

# Quantum optical signatures of coherent vibronic dynamics in bio-inspired light harvesting systems

*Valentina Notararigo*

Dissertation submitted in partial fulfilment  
of the requirements for the degree of  
**Doctor of Philosophy**  
of  
**University College London**

Department of Physics and Astronomy  
University College London

December 13, 2019



**Declaration of originality**

I, Valentina Notararigo, confirm that the work presented in this thesis is my own. Where information has been derived from other sources, I confirm that this has been indicated in the thesis.

**Declaration of copyright**

The copyright of this thesis rests with the author and is made available under a Creative Commons Attribution Non-Commercial No Derivatives licence. Researchers are free to copy, distribute or transmit the thesis on the condition that they attribute it, that they do not use it for commercial purposes and that they do not alter, transform or build upon it. For any reuse or redistribution, researchers must make clear to others the licence terms of this work.



## **Acknowledgements**

I would like to first thank my supervisor, Alexandra Olaya-Castro, for the supervision, the support, the sharing of the physical insight and the help, both in physics and in life. It has been a pleasure working with you.

I am also thankful to all people I have shared the office with: Stefan, Robert, TK, thanks for every stimulating discussion and the good time. David, thanks for having patiently helped me whenever I needed, it has always been a pleasure to chat with you. And Richard, thank you for being such a good friend and for having shared with me so much of your time: the office was not the same after you left.

Many thanks to all my dearest friends, those who have been there since I was born, and the new ones met in this beautiful city.

A huge thank you goes to my family, for all the support and the help: you have been fundamental in these years in so many ways... Our bond is stronger than any physical distance.

And last, but definitely not least, Federico: thank you for always being here for me, thanks for the help in any kind of situation, thanks for the support whenever I needed it the most. I could not have done this without you.



## LIST OF PUBLICATIONS

This thesis is based upon the following publications.

- *Perturbation approach for computing frequency- and time-resolved photon correlation functions*, David I. H. Holdaway, **Valentina Notararigo**, and Alexandra Olaya-Castro, Phys. Rev. A **98**, 063828, 2018.

Other works carried out during the PhD (not directly included in the thesis):

- *Effect of boundaries on vacuum field fluctuations and radiation-mediated interactions between atoms*, F. Armata, S. Butera, G. Fiscelli, R. Incardone, **V. Notararigo**, R. Palacino, R. Passante, L. Rizzuto, S. Spagnolo, J. Phys. Conf. Series - Proceedings of the Eighth International Workshop DICE 2016 Spacetime-Matter-Quantum Mechanics, 880, 012064, 2017.
- *Resonance interaction energy between two entangled atoms in a photonic bandgap environment*, **Valentina Notararigo**, Roberto Passante, and Lucia Rizzuto, Scientific Reports **8**, 5193, 2018.



# Abstract

The study of quantum phenomena in biology has received significant attention in the last decade. One of the problems of most interest is the understanding of quantum effects during the first steps of photosynthesis. Ultrafast two-dimensional electronic spectroscopy has revealed that pigment-protein complexes responsible for light-harvesting and charge separation in photosynthetic organisms can support quantum coherent dynamics in the excited state, for up to few hundreds of femtoseconds. The leading hypothesis on the mechanisms supporting this coherent behaviour is quantum interactions between electronic and some specific vibrational motions in the excited state. This hypothesis, however, awaits unambiguous confirmation. Among the most powerful techniques to investigate the quantum behaviour of an emitter is the study of quantum optical properties of the light it emits. This thesis develops theoretical studies showing that frequency-filtered and time-resolved photon counting statistics of the light emitted by a prototype photosynthetic unit can give important insight into the quantum coherent nature and the mechanisms underlying excited state dynamics in single photosynthetic complexes. By developing a perturbative and efficient approach to the computation of frequency- and time- resolved photon correlation functions, we show that such correlations have the potential to give unambiguous signatures of coherence contributions to the steady state emission. For a light-harvesting unit emitting in free space, the signatures of excited state coherence manifest themselves as non-trivial antibunching. This feature cannot be probed by measuring unfiltered photon correlations. We then consider the situation in which a prototype energy transfer unit is embedded in an optical cavity such that its emission rate is enhanced. In this case we observed a rich behaviour of the frequency-filtered, second-order photon correlations that allows a clear distinction of coherence contributions, and their variation, depending of the electronic and vibrational interactions in the system of interest.



# Impact Statement

The investigations carried out in this thesis have the potential to answer one of the most relevant questions debated inside the community. In fact, the theoretical approach developed in Chapter 2 to compute frequency-filtered and time-resolved correlation functions represents a promising innovative tool to prove, without any ambiguity, the presence of quantum coherent effects occurring in the first stages of photosynthesis in living organisms.

Thanks to the development of two-dimensional electronic spectroscopy, a lot of experiments have already been performed on biological systems that seem to show the presence of such effects. However, the leading hypothesis behind them needs further confirmations from different experimental techniques. The new proposed formalism, indeed, is based on the calculation of correlation functions, which are able to overcome some challenges met in spectroscopic experiments.

The research carried out in Chapter 3 contains theoretical simulations of very potentially promising experiments. Even in simple bio-inspired models, such simulations display that the frequency- and time-resolved correlation functions witness coherences between the excited states of the system of interest, that can occur only if it undergoes quantum coherent dynamics. These results are very powerful, since they pave the way for new potential experiments that can probe unambiguous signatures of the existence of quantum coherence in biological complexes.

The work presented in Chapter 4 goes even more towards the realisation of a possible photon counting statistics experiment. The introduction of an optical cavity, in resonance with a characteristic frequency of the electronic system, increases the light emission. In such a way, the emission from an individual complex allows to compute photon correlations, which otherwise would not be possible due to the too weak signal in comparison to the noise level.

Finally, the code written for the computations in this thesis might be used for future developments in this research field. Some results in this thesis have been published in a scientific journal and others will be submitted for publication.



# Contents

<b>Introduction</b>	<b>17</b>
Thesis outline . . . . .	19
<b>1 Background</b>	<b>21</b>
1.1 Overview . . . . .	21
1.2 The world of Quantum Biology . . . . .	22
1.2.1 Photosynthesis . . . . .	24
1.2.2 Classical photosynthesis . . . . .	24
1.2.3 Quantum photosynthesis . . . . .	26
1.2.3.1 Excitons (first key quantum effect) . . . . .	27
1.2.3.2 Excitons and vibrations (second key quantum effect) . . . . .	28
1.2.3.3 Optimal balance (third key quantum effect) . . . . .	30
1.3 Open quantum system approach . . . . .	31
1.3.1 Closed quantum systems . . . . .	31
1.3.2 Open quantum systems . . . . .	33
1.3.3 Born-Markov master equation: weak coupling limit . . . . .	34
1.3.3.1 Markov approximation with eigenoperators approach: the Redfield master equation . . . . .	34
1.3.3.2 Markov approximation with Kraus operators approach: the Linblad master equation . . . . .	38
1.3.4 Lindblad dynamics represented by a matrix-vector notation	43
1.4 Hamiltonian of bio-inspired light harvesting systems . . . . .	44
1.4.1 Electronic Hamiltonian . . . . .	46
1.4.2 Vibrational Hamiltonian . . . . .	49
1.4.3 Interaction Hamiltonian . . . . .	50
1.4.4 Full Hamiltonian . . . . .	51
1.5 Probing quantum coherence . . . . .	53
1.5.1 Theoretical approach . . . . .	53

1.5.2	Experimental approach	54
1.6	Blind and coloured photon counting statistics	58
1.6.1	Blind correlation functions	58
1.6.2	Frequency-filtered correlation functions	60
1.6.3	Sensor method for spectrally filtered photon correlations	61
<b>2</b>	<b>Perturbative method for computing frequency-filtered and time-resolved photon correlation</b>	<b>67</b>
2.1	Introduction	67
2.2	Why an alternative sensor method?	69
2.3	Frequency-filtered spectrum and photon correlations at zero time delay	72
2.3.1	$M = 1$ : power spectrum	72
2.3.2	$M = 2$ : zero-delay correlations	75
2.3.3	$M > 2$ : numerical procedure to compute zero time delay correlations at higher orders	77
2.4	Frequency-filtered correlations at finite delay time	80
2.4.1	Behaviours at short time delays	84
2.4.2	Behaviours at large time delays	85
2.5	Consistency check about the equivalence of the sensor and the integral methods	87
2.6	Comparison between results obtained with new and original formalism	89
2.7	Conclusion	95
<b>3</b>	<b>Frequency-filtered and time-resolved photon counting statistics of prototype light harvesting dimers</b>	<b>97</b>
3.1	Introduction	97
3.2	Model in free space	99
3.3	Dynamics	102
3.4	Counting statistics in free space	104
3.4.1	First order correlations	104
3.4.2	Second order correlations: zero time delay	105
3.4.3	Second order correlations: finite time delay	106
3.5	Relations between coherent contribution dynamics and filtering analysis	112
3.6	Conclusion	115

<b>4 Coloured photon counting statistics of bio-inspired dimers coupled to a cavity</b>	<b>117</b>
4.1 Introduction	117
4.2 Motivation	119
4.3 Model: vibronic system coupled to a cavity	120
4.4 Counting statistics in the cavity	122
4.4.1 Numerical simulations	122
4.4.2 First order correlations $S_{\Gamma}^{(1)}(\omega_1)$	123
4.4.3 Zero time delay second order correlations $g_{\Gamma}^{(2)}(\omega_1, R_3)$	124
4.4.4 Finite time delay second order correlations $g_{\Gamma}^{(2)}(R_4, R_3, \tau)$	125
4.5 Conclusion	128
<b>Conclusions and outlook</b>	<b>129</b>
<b>Appendix</b>	<b>132</b>
<b>A Convergence for L in free space</b>	<b>133</b>
<b>B Numerical checks in the cavity configuration</b>	<b>135</b>



# List of Figures

1.1	<i>Solar radiation spectrum as a function of wavelength [70]. . . . .</i>	24
1.2	<i>A photosystem is formed of a reaction centre and an antenna complex. Light is absorbed by the light-harvesting complex, containing proteins and molecules of chlorophylls (of type a and b) and carotenoids, and then transferred to the reaction centre. It contains one or more molecules of chlorophylls, together with the primary electron acceptor: here the sunlight energy is transformed into chemical energy. Figure taken from Ref. [71]. . . . .</i>	25
1.3	<i>The figure (from Ref. [77]) represents the structural organization of the Fenna-Matthews-Olson (FMO) pigment-protein complex: it contains seven bacterio-chlorophyll (BChl) molecules, indicated with italic numbers. The exciton delocalisation over the different chromophores is indicated with bold numbers and coloured shades. For example, excitons 3 and 7 (green, bold numbers) are both delocalised over the same BChls 1 and 2 (italic numbers). The red and green arrows refer to the main two photoexcitation transfer pathways. . . . .</i>	28
1.4	<i>The table summarises the three quantum secrets involved in the photosynthetic process. . . . .</i>	30
1.5	<i>The figure shows the system under study before and after diagonalising the electronic Hamiltonian, both for the electronic part only (a), and for the collective exciton-vibration description (b). . . . .</i>	52
1.6	<i>Representation of the pump-probe setup [90]. . . . .</i>	55
1.7	<i>Representation of the geometry for a two-pulse photon echo experiment [93].</i>	55
1.8	<i>Representation of the scheme for a 2D spectroscopy experiment [94], where <math>\tau</math> corresponds to the coherence time passing until the first laser pulse, <math>T</math> is the waiting time between the second and third pulse, and <math>t</math> is the time delay with respect to the second pulse. . . . .</i>	56

1.9	<i>Power spectra of emission probed by weak incoherent excitation (<math>P_\sigma = \gamma_\sigma = 0.01g</math>) for three cavities of decreasing quality <math>\gamma_a = 0.01g</math> (solid line), <math>\gamma_a = 0.1g</math> (dashed) and <math>\gamma_a = 0.5g</math> (dotted). The values of the parameters are: <math>g = 1</math>, <math>\epsilon_1 = 10^{-5}</math> and <math>\Gamma = 0.001g</math>. The figure is in semilog scale and it is plotted in arbitrary units. . . . .</i>	64
1.10	<i>Two-photon correlations at zero delay with <math>\omega_2 = R</math>. Same parameters as figure 1.9. . . . .</i>	64
1.11	<i>Time-resolved correlation function without using the normal order of the sensor operators. Positive times correspond to detection of frequencies as reported in the legend, negative times to the opposite order. . . . .</i>	65
1.12	<i>Time-resolved second order correlation function. Positive times correspond to detection of frequencies as reported in the legend, negative times to the opposite order. Parameters: <math>\Gamma = \gamma_2</math> for both sensors, <math>P_\sigma = \gamma_\sigma = 0.01g</math>, <math>\gamma_a = 0.1g</math>. . . . .</i>	65
2.1	<i>(a) Potential experimental setup to measure frequency-filtered and time-resolved correlation functions, similar to that used in Ref. [48]. (b) Diagram of the sensor method proposed in Ref. [46, 47] to compute frequency-filtered correlations. Each sensor is modelled as a two-level system coupled to the quantum emitter through the strength parameter <math>\epsilon_m</math>, with <math>m = 1, \dots, M</math>. Photon correlations are recovered in the limit of small coupling <math>\epsilon_1, \dots, \epsilon_M \rightarrow 0</math>. . . . .</i>	70
2.2	<i>Power spectra <math>S_\Gamma(\omega_1)</math> for the system under study as a function of the frequency <math>\omega_1</math>. The figure is in log scale and compares the results with the new proposed method and the original sensor method. . . . .</i>	92
2.3	<i>(a) Intensity of power spectrum at a fixed frequency, <math>S_\Gamma(\omega_1 = R_3)</math> in log-log scale, and (b) zero-delay time second-order correlation <math>g_\Gamma^{(2)}(R_4, R_3)</math> in semilog scale, as functions of <math>\epsilon</math>. Both functions are calculated with the <math>\epsilon</math>-dependent method for our vibronic dimer. . . . .</i>	92
2.4	<i>(a) Comparison between the second order photon correlations at zero time delay <math>g_\Gamma^{(2)}(\omega_1, R_3)</math> versus <math>\omega_1</math> computed with the new method and the <math>\epsilon</math>-dependent sensor method for different values of <math>\epsilon</math>. (b) <math> \Delta g_\epsilon^{(2)}(0) </math>, the absolute difference value between the predictions of the two methods, versus <math>\omega_1</math> for two values of <math>\epsilon</math>. . . . .</i>	93

2.5	<i>Frequency- and time-resolved correlation function <math>g_{\Gamma}^{(2)}(R_4, R_3, \tau)</math> versus <math>\tau</math> predicted with (a) the perturbative method and (b) the <math>\epsilon</math>-dependent method. Inset (i) in panel (a) depicts the short time behaviour of <math>\nu\tilde{I}_0(\tau)</math> as defined in the text. Inset (ii) in (a) and inset in (b) report long time regime of <math>g_{\Gamma}^{(2)}(\omega_1, \omega_2, \tau)</math>.</i>	94
3.1	<i>Picture (a) represents the dimer under study and is based on the protein structure of PE545. Table (b) reports the set of parameters common to both the regimes analysed, while table (c) indicates the parameters for the two specific configurations.</i>	100
3.2	<i>Dynamics (populations and coherences) of the electronic system only without the sensors: (a) for dimer 1 (quasi-localised model) and (b) dimer 2 (more delocalised model), with parameters in Fig.3.1(b) and 3.1(c) and <math>\rho_{el} = Tr_{vib}\{\rho(t)\}</math>.</i>	102
3.3	<i>Vibronic dynamics of the system without the sensors. The figure represents some populations (a) and coherences (c) for dimer 1 (quasi-localised model) and for dimer 2 (b) and (d) (more delocalised model), with parameters in Fig.3.1(b) and 3.1(c).</i>	103
3.4	<i>Power spectra of the exciton emission for: (a) dimer 1 (quasi-localised model) and (b) dimer 2 (more delocalised model), with parameters in Fig.3.1(b) and 3.1(c). The figure is in log scale.</i>	105
3.5	<i>Two color-photon correlations at zero time delay for (a) dimer 1 (quasi-localised model) and (b) dimer 2 (more delocalised model), with parameters in Fig.3.1(b) and 3.1(c). The figure is in semilog scale.</i>	106
3.6	<i>Blind two-photon correlations at finite time delay for (a) dimer 1 (quasi-localised model) and (b) dimer 2 (more delocalised model), with parameters in Fig.3.1(b) and 3.1(c).</i>	107
3.7	<i>Frequency- and time-resolved auto-correlation function <math>g_{\Gamma}^{(2)}(R_4, R_4, \tau)</math> versus <math>\tau</math> predicted for (a) dimer 1 (quasi-localised model) and (b) dimer 2 (more delocalised model), with parameters in Fig.3.1(b) and 3.1(c). The inserts in panels (a) and (b) show the short time behaviour of <math>\nu\tilde{I}_1(\tau)</math> and <math>\nu\tilde{I}_2(\tau)</math> (with <math>\nu = [(\tilde{n}_1\tilde{n}_2)]^{-1}</math>).</i>	108
3.8	<i>Frequency- and time-resolved cross-correlation function <math>g_{\Gamma}^{(2)}(R_4, R_3, \tau)</math> for (a) dimer 1 (quasi-localised model) and (b) dimer 2 (more delocalised model), with parameters in Fig.3.1(b) and 3.1(c). The inserts in panels (a) and (b) show the short time behaviour of <math>\nu\tilde{I}_1(\tau)</math> and <math>\nu\tilde{I}_2(\tau)</math>.</i>	109

3.9	<i>Frequency- and time-resolved cross-correlation functions <math>g_{\Gamma}^{(2)}(R_4, R_3, \tau)</math> for dimer 1 comparing different couplings <math>g</math> to the phonon bath (other parameters in Fig.3.1(b) and 3.1(c)).</i>	111
3.10	<i>Frequency- and time-resolved auto-correlation functions <math>g_{\Gamma}^{(2)}(R_4, R_4, \tau)</math> for (a) dimer 1 (quasi-localised model) and (b) dimer 2 (more delocalised model), for different pumping rates <math>P</math>, with the other parameters in Fig.3.1(b) and 3.1(c).</i>	112
3.11	<i>Frequency- and time-resolved cross-correlation functions <math>g_{\Gamma}^{(2)}(R_4, R_3, \tau)</math> for (a) dimer 1 (quasi-localised model) and (b) dimer 2 (more delocalised model), for different pumping rates <math>P</math>, with the other parameters in Fig.3.1(b) and 3.1(c).</i>	113
3.12	<i>Frequency- and time-resolved auto-correlation functions <math>g_{\Gamma}^{(2)}(R_4, R_4, \tau)</math> for (a) dimer 1 (quasi-localised model) and (b) dimer 2 (more delocalised model), for different damping rates <math>\Gamma_{th}</math> for the mode, with the other parameters in Fig.3.1(b) and 3.1(c).</i>	114
3.13	<i>Frequency- and time-resolved cross-correlation functions <math>g_{\Gamma}^{(2)}(R_4, R_3, \tau)</math> for (a) dimer 1 (quasi-localised model) and (b) dimer 2 (more delocalised model), for different damping rates <math>\Gamma_{th}</math> for the mode, with the other parameters in Fig.3.1(b) and 3.1(c).</i>	114
4.1	<i>Representation of the system we analyse in this chapter: a bio-inspired system, undergoing incoherent pumping, is located inside a cavity weakly coupled to sensors, which detect outcoming photons at specific frequencies.</i>	119
4.2	<i>Power spectra for: (a) the quasi-localised model in dimer 1 and (b) the more delocalised in dimer 2, with parameters given in Tables 3.1(b) and 3.1(c). The yellow line corresponds to the spectrum with the largest value of coupling. The plots are in arbitrary units and the spectra have been translated with respect each other to better distinguish their features. The figure is in log scale.</i>	124
4.3	<i>Second order correlations at zero time delay for: (a) dimer 1 and (b) dimer 2, with parameters in Fig.3.1(b) and 3.1(c). The figure is in semilog scale. The yellow line corresponds to the spectrum with the largest value of coupling.</i>	125
4.4	<i>Frequency- and time-resolved cross-correlation function <math>g_{\Gamma}^{(2)}(R_4, R_3, \tau)</math> for: (a) the quasi-localised configuration in dimer 1 and (b) the more delocalised model in dimer 2, with parameters in Fig.3.1(b) and 3.1(c).</i>	125

4.5	<i>Frequency- and time-resolved cross-correlation functions <math>g_{\Gamma}^{(2)}(R_4, R_4, \tau)</math> for: (a) the quasi-localised configuration in dimer 1 and (b) the more delocalised model in dimer 2, for different damping rates <math>\Gamma_{th}</math> for the modes, with the other parameters in Fig.3.1(b) and 3.1(c).</i>	126
A.1	<i>The figure represents (a) the power spectra, (b) the zero time delay and (c) the time-resolved photon correlations for dimer 1, considering different values of the maximum number of excitations <math>L</math> in the collective vibrational mode.</i>	133
B.1	<i>Power spectra (a) and (b) and time-resolved correlation functions (c) and (d) for both dimers, with coupling to the cavity <math>g_c = (1.33ps)^{-1} = 25 \text{ cm}^{-1}</math> and other parameters given in Tables 3.1(b) and 3.1(c), comparing different values of the maximum number of excitations <math>L''</math> in the cavity mode. (The figure for the power spectra is in log scale.)</i>	136
B.2	<i>Power spectra (a) and (b) and time-resolved correlation functions (c) and (d) for both dimers, with coupling to the cavity <math>g_c = (0.67ps)^{-1} = 50 \text{ cm}^{-1}</math> and other parameters given in Fig.3.1(b) and 3.1(c), comparing different values of the maximum number of excitations <math>L''</math> in the cavity mode. (The figure for the power spectra is in log scale.)</i>	136



# Introduction

Quantum mechanics offers the most accurate description of the microscopic world, in contrast to classical mechanics which focuses on the investigation of macroscopic systems. However, thanks to the recent theoretical and experimental developments, the domain in which quantum mechanical phenomena can be explored has enlarged significantly. As a result, this has provided technological capabilities to question the importance of quantum effects in life processes. This is, indeed, the goal of quantum biology, which is an emerging field of research studying quantum mechanical effects in biological systems and paving the way to bio-inspired technologies in the near future.

Biological systems interact with their surrounding environments, they exist at room temperature and need external energy to guarantee the out of equilibrium state which characterises life [1]. At first glance, it would seem difficult to think that non-trivial quantum mechanical effects can survive in biological processes and have a significant impact on them. However, some biological processes happening at molecular level can occur on very short time scales and be well localised, thus potentially showing quantum effects before the environment destroys them. Nonetheless, environmental noise might support the existence of quantum coherence and entanglement [2]. This means that the presence of a quantum dynamics in these systems is not just related to short length and time scales, but it is rather the result of a more complex and constructive interplay between the environment and the system.

The most fundamental example of quantum phenomena in biology is photosynthesis, in particular its first stages involving the processes of light harvesting and energy transfer [3]. Such processes occur thanks to specialised antennae, which are formed of chromophores arranged in specific configurations within protein scaffolds. The efficiency of the energy transfer in living organisms is exceptionally high: more than 90% of photons absorbed activate chemical reactions, meaning that almost every photon initiates a charge separation [4–6]. In photosynthesis certain living organisms, such as plants and some bacteria, capture light coming from the sun,

thanks to collective electronic states, called excitons. This energy is then transferred within the antenna and used to produce chemical energy [7].

The study of the exciton dynamics and the mechanism of energy transfer from the light harvesting antenna to the reaction centres has been of interest for different research groups, due to the many optical experiments carried out with photosynthetic complexes [8–12]. It has been shown that exciton states are delocalised over different chromophores and that an interesting interaction between quantum processes and environmental noise is key to understand the exceptionally high efficiency of the energy transfer process [13–21]. However, it is not clear yet if this process can be explained through classical equations or, on the contrary, if it involves non-trivial quantum phenomena [22]. The presence of these phenomena and the biological function of this quantum behaviour are still open questions in the field of quantum photosynthesis.

Important steps forward regarding these questions have been made thanks to the development of two-dimensional electronic spectroscopy [23,24]. Over the last years, indeed, ultrafast two-dimensional spectroscopy on biological complexes has shown oscillatory electronic dynamics lasting from a few hundred of femtoseconds [9,25] up to picoseconds [12]. This is an unexpected long time scale, considering the rapidly decaying electronic quantum coherence happening on a timescale of tens of femtoseconds.

There is an ongoing discussion about the origin of the beating patterns observed in two-dimensional electronic spectroscopy, which can be illustrated by comparing three very recent works. Ref. [26] indicates that the observed oscillations correspond to vibrational coherence in the electronic ground state of Fenna-Matthews-Olson (FMO) complexes, while Ref. [27] points out that they detect vibronic coherences in the excited state of FMO. Ref. [28], instead, shows that the oscillations observed correspond to both electronic and vibrational coherences. While there is yet no consensus, it seems that the leading hypothesis underlying the experimental observation of long-lived coherent dynamics is the involvement of a vibronic mechanism, that is the quantum interaction between joint electronic and vibrational degrees of freedom [29–34]. In other words, the vibronic coupling could be the reason behind the quantum energy exchange between electronic states and specific vibrations [22,35]. Within this interpretation, the interaction with the intramolecular vibration affects the excited state dynamics of the system. It leads then to the formation of vibronic states, that is superpositions of quantum states of excitons and vibrations, causing the long-lived oscillations in the dynamics. However, there is some controversy on

the origin of these oscillations [36], therefore the need of better understanding the exciton-vibration interaction.

Although multidimensional spectroscopy represents a powerful tool to investigate quantum coherent dynamics in biological systems, it does not allow to clearly understand the origin of the beatings observed. One of the main challenges is that these experiments deal with the average behaviour of a large ensemble of biomolecules, limiting then the understanding of the quantum behaviour happening at a level of single molecule. In addition, the observation of the beatings in the dynamics does not represent an incontrovertible proof of quantum behaviour [22, 37].

Given the questions still open in the field of quantum photosynthesis, it becomes essential to provide alternative and unambiguous confirmations of the quantum mechanism underlying the energy transfer in biomolecular systems. To this end, it is fundamental to understand its origin at a level of a single molecule. One of the most common ways to investigate and define quantum properties of both light [38–41] and emitters [42–44] is the measurement of photon correlation functions. Indeed, they allow to gain conceptual clarity on the contribution of quantum coherent processes to the emission statistics and also provide alternative experimental setups to probe non-trivial quantum effects in the dynamics of biological systems [45].

The aim of this work is to investigate the quantum coherent interaction in bio-inspired single molecules through the analysis of the coloured photon counting statistics. Indeed, spectral filtering of optical signals, and the consequent trade-off between frequency and time resolution, gives insight on many quantum phenomena [46–50], including quantum dynamics of complex molecular systems [49, 50].

## Thesis outline

This thesis is divided as follows.

The first Chapter describes the context of quantum biology, focusing on the first stages of photosynthesis. It presents the open quantum system approach used to study biomolecules and the experimental spectroscopical setups employed to investigate them. It also introduces the correlation functions, with particular emphasis on frequency-filtered and time-resolved photon correlations.

The second Chapter develops an alternative technique to the sensor procedure proposed in [46, 47] to compute coloured correlation functions. This method shows that frequency- and time-resolved photon correlations can probe coherent contribu-

tions to the light emitted by the biomolecule. The results here obtained represent the theoretical scaffolding on which the next chapters are built.

The third Chapter presents the analysis of the statistical properties of the light emitted by two different bio-inspired toy models, in free space. The results, obtained using the formalism developed in Chapter two, reflect signatures of quantum coherent dynamics within the excited state manifold, even in the steady state.

Last Chapter examines the same two photosynthetic complexes, now weakly coupled to a cavity mode. The weak coupling regime assures that the cavity does not affect the dynamics of the systems. The presence of the cavity guarantees to selectively increase the emission of photons emitted by the system, due to the resonance condition with one particular frequency, as shown by the analysis of the frequency-filtered and time-resolved correlation functions.

# Chapter 1

## Background

This chapter gives a brief introduction to the field of quantum biology with particular emphasis on quantum effects in photosynthesis, the main subject of this thesis. The chapter presents the theoretical framework and the experimental techniques used to investigate quantum effects in photosynthetic systems.

We introduce the open quantum system approach that describes quantum dynamics of molecular systems and which will be used to characterise the prototype photosynthetic complexes of interest. The last part of the chapter is dedicated to the theoretical framework used to examine quantum optical properties of the light emitted by these systems.

### 1.1 Overview

Quantum biology is an emerging field of research which aims to explore quantum mechanical effects in the functioning of biological systems and to draw lessons for the next generation of bio-inspired technologies [1]. The field has gained significant attention in the last ten years thanks to the development of new experimental techniques that have allowed observation of quantum phenomena in biological systems [8–12]. However, the term “quantum biology” is almost a century old, coined by Jordan in his book (“The physics and the secret of life”) in 1943 as he wondered whether quantum mechanics played a role in life [51]. One year later, in his book “What is life?”, Schrödinger also argued that quantum mechanics must affect the processes and reactions that happen in living organisms, since it governs the stability and structure of molecules [52]. He also underlined that every process in life has a statistical and stochastic nature, meaning that every event is random and that order is only obtained with the statistical average of disordered situations. In contrast, Davydov, in his book “Biology and quantum mechanics” (1982) [53] asserts that

quantum mechanics is significant only for isolated systems in pure states, hence it could not be relevant for biological processes happening in open systems at thermal equilibrium.

For a long time quantum biology was seen as a speculative field. Nowadays, however, the progress in science and technology has allowed a significant improvement and development of the experimental techniques, which have led to obtain very promising results on the matter of quantum effects in nature [9–12].

This, in turn, has opened new challenges from a theoretical point of view, such as the development of advanced models and approaches to understand the physics of living systems. At this point it is important to clarify what we mean by “quantum biology” and where its effects become tangible.

## 1.2 The world of Quantum Biology

In general, quantum phenomena can be observed on microscopic scale in systems “protected” long enough from the influence of the surrounding environment, thus allowing quantum coherences to survive sufficiently long across relevant timescales. Biological systems, even at the protein scale, are the exact opposite by definition: they constantly interact with their environment, they operate at room temperature and need to be provided with energy to guarantee the out of equilibrium state that characterises life [1]. Consequently, it would seem that quantum mechanics does not affect biological processes, except for the “trivial” quantum effects involving, for instance, molecular bonds.

However, the reality is more nuanced. First of all, some processes in biological systems happen on very short time scales (of the order of picoseconds), and in very localised regions (over the size of the protein, namely a few nanometers). This implies that molecular complexes could manifest quantum dynamical behaviour on the relevant time and length scales, before the environmental fluctuations cancel it. Secondly, it has been suggested that environmental noise could indeed aid quantum coherence and entanglement [2, 14, 54, 55]. As a consequence, quantum dynamical behaviour associated to a biological process in relevant time and length scales is strongly dependent on non-trivial interactions between the system and its surroundings.

Within this scenario there are already some known biological phenomena that can only be explained through quantum mechanics [56]. The mechanism of vision is an example: the absorption of light by a chromophore leads to a quantum me-

chanical arrangement of electronic states with a specific symmetry that produces a photochemical isomerization. After a series of enzymes and reactions are activated, an electrical impulse is generated and transferred to a nerve cell [56]. Other examples of photochemical processes in biology, that can be understood only from a quantum mechanical point of view, are the deactivation of excited states in DNA to avoid photodamage into the genetic code [57], photoprotection using melanin [58] and bioluminescence used by coral [59].

Electron flow (over 15 Å) is another essential process in respiration [60] and photosynthesis [61]. Since proteins are not electrical conductors, quantum mechanical tunnelling intervenes to overcome the classical energy barriers thanks to the time uncertainty principle. Therefore, this tunnelling effect allows electron transfer within the protein scaffold [62, 63]. More specifically, the presence of the protein provides electronic states associated with pathways along its structure which help donor and acceptor wavefunctions to delocalise towards each other, thus speeding up the tunnelling rates by 10 orders of magnitude in comparison to the same situation in the vacuum [63, 64]. Proton tunnelling also has a key role in many enzymatic catalytic reactions involving the transfer of a proton [65]. Inelastic tunnelling assisted by specific high-energy vibrations has been suggested to play a role in olfaction. [66]. It has been proposed that odorants (that is the proteins secreted in the nasal mucus) are discriminated by some specific olfactory receptors not only through their shapes but also through their vibrational spectrum. This means that an electron tunnelling assisted by a phonon happens between two receptors via the protein [67].

Of a different nature is the mechanism of magnetoreception characterising some living organisms that use the Earth's magnetic field [68]. A radical pair mechanism has been suggested as the built-in magnetic compass that uses the Earth's magnetic field. At the same time, various decoherence processes take place, such that the subsequent signal produced depends on the system's orientation with respect to the magnetic field [69].

The most emblematic example of quantum phenomena in biology is photosynthesis, more specifically the processes of light harvesting and energy transfer [3]. Light harvesting happens in living organisms with a remarkably high efficiency: under conditions of low irradiance, more than 90% of photons absorbed drive photochemistry, in other words almost every photon initiates a charge separation [4–6]. Given the importance of this topic for the thesis, this process will be described in the following both from a classical and quantum point of view.

### 1.2.1 Photosynthesis

Photosynthesis is a biological process where plants, algae and some bacteria capture light coming from the sun and then convert this energy into biochemical energy, providing the resources necessary for life [7]. Photosynthetic process involves not only the well known mechanism of production of biomass based on chlorophylls, but also other photoreception processes carried out by some bacteria [7].

### 1.2.2 Classical photosynthesis

In photosynthesis, sunlight is used to initialise a chain of chemical reactions, as it will be discussed in the following. The sun emission spectrum is very broad, ranging from gamma rays to radio waves (see Fig.1.1).

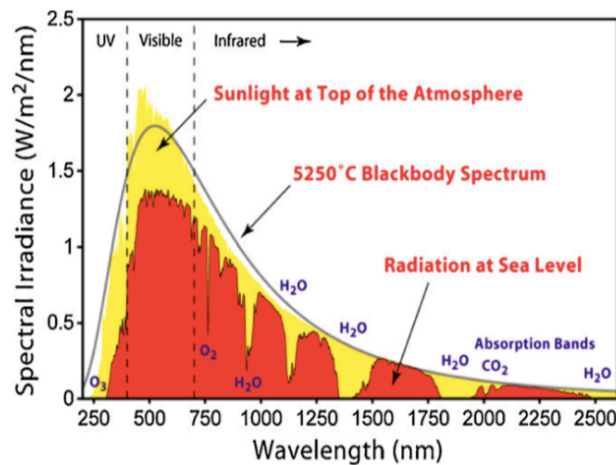


Figure 1.1: *Solar radiation spectrum as a function of wavelength [70].*

However, the light reaching the surface of the Earth is reduced both by scattering and by the absorption of molecules in the atmosphere, such as carbon dioxide that absorbs in the infrared region and ozone that absorbs in the ultraviolet [7]. In comparison, many chlorophyll-pigments use visible light (400-700nm) to activate photosynthesis. In aquatic systems the situation is different: the intensity of light decreases with depth. Here, water absorbs mainly in the red region of the spectrum, therefore the wavelengths suited to chlorophyll-pigments do not reach the organisms at the bottom. Furthermore, water also scatters light: the scattering is inversely proportional to the fourth power of the wavelength, meaning that this phenomenon affects mainly blue light. As a consequence, only green light from the middle region “survives”: chlorophylls do not absorb much in this range, but some other photosynthetic pigments, such as carotenoids or chromophores in cryptophyte algae, do and they are present in many aquatic organisms.

Photosynthesis can happen in two different ways, oxygenic and anoxygenic, depending on the kind of atom that acts as donor in the chemical reaction. The oxygenic form of photosynthesis uses the photon energy to produce glucose and oxygen from carbon dioxide and water ( $6CO_2 + 6H_2O \xrightarrow{\text{light}} C_6H_{12}O_6 + 6O_2$ ). This is typical of all plants, algae and cyanobacteria. The anoxygenic process, instead, starts from a molecule of the form  $H_2S$  (hydrogen sulfide) where the final product is not oxygen, but another molecule, for example sulphur. This mechanism happens in purple, green and heliobacteria [7].

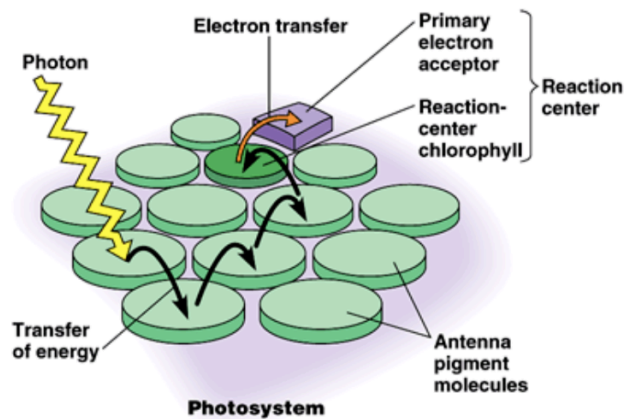


Figure 1.2: A photosystem is formed of a reaction centre and an antenna complex. Light is absorbed by the light-harvesting complex, containing proteins and molecules of chlorophylls (of type a and b) and carotenoids, and then transferred to the reaction centre. It contains one or more molecules of chlorophylls, together with the primary electron acceptor: here the sunlight energy is transformed into chemical energy. Figure taken from Ref. [71].

In plants photosynthesis takes place inside the chloroplasts, subcellular structures that contain the chlorophyll pigments, and it occurs in four main steps (summarised in Fig.1.2).

The first is the absorption of energy from sunlight by one of the collective pigments states in the light harvesting complex. Pigments (also called chromophores or sites) are organised in protein scaffolds that hold them in specific orientations. This structure is such that the inter-pigment electronic coupling creates delocalised excited states (called “excitons”) that increase the absorption cross-section. In other words, the presence of the proteins generates antennae that optimise the absorption surface and efficiency. Once an electronic excitation is created, the energy is transferred through the collective states, until it reaches the reaction centre, where, eventually, it leads to charge separation. The photon absorption process within antennae works in such a way that excitations are funnelled from higher to lower

energy excitons.

The second phase of photosynthesis involves primary electron transfer in reaction centres. These contain pigments, chemically similar to those in the rest of the antenna, but with particular properties due to the surrounding protein environment: here a chlorophyll dimer, called the special pair, acts as a primary electron donor to initiate an electron transfer cascade [7]. The excited state of the pigment releases an electron that binds to an acceptor, generating a ionised molecule: at this stage the excitation energy has been transformed into chemical energy, but the new state is very unstable, therefore the electron can be transferred back and the energy can be converted into heat.

To avoid energy losses, the system enters into the third phase of the photosynthesis, where a series of secondary chemical reactions takes place, in order to separate positive and negative charges and fight the recombination process. This process happens in very short time (within one nanosecond) and creates a pH difference, or electrochemical gradient, which is used to synthesise ATP (adenosine triphosphate). The last stage sees the production of stable high-energy molecules which will be used as fuel for processes needed in cells, in particular the ATP produced in the previous step is needed to reduce carbon dioxide to sugars.

In principle, the whole photosynthesis event seems to involve only trivial quantum effects, such as the formation of collective electronic states. However, other quantum mechanisms could play a key role during the energy dynamics, as it will be explained in more detail in the following section.

### 1.2.3 Quantum photosynthesis

Within the photosynthesis mechanism, it is the first phase that has attracted the attention regarding the question about the presence of quantum effects. This is due to the very short time needed for absorption and energy transfer, from femto to picoseconds (this time is short in comparison to relaxation to the ground state), and to the high efficiency of the process itself, that is the high probability that an absorbed photon is converted into a charge-separated state [4–6]. This efficiency is due to the ultrafast energy transfer to the reaction centre that occurs before the relaxation to the ground state [72].

In the light absorption event, an incoming photon with a specific frequency in the visible spectrum is captured by an exciton in the antenna, which is a complex formed of different kind of chlorophylls or bacteriochlorophylls (for oxygenic organisms or anoxygenic bacteria, respectively) bound to a protein scaffold.

In what follows, we summarise the main quantum features of the light absorption and energy transfer process in the first stages of the photosynthetic process.

### 1.2.3.1 Excitons (first key quantum effect)

The process of light absorption by a light harvesting complex happens thanks to the superposition of transition dipoles of the pigments that form the antennae. Within a simplified model, a pigment inside the antenna complex can be modelled as a two-state system [73]. This assumption is based on the fact that in the description of excitation transport it is common to reduce the dynamics of individual molecules to a single HOMO/LUMO transition. Most of the energy absorbed by photosynthetic organisms, indeed, comes from the strongest optically allowed transition, which is in the  $Q_y$  band of the power spectrum between 750 and 850 nm [74]. Within this model, an incoming photon with the same energy as the electronic gap causes a transition from the ground to the excited state which has a lifetime of about 6 ns [72, 75].

Chromophores in light harvesting complexes are very close to each other: the centre-centre distance is around few Angstroms. Therefore, since the electronic coupling scales as the inverse of chromophore separation cubed ( $V \sim 1/r^3$ ), pigments can strongly interact within the antenna, giving rise to the formation of collective electronic states or excitons. Excitonic states induce broadening or modulation of the absorption spectrum [3].

Under the condition that all the pigments have a comparable HOMO/ LUMO energy gap and the transport time is much faster than the absorption rate, it is possible to assume that the collective state hosts a single excitation at a time [76]. Formally, this means that the attention can be focused onto the single-excitation subspace. This hypothesis is particularly reasonable when dealing with photosynthetic bacteria, such as purple bacteria or green sulphur bacteria, where the photosynthetic process occurs in extremely low light conditions at the bottom of the sea. However, usually it also holds for light-harvesting complexes of higher plants [7].

To clarify the importance of excitonic states, let us consider an antenna with two interacting single chromophores having the same transition energy. This leads to a situation with three states: a common ground state and two local states. Coulomb interaction between the last two gives rise to quantum superposition of excitations coherently delocalised over both sites: these new eigenstates of the system are called excitons. The dipole moments of the individual chromophores combine in such a way that the dipole moment of one exciton will be larger (bright exciton), while the other will be smaller (dark exciton).

As a result, the bright exciton state couples more strongly to the electromagnetic field and, therefore, has a higher probability of absorbing a photon at its transition frequency. For an ensemble of pigments with the same energy, the excitons are delocalised over all the sites with the same amplitude of probability. This is the *first key quantum effect* in photosynthesis: the collective electronic states, namely the excitations delocalised over the chromophores in the antenna, allow a stronger coupling of the bright excitons to the electromagnetic field and, therefore, a higher probability to absorb photons. Of course, in reality, the process is more complicated, because the chromophores do not have the same transition energy, due to the interactions with different local environments. This implies that the excitons are delocalised over some chromophores with higher probability amplitudes (see Fig.1.3).

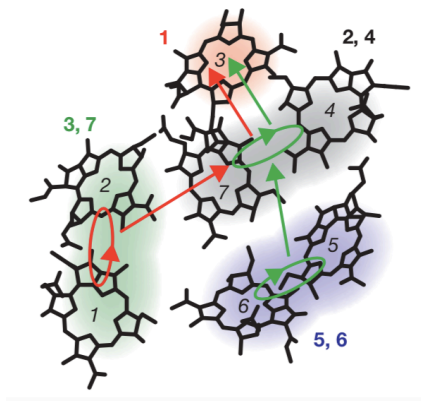


Figure 1.3: *The figure (from Ref. [77]) represents the structural organization of the Fenna-Matthews-Olson (FMO) pigment-protein complex: it contains seven bacterio-chlorophyll (BChl) molecules, indicated with italic numbers. The exciton delocalisation over the different chromophores is indicated with bold numbers and coloured shades. For example, excitons 3 and 7 (green, bold numbers) are both delocalised over the same BChls 1 and 2 (italic numbers). The red and green arrows refer to the main two photoexcitation transfer pathways.*

### 1.2.3.2 Excitons and vibrations (second key quantum effect)

The importance of the excitons for the whole antenna complex can be better understood through the explanation of other two phenomena, whose relevance is connected to their relation with the electronic coupling  $V$ : the energetic disorder and the electron-phonon coupling [72].

The “energetic disorder” is an effect related to the degree of delocalisation of the excitons over the sites, which depends on the relation between the energy difference  $\Delta\alpha = \alpha_i - \alpha_j$  between sites  $i$  and  $j$  and their electronic coupling  $V_{ij}$ . When this

energy difference is larger than the electronic coupling,  $\Delta\alpha \gg V_{ij}$ , that is when molecules have off-resonant electronic transitions, the excitons are quasi-localised over the sites. In the opposite scenario, when transitions are near resonant, namely  $\Delta\alpha \ll V_{ij}$ , the excitons have a large degree of delocalisation over the sites.

The research work of this thesis uses models falling into different degrees of exciton delocalisation over the sites.

Pigments with detuned energies are commonly found in antenna complexes. For instance, identical molecules that experience different local protein environment can have different transition energies. Slow protein motions produce random fluctuations in electronic parameters, resulting in the so called “static disorder”. It changes the electronic parameters in long timescales with respect to the exciton dynamics. In some antenna complexes, the presence of different types of chromophores, with different transition energies, increases even more the spectral cross-section for light absorption. This occurs, for example, in phycobilisomes antenna from cyanobacteria and red algae, and in the antenna proteins of cryptophyte algae, such as phycoerytherin 545 (PE545) and phycocyanin 645 (PC645). An example of how the energetic disorder affects an antenna can be seen in the B850 ring in light harvesting complex 2 (LH2): here, the eigenstates of the system can delocalise over the complex in a perfectly symmetric way. However, the energetic disorder breaks the symmetry of the site absorption, which leads to more localised excitons [78, 79].

The other phenomenon influencing the extent of delocalisation of the excitons is the competition between electronic interactions and electron-phonon coupling. This coupling is due to the interplay between the electronic and vibrational degrees of freedom, where the latter are affected by the stochastic fluctuations in the environment. These fluctuations affect the system destroying phase relations between the excitations of different chromophores and, therefore, giving rise to an excitation more localised than that of an isolated electronic system. This interplay generates the so called “dynamic disorder” as, contrarily to the static disorder, it affects electronic parameters on a timescale comparable to excitation dynamics.

Some vibrational fluctuations are spectrally narrow in frequency and therefore quasi-coherent. Depending on their energy scale, collective vibronic effects can emerge supporting coherence among excitons. In contrast, spectrally broad vibrations lead to dephasing. This is related to the *second key quantum effect* in photosynthesis, since the interaction between electronic and quasi-coherent vibrations allows energy to transfer between excitons and can create quantum coherence between them.

### 1.2.3.3 Optimal balance (third key quantum effect)

At this point it is essential to distinguish between two types of phonon environments: the coherent and the incoherent vibrational motions. The presence of one or the other determines the kind of pathway followed by the electronic excitation during the transfer of energy to the reaction centre [80]. This depends on the ratio between two characteristic times: the intramolecular (or vibrational) relaxation time,  $T_g$ , and the intermolecular transitions time,  $T_V$ . When the intermolecular transitions time is smaller than the vibrational relaxation time,  $T_V < T_g$ , the excitation can move as a delocalised state through the antenna, therefore the excitation energy transfer is a *coherent* process. Viceversa, if the intermolecular transitions time is larger than the vibrational relaxation time,  $T_V > T_g$ , the excitation remains localised and the excitation energy transfer is called *incoherent*. Related to these two concepts, we find the *third key quantum effect* in photosynthesis, for which nature has found the optimal balance between these two kinds of vibrations to guarantee the most efficient energy transfer during the photosynthetic process.

QUANTUM SECRETS OF PHOTOSYNTHESIS	
1) Excitons	Coulomb interactions between single chromophores lead to quantum superposition of excitations over the sites. The dipole moments of the brighter excitons couple stronger to the electromagnetic field, giving a higher probability of absorbing photons.
2) Excitons and vibrations	The interaction between electronic degrees of freedom and quasi-coherent vibrations (namely those spectrally narrow in frequency) generates energy transfer between excitons and can create quantum coherence between them.
3) Optimal balance	Nature has found the optimal balance between coherent and incoherent vibrational motions, which guarantees the most efficient energy transfer during photosynthesis.

Figure 1.4: *The table summarises the three quantum secrets involved in the photosynthetic process.*

Photosynthetic complexes exchange energy and information with their surrounding environments, which can have a very complex structure. Since these systems are formed by electronic excitations of pigments coupled to the surrounding chromophore molecules and proteins, they are characterised by many interacting degrees

of freedom. This kind of scenario falls under the definition of open quantum system. In addition, experimentally, it is possible to have access to all electronic and vibrational environments that determine excitation dynamics, but usually experiments probe certain degrees of freedom. For these reasons, the theoretical description of the energy transfer in biological systems is based on the open quantum systems approach. The specific tools needed, the various limits in each model and the way to treat the system, the bath and the interaction between them will be explained in the following section.

## 1.3 Open quantum system approach

### 1.3.1 Closed quantum systems

Quantum mechanics provides a mathematical framework capable of describing the microscopic nature of particles. It is based on some fundamental concepts, which are the starting points of the theory itself. First of all, every physical system is associated to a linear space called Hilbert space  $\mathcal{H}$ , where each state is represented by a ket  $|\psi\rangle$ , or, alternatively, by a density operator  $\rho = |\psi\rangle\langle\psi|$  [56]. Every observable is described by a Hermitian operator in the Hilbert space and the only possible results of a measurement are given by the (real) eigenvalues of this operator itself. When the system is in a specific state  $|\psi\rangle$ , the probability that the observable  $\mathcal{A}$  gives the eigenvalue  $a_n$  as a result is the inner product  $|\langle a_n|\psi\rangle|^2$ . If the measure of the observable  $\mathcal{A}$  on the state  $|\psi\rangle$  gives the eigenvalue  $a_n$ , the state of the system is the normalised eigenstate  $|a_n\rangle$ . Finally, the time evolution of a quantum system represented by the state  $|a_n\rangle$  is described by the Schrödinger equation [81]:

$$\frac{d}{dt} |\psi(t)\rangle = -\frac{i}{\hbar} [H(t), |\psi(t)\rangle], \quad (1.1)$$

where  $H(t)$  is the Hamiltonian of the system. Its solution is obtained in terms of a unitary evolution operator  $U(t, t_0)$ , which evolves the initial state  $|\psi(t_0)\rangle$  at time  $t_0$  to the final state  $|\psi(t)\rangle = U(t, t_0)|\psi(t_0)\rangle$  at time  $t$ . Putting this formal solution into the Schrödinger equation (1.1), an equation for the time evolution operator can be obtained as follows:

$$\frac{\partial}{\partial t} U(t, t_0) = -\frac{i}{\hbar} H(t)U(t, t_0), \quad (1.2)$$

with initial condition  $U(t, t_0) = I$ . Using these last two equations it is possible to show that  $U^\dagger(t, t_0)U(t, t_0) = U(t, t_0)U^\dagger(t, t_0) \equiv I$ , therefore  $U(t, t_0)$  is a unitary

operator. For an isolated system with a Hamiltonian that does not depend on time, the evolution operator is given by:

$$U(t, t_0) = e^{-\frac{i}{\hbar}H(t-t_0)}. \quad (1.3)$$

However, if the system is closed with a time-dependent Hamiltonian, its form changes in:

$$U(t, t_0) = T_{\leftarrow} e^{-\frac{i}{\hbar} \int_{t_0}^t ds H(s)}, \quad (1.4)$$

where  $T_{\leftarrow}$  indicates the chronological time-ordering operator for which the time arguments in time-dependent operators increase from right to left.

If the system under scrutiny is in a mixed state, it can be described by the density matrix  $\rho$ . Its dynamical evolution can be determined by the Schrödinger equation (1.1), starting from the initial condition:

$$\rho(t_0) = \sum_i \kappa_i |\psi_i(t_0)\rangle \langle \psi_i(t_0)|, \quad (1.5)$$

where  $\kappa_i$  are positive weights and  $|\psi_i(t_0)\rangle$  are normalised state vectors. At time  $t$ , the state of the system will be:

$$\begin{aligned} \rho(t) &= \sum_i \kappa_i U(t, t_0) |\psi_i(t_0)\rangle \langle \psi_i(t_0)| U^\dagger(t, t_0) \\ &= U(t, t_0) \rho(t_0) U^\dagger(t, t_0). \end{aligned} \quad (1.6)$$

Differentiating this equation with respect to time, it is possible to obtain the equation of motion for the density matrix:

$$\frac{d}{dt} \rho(t) = -\frac{i}{\hbar} [H(t), \rho(t)], \quad (1.7)$$

which is called *Liouville-von Neumann equation* and can be also written as

$$\frac{d}{dt} \rho(t) = \mathcal{L}\rho(t), \quad (1.8)$$

to stress the analogy with the equation of motion for probability density in classical statistics.  $\mathcal{L}$  is defined as Liouville super-operator since it acts on an operator ( $\rho(t)$ ) to give another operator ( $\mathcal{L} = -i[H(t), \cdot]$ ). Again, for an isolated system, the time evolution operator is given by:

$$\rho(t) = e^{\mathcal{L}(t-t_0)} \rho(t_0), \quad (1.9)$$

while for a closed system the density matrix has the form:

$$\rho(t) = T_{\leftarrow} e^{\int_{t_0}^t ds \mathcal{L}(s)} \rho(t_0). \quad (1.10)$$

In the Schrödinger picture, where the states evolve, the dynamics of the density matrix is characterised by the Liouville-von Neumann equation (1.8). The evolution can also be described through the evolution of the operators of the system, using in this case the Heisenberg representation. At the initial time  $t_0$ , the states coincide in both pictures, such that  $\rho(t_0) = \rho_H(t_0)$ . The operators at time  $t$ , instead, are related through the canonical transformation:

$$A_H(t) = U^\dagger(t, t_0)A(t)U(t, t_0), \quad (1.11)$$

where here the operator in Schrödinger picture explicitly depends on time. At the initial time  $t_0$ , the Schrödinger and Heisenberg pictures also coincide for the operators:  $A_H(t_0) = A(t_0)$ . The equivalence of the two pictures can be seen through the calculation of the expectation value of an observable:

$$\langle A(t) \rangle = \text{tr}\{A(t)\rho(t)\} = \text{tr}\{A_H(t)\rho_H(t_0)\}. \quad (1.12)$$

The equation of motion for an operator in Heisenberg picture can be obtained differentiating Eq.(1.11) with respect to time:

$$\frac{d}{dt}A_H(t) = \frac{\partial}{\partial t}A_H(t) + \frac{i}{\hbar}[H_H(t), A_H(t)], \quad (1.13)$$

where  $H_H(t) = U^\dagger(t, t_0)H(t)U(t, t_0)$  is the Hamiltonian in the Heisenberg picture. The partial derivative in Eq.(1.13) is given by  $\frac{\partial}{\partial t}A_H(t) = U^\dagger(t, t_0)\frac{\partial}{\partial t}A(t)U(t, t_0)$ . If  $\frac{dA_H(t)}{dt} = 0$ , then  $A_H$  is a constant of motion. An important special case is given when  $A = H$ : for an isolated system  $\frac{\partial}{\partial t}H(t) = 0$  and the time evolution operator has the form of Eq.(1.3), meaning that the Hamiltonian commutes with it. In this case the Heisenberg picture Hamiltonian is a constant of motion:  $\frac{d}{dt}H_H = 0$ .

In addition, if the operator in Schrödinger picture does not depend explicitly on time and the system is isolated, the equation of motion (1.13) becomes:

$$\frac{d}{dt}A_H(t) = \frac{i}{\hbar}[H_H(t), A_H(t)]. \quad (1.14)$$

### 1.3.2 Open quantum systems

An open system is a quantum system coupled to an environment: the interaction between them causes correlations leading to non-unitary system evolution. If the Hilbert space of the system is denoted by  $\mathcal{H}_S$  and that of the environment by  $\mathcal{H}_E$ , the total Hilbert space is given by the tensor product of the two  $\mathcal{H} = \mathcal{H}_S \otimes \mathcal{H}_E$ , while the total Hamiltonian is

$$H = H_S + H_E + H_{SE}, \quad (1.15)$$

where  $H_S$  is the Hamiltonian of the system only,  $H_E$  is the free environment Hamiltonian and  $H_{SE}$  characterises the interaction between them. An environment that has an infinite number of degrees of freedom (such that the frequencies of the modes form a continuum) is called reservoir. If the reservoir is in thermal equilibrium, it is called a bath.

It is possible to study the dynamics of the system only by tracing over the environment degrees freedom:

$$\rho_S(t) = \text{Tr}_E \{ \rho(t) \} \quad (1.16)$$

and the expectation values of observables acting on the system Hilbert space are given by

$$\langle A \rangle = \text{Tr}_S \{ A \rho_S \}. \quad (1.17)$$

The interaction with the environment affects the dynamics of the system, which, therefore, needs to be treated differently with respect to the case of a closed system.

### 1.3.3 Born-Markov master equation: weak coupling limit

Since in the rest of this thesis the bio-inspired systems will be analysed in the Markovian regime, it is useful to see which approximations lie behind this model. The most important condition is the weak coupling between the system and the reservoir and we are going to explain it with two different approaches.

The first is more formal and passes through the calculation of the eigenoperators of the interaction Hamiltonian. This calculation can be quite complicated for systems with many interactions, but it is worth going through the formalism because it shows very clearly at what stage and how the Markov approximation takes place in the evolution.

The second approach is more phenomenological and relies on the formalism of Kraus operators to write the master equation: this is the method we are going to use to describe our bio-inspired systems.

#### 1.3.3.1 Markov approximation with eigenoperators approach: the Redfield master equation

To understand in more detail the formal procedure to write the master equation for a system, it is necessary to focus on the Hamiltonian describing the whole system (in Eq.(1.15)). The starting point is the Schrödinger equation (1.7), that can be transformed into the interaction picture, separating the rapid motion generated by  $H_S + H_E$  from the slow motion generated by the interaction  $H_{SE}$  [81, 82]:

$$\frac{d}{dt} \tilde{\rho}_I(t) = -\frac{i}{\hbar} \left[ \tilde{H}_I, \tilde{\rho}_I(t) \right], \quad (1.18)$$

where  $\tilde{\rho}_I(t)$  is the density matrix of the whole system in the interaction picture, that takes the form  $\tilde{\rho}_I(t) = e^{(i/\hbar)(H_S+H_E)t} \rho(t) e^{-(i/\hbar)(H_S+H_E)t}$ , and  $\tilde{H}_I$  is given by  $\tilde{H}_I(t) = e^{(i/\hbar)(H_S+H_E)t} H_{SE} e^{-(i/\hbar)(H_S+H_E)t}$ . From now on, the tilde and the subscript in  $\tilde{\rho}_I$  will be omitted for sake of simplicity, therefore the integral form of the previous equation is:

$$\rho(t) = \rho(0) - \frac{i}{\hbar} \int_0^t ds [H_{SE}(s), \rho(s)]. \quad (1.19)$$

The next step is to assume that at the initial time  $t = 0$  there are no correlations between the system and the reservoir (the interaction has been switched on at that instant). This leads to the following factorised form for the total density matrix  $\rho(0) = \rho_S(0) \otimes \rho_E$ . The substitution of this expression in the commutator within the master equation and the trace over the reservoir degrees of freedom give:

$$\frac{d}{dt} \rho_S(t) = - \int_0^t ds \text{Tr}_E \left[ H_{SE}(t), [H_{SE}(s), \rho(s)] \right]. \quad (1.20)$$

Here, it has been assumed that  $\text{Tr}_E [H_{SE}(t), \rho(0)] = 0$ , which is guaranteed if the reservoir has zero mean in the state  $\rho_E$ : this can always be achieved by including the term  $\text{Tr}_E [H_{SE} \rho_E]$  in the system Hamiltonian.

Even if the total density matrix is factorised at time  $t = 0$ , this does not mean that at later times the interaction with the reservoir leaves this condition unchanged. However, the model relies on the condition of weak coupling, meaning that the reservoir is a very large system that is not affected by the coupling to the system, hence:

$$\rho(t) \approx \rho_S(t) \otimes \rho_E. \quad (1.21)$$

This is the first main approximation within this model which is called *Born approximation*. Substituting this expression in the equation above, an integro-differential equation for the reduced density matrix can be obtained:

$$\frac{d}{dt} \rho_S(t) = - \int_0^t ds \text{Tr}_E \left[ H_{SE}(t), [H_{SE}(s), \rho_S(s) \otimes \rho_E] \right]. \quad (1.22)$$

At this stage, the future behaviour of  $\rho(t)$  still depends on its past through the

integration over  $s$ . Here, the second main approximation within the weak coupling regime is performed: the *Markovian approximation* asserts that the future evolution of the system only depends on its present, therefore replacing  $\rho(s)$  with  $\rho(t)$  in the equation above, this condition is guaranteed:

$$\frac{d}{dt} \rho_S(t) = - \int_0^t ds \operatorname{Tr}_E \left[ H_{SE}(t), [H_{SE}(s), \rho_S(t) \otimes \rho_E] \right]. \quad (1.23)$$

This equation is called *Redfield equation*: it is local in time but the evolution of the reduced density matrix still depends on the choice of the initial state. To avoid this, the relaxation time scale  $\tau_r$  over which the state of the system changes significantly has to be very large in comparison to the time scale  $\tau_c$  over which the environment correlation functions decay ( $\tau_r \gg \tau_c$ ). This condition can mathematically be satisfied by letting the upper limit of the integral go to infinity and substituting  $s$  with  $t - s$  to obtain:

$$\begin{aligned} \frac{d}{dt} \rho_S(t) &= - \int_0^\infty ds \operatorname{Tr}_E \left[ H_{SE}(t), [H_{SE}(t-s), \rho_S(t) \otimes \rho_E] \right] \\ &= + \int_0^\infty ds \operatorname{Tr}_E \left\{ - H_{SE}(t) H_{SE}(t-s) \rho_S(t) \otimes \rho_E + H_{SE}(t-s) \rho_S(t) \otimes \rho_E H_{SE}(t) \right\} + h.c. \end{aligned} \quad (1.24)$$

At this point a further approximation needs to be made, the *rotating wave approximation*, in which the rapidly oscillating terms in the master equation can be neglected. To explain this, we write the Hamiltonian in the interaction picture in the general form:

$$H_{SE} = \sum_{\alpha} A_{\alpha} \otimes B_{\alpha}, \quad (1.25)$$

where  $A_{\alpha}^{\dagger} = A_{\alpha}$  and  $B_{\alpha}^{\dagger} = B_{\alpha}$ . The secular approximation mentioned above can be easily seen if the interaction Hamiltonian is decomposed into eigenoperators of the system Hamiltonian  $H_S$ . Indicating the eigenvalues of  $H_S$  with  $\epsilon$  and the projection on the eigenspace belonging to  $\epsilon$  with  $\mathbb{1}(\epsilon)$ , it is possible to decompose the operators as:

$$A_{\alpha}(\omega) = \sum_{\omega=\epsilon'-\epsilon} \mathbb{1}(\epsilon) A_{\alpha} \mathbb{1}(\epsilon'), \quad (1.26)$$

where the sum acts over all fixed energy difference  $\omega$  between two eigenvalues  $\epsilon$  and  $\epsilon'$ . As a consequence:

$$\begin{aligned} [H_S, A_{\alpha}(\omega)] &= -\omega A_{\alpha}(\omega) \\ [H_S, A_{\alpha}^{\dagger}(\omega)] &= +\omega A_{\alpha}^{\dagger}(\omega). \end{aligned} \quad (1.27)$$

Hence, the operators  $A_\alpha(\omega)$  and  $A_\alpha^\dagger(\omega)$  are called eigenoperators of  $H_S$  belonging to the frequencies  $\pm\omega$ , respectively. Using the completeness relation, the sum over all the energy differences gives  $\sum_\omega A_\alpha(\omega) = \sum_\omega A_\alpha^\dagger(\omega) = A_\alpha$ . Therefore, the interaction Hamiltonian (1.25) can be rewritten as:  $H_{SE} = \sum_{\alpha,\omega} A_\alpha(\omega) \otimes B_\alpha = \sum_{\alpha,\omega} A_\alpha^\dagger(\omega) \otimes B_\alpha^\dagger$ .

In turn, the interaction Hamiltonian in the interaction picture can be expressed as:

$$H_{SE}(t) = \sum_{\alpha,\omega} e^{-i\omega t} A_\alpha(\omega) \otimes B_\alpha(t) = \sum_{\alpha,\omega} e^{+i\omega t} A_\alpha^\dagger(\omega) \otimes B_\alpha^\dagger(t), \quad (1.28)$$

where  $B_\alpha(t) = e^{iH_E t} B_\alpha e^{-iH_E t}$  are the environment operators in the interaction picture. Replacing Eq.(1.28) in the master equation (1.24) and rearranging the terms, the following form can be obtained:

$$\frac{d}{dt} \rho_S(t) = \sum_{\omega,\omega'} \sum_{\alpha,\beta} e^{i(\omega'-\omega)t} \Gamma_{\alpha\beta}(\omega) \left( A_\beta(\omega) \rho_S(t) A_\alpha^\dagger(\omega') - A_\alpha^\dagger(\omega') A_\beta(\omega) \rho_S(t) \right) + h.c. \quad (1.29)$$

where  $h.c.$  indicates the Hermitian conjugate of the previous expression and

$$\Gamma_{\alpha\beta}(\omega) \equiv \int_0^\infty ds e^{i\omega s} \langle B_\alpha^\dagger(t) B_\beta(t-s) \rangle = \int_0^\infty ds e^{i\omega s} \text{Tr}_E \left\{ B_\alpha^\dagger(t) B_\beta(t-s) \rho_E \right\} \quad (1.30)$$

is the one-sided Fourier transform of the environment correlation functions. If the environment is in a stationary state  $\rho_E$ , then  $[H_E, \rho_E] = 0$ , which means the reservoir correlation functions do not depend explicitly on time, but only on the time difference:  $\langle B_\alpha^\dagger(t) B_\beta(t-s) \rangle = \langle B_\alpha^\dagger(s) B_\beta(0) \rangle$ . As already stated, the Markov approximation relies on the condition that the environment correlation functions decay faster than the system relaxation time ( $\tau_c \ll \tau_r$ ). This condition is verified only for a reservoir which has an infinite number of degrees of freedom and a continuum spectrum of frequencies (if the spectrum is discrete, the correlation functions are quasi-periodic). At this stage, it is possible to introduce the rotating wave approximation. Let us denote by  $\tau_S$  the time scale of the intrinsic evolution of the system, which is of the order of the inverse of the energy differences involved. If this time is smaller than the relaxation time, that is  $\tau_S \sim \frac{1}{|\omega'-\omega|} \ll \tau_r$ , then terms for which  $\omega \neq \omega'$  oscillate very rapidly during the time  $\tau_r$  over which the system varies ap-

preciably. This implies that only terms with  $\omega = \omega'$  survive in the master equation (1.29): this condition is satisfied for optical quantum systems. Therefore we obtain:

$$\frac{d}{dt} \rho_S(t) = \sum_{\omega} \sum_{\alpha, \beta} \Gamma_{\alpha\beta}(\omega) \left( A_{\beta}(\omega) \rho_S(t) A_{\alpha}^{\dagger}(\omega) - A_{\alpha}^{\dagger}(\omega) A_{\beta}(\omega) \rho_S(t) \right) + h.c. \quad (1.31)$$

At this point, some calculations have to be performed, introducing a decomposition for the Fourier transform of the reservoir correlation functions and also adding and subtracting certain quantities. This allows to rewrite the expression above as:

$$\frac{d}{dt} \rho_S(t) = -i [H_{LS}, \rho_S(t)] + \mathcal{D}(\rho_S(t)), \quad (1.32)$$

where the following definition has been used

$$H_{LS} = \sum_{\omega} \sum_{\alpha, \beta} S_{\alpha\beta}(\omega) A_{\alpha}^{\dagger}(\omega) A_{\beta}(\omega), \quad (1.33)$$

with  $S_{\alpha\beta}(\omega) = \frac{1}{2i} (\Gamma_{\alpha\beta}(\omega) - \Gamma_{\beta\alpha}^*(\omega))$ . The Hermitian operator  $H_{LS}$  is often called the Lamb-shift Hamiltonian, as it gives a renormalization of the unperturbed system energies caused by the coupling to the reservoir. It also commutes with the unperturbed Hamiltonian,  $[H_S, H_{LS}] = 0$ . The second term in Eq.(1.32) reads as:

$$\mathcal{D}(\rho_S(t)) = \sum_{\omega} \sum_{\alpha, \beta} \gamma_{\alpha\beta}(\omega) \left( A_{\beta}(\omega) \rho_S(t) A_{\alpha}^{\dagger}(\omega) - \frac{1}{2} \{ A_{\alpha}^{\dagger}(\omega) A_{\beta}(\omega), \rho_S(t) \} \right), \quad (1.34)$$

with  $\gamma_{\alpha\beta}(\omega) = \Gamma_{\alpha\beta}(\omega) + \Gamma_{\beta\alpha}^*(\omega) = \int_{-\infty}^{\infty} ds e^{i\omega s} \langle B_{\alpha}^{\dagger}(s) B_{\beta}(0) \rangle$ . With these definitions, Eq.(1.32) is the master equation in the interaction picture describing a system weakly coupled to a reservoir, under the specific approximations explained above and calculating explicitly the eigenoperators of the Hamiltonian.

### 1.3.3.2 Markov approximation with Kraus operators approach: the Linblad master equation

A different approach to obtain a phenomenological master equation relies on the formalism of Kraus operators [83]. The purpose is to write a master equation with time-independent coefficients for the density matrix of the system.

First of all, any superoperator in quantum mechanics can be written in the form:

$$\mathcal{L}_{\delta t}[\rho] = \sum_{\mu} K_{\mu}(\delta t) \rho K_{\mu}^{\dagger}(\delta t), \quad (1.35)$$

where  $\delta t$  is the infinitesimal time interval and  $K_\mu$  are linear operators, such that  $\sum_\mu K_\mu K_\mu^\dagger = \mathbb{1}$ . Eq.(1.35) is called *Kraus representation*. To write the master equation, the idea is to express the transformation from  $\rho_S(t)$  to  $\rho_S(t + \delta t)$  as a Kraus sum. If at time  $t$  the environment is in a steady state  $\rho_E$  and the state of the whole system is separable  $\rho(t) \approx \rho_S(t) \otimes \rho_E$  (as in Eq.(1.21)), then the Kraus formalism can be applied to obtain the density matrix of the system at time  $t + \delta t$ :

$$\rho_S(t + \delta t) = \mathcal{L}_{\delta t}[\rho_S(t)] = \sum_\mu K_\mu(\delta t) \rho_S(t) K_\mu^\dagger(\delta t), \quad (1.36)$$

where the Kraus operators  $K_\mu$  depend on time  $\delta t$ , on the interaction between the system and the environment and on the state of the environment  $\rho_E$ . This expression leads to the master equation we are looking for. However, before proceeding, it is important to notice that a significant physical assumption has been made in Eq.(1.21), since two physical processes have been neglected. One of them is related to the environment: at time  $t$  its state is subjected to a fluctuation  $\delta\rho_E(t)$  around its steady state, because of the previous interaction with the system S. Secondly, such interaction also implies that system and environment can be in an entangled state, which manifests in an additional term  $\delta\rho_{SE}(t)$  in the total density matrix. This means that the exact form of Eq.(1.21) would be:

$$\rho(t) = \rho_S(t) \otimes [\rho_E + \delta\rho_E(t)] + \delta\rho_{SE}(t). \quad (1.37)$$

However, this exact expression carries some issues. First of all, the presence of correlations between the system and the environment would make difficult to link linearly  $\rho_S(t)$  and  $\rho_S(t + \delta t)$ . In addition, even if this was possible, the Kraus operators  $K_\mu$  would depend on time  $t$ , due to the fluctuating initial state of the environment, and this would lead to time-dependent coefficients in the master equation.

However, the *Markovian approximation* helps solve these problems. In fact, if the environment is big enough, the system S evolves over the finite time interval  $\delta t$  as if it was not entangled with the environment, allowing a description of the total density matrix as given in Eq.(1.21). When the environment is very large, its levels span a wide range of energy  $\Delta\omega$ . As a consequence, the correlation time of its observable is very short, being of the order of  $\tau_c = \hbar/\Delta\omega$ . For time intervals smaller than  $\tau_c$ , the observables of the environment remain constant, and the system and

the environment undergo a coherent evolution. During the next time interval  $\tau_c$ , the phase relations between them are lost and a new coherent evolution starts again. This implies that the environment fluctuation  $\delta\rho_E$  and the correlations between the system and the environment  $\delta\rho_{SE}$  have a very short correlation time, of the order of  $\tau_c$ . Therefore, products of two matrix elements of these quantities, taken at times differing by more than  $\tau_c$ , vanish on average.

Based on the previous discussion, it is possible to estimate the time scale  $\tau_r$  of the evolution of the system S. Every step in the evolution of  $\rho_S$  has duration  $\tau_c$  and each element in it undergoes a quantum phase variation of  $g\tau_c/\hbar$ , being  $g$  the coupling between the system and the environment, with order of magnitude of  $H_{SE}$ . After a time  $t$ , namely after a number of  $t/\tau_c$  steps, and considering that steps corresponding to successive  $\tau_c$  intervals add quadratically, the quantum phase accumulated is:

$$[\Delta\Phi(t)]^2 = \left(\frac{g\tau_c}{\hbar}\right)^2 \frac{t}{\tau_c} = \frac{t}{\tau_r}, \quad (1.38)$$

where the evolution time scale  $\tau_r$  is defined as:

$$\tau_r = \left(\frac{\hbar}{g\tau_c}\right)^2 \tau_c. \quad (1.39)$$

The Markov condition of an environment that does not have memory of its past is:  $\tau_c \ll \tau_r$  meaning that  $g\tau_c/\hbar \ll 1$ . Choosing a time  $\delta t$  such that  $\tau_c \ll \delta t \ll \tau_r$ , the value of  $\rho_S(t + \delta t)$  does not change significantly with respect to  $\rho_S(t)$ , if the reservoir fluctuations and correlations between the system and the environment are neglected. Therefore, under Markovian approximation, Eq.(1.37) can be replaced by Eq.(1.21).

At this point it is easier to go back to the goal of this formulation: to find a phenomenological expression of the master equation. Using Eq.(1.36), the derivative of the density matrix of the system can be written as:

$$\frac{d\rho_S(t)}{dt} = \frac{\mathcal{L}_{\delta t}[\rho_S(t)] - \rho_S(t)}{\delta t}. \quad (1.40)$$

Since  $\mathcal{L}_{\delta t}[\rho_S(t)] = \rho_S(t + \delta t) = \rho_S(t) + O(\delta t)$  is a first order contribution in  $\delta t$ , it is reasonable to say that one of the Kraus operators should be of the order of unity, that is:

$$K_0 = \mathbb{1} - iA\delta t + O(\tau^2), \quad (1.41)$$

where  $A$  is an operator independent on time that can be defined as:

$$A = \frac{H}{\hbar} - iJ. \quad (1.42)$$

The Hermitian and anti-Hermitian operators of  $A$  have been divided in the two Hermitian operators

$$H = \hbar \frac{A + A^\dagger}{2}, \quad J = i \frac{A - A^\dagger}{2}. \quad (1.43)$$

Substituting Eq.(1.42) into the first order in  $\delta t$ , we obtain:

$$K_0(\delta t) \rho_S K_0^\dagger(\delta t) = \rho_S - \frac{i}{\hbar} \delta t [H, \rho_S] - \delta t (J \rho_S + \rho_S J). \quad (1.44)$$

In the right-hand side, it can be noticed a commutator with a Hamiltonian-like term  $H$ , which describes a unitary evolution of the system  $\rho_S$ . This term is the sum of the free Hamiltonian  $H_S$  and the energy shift contributions induced by relaxation, due to the coupling of the system with the environment. They describe a renormalization of the energy levels of the system and are assumed included in the “naked” energy levels, therefore  $H$  in Eq.(1.44) can be replaced by  $H_S$ .

The other terms in Kraus sum are of the order of  $\delta t$ , hence:

$$K_\mu(\delta t) = \sqrt{\delta t} L_\mu. \quad (1.45)$$

The normalisation condition on Kraus operators requires  $\sum_\mu K_\mu^\dagger(\delta t) K_\mu(\delta t) = \mathbb{1} - 2J\delta t + \sum_{\mu \neq 0} \delta t L_\mu^\dagger L_\mu = \mathbb{1}$ , from which it is possible to define  $J$  as:

$$J = \frac{1}{2} \sum_{\mu \neq 0} L_\mu^\dagger L_\mu. \quad (1.46)$$

Reorganising all terms, the *Lindblad master equation* can be obtained in the form:

$$\frac{d\rho_S(t)}{dt} = -\frac{i}{\hbar} [H_S, \rho_S] + \sum_{\mu \neq 0} \left( L_\mu \rho_S L_\mu^\dagger - \frac{1}{2} L_\mu^\dagger L_\mu \rho_S - \frac{1}{2} \rho_S L_\mu^\dagger L_\mu \right), \quad (1.47)$$

where  $L_\mu$  are called *jump operators* and represent processes due to the interaction with the environment. This derivation of the master equation is based only on the

assumptions that the evolution of the system occurs under Markovian approximation and that it is described through the Kraus sum formulation.

For completeness, it can be noticed that, as for closed systems, also for open quantum systems it is possible to define an operator in the Heisenberg picture for each operator in the Schrödinger picture. In the limit of Markovian approximation, this leads to the following equation:

$$\frac{d}{dt} A_H(t) = V^\dagger(t, 0) \{ \mathcal{L}^\dagger(t) A \}, \quad (1.48)$$

which is called *adjoint master equation*. If the generator  $\mathcal{L}^\dagger$  does not depend explicitly on time, it commutes with  $V^\dagger(t, 0)$ , therefore the equation above takes the following simpler form:

$$\begin{aligned} \frac{d}{dt} A_H(t) &= \{ \mathcal{L}^\dagger(t) A \} \\ &= -\frac{i}{\hbar} [H, A_H(t)] + \sum_k \gamma_k \left( A_k A_H(t) A_k^\dagger - \frac{1}{2} A_k^\dagger A_k A_H(t) - \frac{1}{2} A_H(t) A_k^\dagger A_k \right). \end{aligned} \quad (1.49)$$

In conclusion, a phenomenological master equation in the form of Eq.(1.47) is expressed in terms of operators acting on the system and related to the quantum jumps it could undergo. It is not based on a rigorous derivation (as it happens in the formalism described in the previous section), but represents a deductive approach, which relies on physical guesses to write down the form of the operators. Although the Linblad master equation is able to reproduce the correct dynamics observed in experiments and it is independent on the nature of the environment, it does not predict the values of the damping rates in the decoherent term of the master equation, as it happens instead in the Redfield master equation.

This procedure to write the master equation is often used in the study of energy transfer in photosynthetic systems: this is precisely the approach we are going to use to describe our bio-inspired toy models. In particular, we assume that the jump operators have a general form  $L_\mu = \sqrt{\gamma_{c_\mu}} c_\mu$ , where  $\gamma_{c_\mu}$  is the rate at which a specific process occurs, and  $c_\mu$  is the operator involved in that process. Therefore, in the next chapters we will rewrite Eq.(1.47) as:

$$\frac{d\rho_S(t)}{dt} = -\frac{i}{\hbar} [H_S, \rho_S] + \sum_{\mu \neq 0} \frac{\gamma_{c_\mu}}{2} \mathcal{L}_{c_\mu}(\rho_S), \quad (1.50)$$

where:

$$\mathcal{L}_{c_\mu}(\rho_S) = 2c_\mu\rho_S c_\mu^\dagger - c_\mu^\dagger c_\mu \rho_S - \rho_S c_\mu^\dagger c_\mu. \quad (1.51)$$

For sake of completeness, we highlight that the analysis in the following chapter was carried out also using the Redfield master equation. However, since the results were analogous to those obtained with the Lindblad master equation, we reported only the latter and performed the other calculations choosing the phenomenological approach.

### 1.3.4 Lindblad dynamics represented by a matrix-vector notation

To numerically solve the Markovian master equation, the dynamics is represented in a matrix-vector notation [84]. This is equivalent to describing the dynamics of the system through a differential equation of the form

$$\frac{d\vec{r}_s}{dt} = L\vec{r}_s, \quad (1.52)$$

with  $L$  a matrix and  $\vec{r}_s$  the vector representing the state of the system. (For sake of simplicity the symbol of vector will be omitted in the following.)

If the density matrix of the system  $\rho_S$  is a  $n \times n$  matrix, the Hilbert space is built starting from the scalar product  $\rho_1 \cdot \rho_2 = \text{Tr}\{\rho_1^\dagger \rho_2\}$ . Within the vec-ing method, the  $n \times n$  matrix  $\rho$  is flattened in a  $n^2$  vector and the super-operator  $\mathcal{L}$  is a  $n^2 \times n^2$  matrix. This can be done by putting the columns of the matrix  $\rho$  one below the other, hence the element in position  $(a, b)$  in the matrix goes in position  $(b-1)n + a$  in the vector representation. To find the right representation for the super-operator  $\mathcal{L}$ , it is necessary to remember that:

- A left multiplication of the density matrix  $\rho$  by a  $n \times n$  matrix  $A$ , that is  $A\rho$ , can be obtained multiplying the vector  $\vec{r}$  by the  $n^2 \times n^2$  matrix  $\mathbb{1} \otimes A$ , where  $\mathbb{1}$  is the  $n \times n$  identity matrix.
- In a similar way, a right multiplication of the matrix  $\rho$  by an  $n \times n$  matrix  $B$ , namely  $\rho B$ , is equivalent to multiplying the vector  $\vec{r}$  by the  $n^2 \times n^2$  matrix  $B^T \otimes \mathbb{1}$ , where T indicates the transpose of the matrix.
- Finally, a simultaneous multiplication on the left and right side, i.e.  $A\rho B$ , is performed multiplying the vector  $\vec{r}$  by the  $n^2 \times n^2$  matrix  $B^T \otimes A$ .

Hence, numerically, the general form of the Lindblad master equation (1.47) can be written as follows. The commutator takes the form:

$$[H, \rho] \rightarrow (\mathbb{1} \otimes H - H^T \otimes \mathbb{1}) \vec{r}, \quad (1.53)$$

while the dissipator becomes:

$$\begin{aligned} c_\mu \rho c_\mu^\dagger &\rightarrow \left( (c_\mu^\dagger)^T \otimes c_\mu \right) \vec{r} \\ c_\mu^\dagger c_\mu \rho &\rightarrow \left( \mathbb{1} \otimes c_\mu^\dagger c_\mu \right) \vec{r} \\ \rho c_\mu^\dagger c_\mu &\rightarrow \left( (c_\mu^\dagger c_\mu)^T \otimes \mathbb{1} \right) \vec{r}. \end{aligned} \quad (1.54)$$

This means that the form for  $L$  in Eq.(1.52) is given by:

$$L = \mathbb{1} \otimes H - H^T \otimes \mathbb{1} + \sum_i \gamma_i \left( (c_\mu^\dagger)^T \otimes c_\mu - \frac{1}{2} \left( \mathbb{1} \otimes c_\mu^\dagger c_\mu + (c_\mu^\dagger c_\mu)^T \otimes \mathbb{1} \right) \right). \quad (1.55)$$

## 1.4 Hamiltonian of bio-inspired light harvesting systems

We have described light-harvesting systems and the open systems formalism required to treat them properly. At this point the attention will be focused onto the detailed description of the Hamiltonian characterising the bio-inspired light harvesting systems of interest, with particular emphasis on the specific models used in this thesis.

As already mentioned, a light harvesting antenna is formed of chromophores interacting between them and bound to proteins. Every chromophore molecule is formed of electrons and nuclei, the latter being represented as a collection of quantised harmonic oscillators given their slow vibrational motion. The Hamiltonian describing such system comprising  $N$  chromophores is given by [85]:

$$\begin{aligned} H = \sum_{k=1}^N &\left[ \frac{1}{2} \omega_k^2 x_k^2 |G\rangle\langle G| + \left( U_k + \frac{1}{2} \omega_k^2 (x_k - q_k)^2 \right) |k\rangle\langle k| + \frac{1}{2} \hat{p}_k^2 \right] \\ &+ \frac{1}{2} \sum_{k,k'=1}^N V_{kk'} (|k\rangle\langle k'| + |k'\rangle\langle k|), \end{aligned} \quad (1.56)$$

Here, it has been assumed that ground and excited states are described by the

same normal mode coordinates  $x_k$  [80]. In Eq.(1.56)  $\omega_k$  represents the frequency of mode  $k$ ,  $x_k$  is the position operator of the same mode and  $q_k$  indicates the shift in its equilibrium position due to the electronic excited state  $|k\rangle$ .  $U_k$  is the bare energy of the electronic state  $k$  at the equilibrium position ( $x_k = q_k$ ), while  $p_k$  is the momentum operator of mode  $k$ . As already explained in Sec.(1.2.3.1), the simplest way to treat electronic excitations in biological systems is to model them as two-level systems, therefore  $|k\rangle$  represents the state with chromophore  $k$  in the excited state and the others in the ground. Finally,  $V_{kk'}$  is the electronic coupling between the two chromophores  $k$  and  $k'$  (assuming a locally balanced charge distribution in each of them,  $V_{kk} = 0$ ), which will be explained in more detail in Sec.1.4.1.

It is important to underline that in the description given by Eq.(1.56) every site is locally coupled only to one high-energy, localized vibrational mode. This quasi-resonant mode (intramolecular vibration) gives the most relevant contribution to the coherent dynamics of the system. All the other low-frequency modes, representing the vibrational environment of the protein and solvent, are far from the condition of resonance with the electronic degrees of freedom and for this reason can be treated phenomenologically, using the Linblad formulation presented in Sec.1.3.3.2, within the Markovian regime, as explained in Secs.1.3.3.2 and 2.6.

Rearranging the terms, it is possible to rewrite Eq.(1.56) as sum of three parts (electronic, vibrational and interaction Hamiltonian):

$$H = H_{\text{el}} + H_{\text{vib}} + H_{\text{el-vib}}, \quad (1.57)$$

where

$$H_{\text{el}} = \sum_{k=1}^N \left[ \frac{1}{2} \omega_k^2 x_k^2 |G\rangle\langle G| + \left( U_k + \frac{1}{2} \omega_k^2 q_k^2 \right) |k\rangle\langle k| \right] + \frac{1}{2} \sum_{k,k'=1}^N \sum_{k \neq k'} V_{kk'} (|k\rangle\langle k'| + |k'\rangle\langle k|) \quad (1.58)$$

$$H_{\text{vib}} = \sum_{k=1}^N \left( \frac{1}{2} \hat{p}_k^2 + \frac{1}{2} \omega_k^2 \hat{x}_k^2 \right) \quad (1.59)$$

$$H_{\text{el-vib}} = - \sum_{k=1}^N \omega_k^2 x_k q_k |k\rangle\langle k|. \quad (1.60)$$

At this point, we focus the attention on each contribution separately in order to arrive at the final expression used in the rest of the thesis.

### 1.4.1 Electronic Hamiltonian

In Eq.(1.58) it is possible to define the reorganisation energy  $\lambda_k = \frac{1}{2} \omega_k^2 q_k^2 = \omega_k S_k$ , where  $S_k$  represents the Huang-Rhys factor. It is related to the Stokes shift and can be measured experimentally by comparing the peak shift between absorption and fluorescence spectra [80]. The reorganisation energy  $\lambda_k$  represents the contribution of mode  $k$  to the site energy  $k$ , that will be indicated with  $\alpha_k = U_k + \lambda_k$ .

It is important to point out that when the vibrational modes have all the same frequency  $\omega_k$  and the displacements of the equilibrium position  $q_k$  are identical for each chromophore, the reorganisation energy gives the same contribution to each site. This means that it only shifts the site energies by the same amount, thus having no effect on the dynamics. This is the case we will consider in the models used in our work, therefore the contribution of the reorganisation energy to each site will be neglected and  $\alpha_k = U_k$  will correspond to the bare energy of the electronic states only.

Substituting the expression above in the Hamiltonian in Eq.(1.58), one obtains [80, 86]:

$$H_{\text{el}} = \alpha_0 |G\rangle\langle G| + \sum_{k=1}^N \alpha_k |k\rangle\langle k| + \frac{1}{2} \sum_{k,k'=1}^N V_{kk'} (|k\rangle\langle k'| + |k'\rangle\langle k|), \quad (1.61)$$

where  $\alpha_0 = \sum_{k=1}^N \frac{1}{2} \omega_k^2 x_k^2$  has been defined as the electronic aggregate ground state energy and  $\mathbb{1}$  is the unity matrix. The energies of the sites  $\alpha_k$  and the strength of the interaction  $V_{kk'}$  depend on the pigment structure and on the charge distribution.

The Coulomb interaction between the sites is given by:

$$V_{kk'} = k_e \iint d\mathbf{r} d\mathbf{r}' \frac{\rho_k(\mathbf{r}_k) \rho_{k'}(\mathbf{r}_{k'})}{|\mathbf{r}_k - \mathbf{r}_{k'}|}, \quad (1.62)$$

where  $k_e = \frac{1}{4\pi\epsilon_0}$  is the Coulomb constant (with  $\epsilon_0$  the vacuum permittivity), and  $\rho_k(\mathbf{r}_k)$  and  $\rho_{k'}(\mathbf{r}_{k'})$  are the charge distributions of molecules  $k$  and  $k'$ , respectively. This charge density indicates the amount of unbalanced charge distribution in the neutral molecule, due to the continuous spatial distribution of the negative electron charge and the localized positive charge of the nuclei [80]. The Coulomb interaction can be expressed in terms of the multiple moments of the respective charge distributions [86]. In the dipole-dipole approximation and in the case of uncharged molecules, the interaction has the following form:

$$V_{kk'}^{\text{dip}} = \frac{\mathbf{D}_k \cdot \mathbf{D}'_k - 3(\mathbf{D}_k \cdot \hat{\mathbf{r}}_{kk'})(\mathbf{D}'_k \cdot \hat{\mathbf{r}}_{kk'})}{|\mathbf{r}_{kk'}|^3}, \quad (1.63)$$

where  $\mathbf{r}_{kk'} = \mathbf{r}_k - \mathbf{r}_{k'}$  is the distance between the two molecules,  $\hat{\mathbf{r}}_{kk'}$  is the corresponding unit vector and  $\mathbf{D}_k$  is the dipole moment:

$$\mathbf{D}_k = \int d\mathbf{r} (\mathbf{r} - \mathbf{r}_k) \rho_k(\mathbf{r}). \quad (1.64)$$

The dipole-dipole interaction is reasonable when the intermolecular distance  $r$  is larger than the size of the molecule, but also when  $r$  is larger than the dipole radius  $a$  (which is of the order of a few angstroms). As a consequence, in many cases, the dipole-dipole coupling term determines spectroscopic and excitation energy transfer properties. Higher order terms fall off more rapidly with distance, hence they are negligible.

On the whole, intermolecular interactions cause very significant changes in the energy spectra, by affecting exciton formation. Excitons, quantum superpositions of excitations that are coherently delocalised over sites, are used to explain energy transfer through the molecular system. These are the eigenstates of Hamiltonian in Eq.(1.61) and can be expressed as a superposition of the sites:

$$|X_i\rangle = \sum_k c_k^i |k\rangle, \quad (1.65)$$

where  $c_k^i$  indicates the amplitude probability of exciton  $i$  over site  $k$ . This can significantly change the electronic excitation spectrum of molecular aggregates with respect to the spectrum of an isolated molecule [86], creating new absorption bands and affecting also the energy transfer dynamics. Indeed, the induced dipole moment of the transitions is accordingly redistributed as:

$$\mu_{X_i} = \sum_k c_k^i \mu_k. \quad (1.66)$$

In normal light conditions, the absorption of sunlight corresponds to a low flux of photons, hence it is possible to consider only one excitation over the chromophores at any time [76].

In terms of the localized states, the Hamiltonian for a dimer is given by Eq.(1.61) with  $N = 2$ . Rearranging some terms and assuming the ground state energy of the aggregate equal to zero ( $\alpha_0 = 0$ ), it can be rewritten as:

$$H_{\text{el}} = \alpha M + \frac{\Delta\alpha}{2} \sigma_z + V \sigma_x, \quad (1.67)$$

where  $\alpha = (\alpha_1 + \alpha_2)/2$  is the mean energy of the sites, and  $\Delta\alpha = \alpha_1 - \alpha_2$  is the energy difference between the excited electronic states, assuming that site 1 has the highest energy. In addition,  $M = |1\rangle\langle 1| + |2\rangle\langle 2|$ ,  $\sigma_z = |1\rangle\langle 1| - |2\rangle\langle 2|$  and  $\sigma_x = |1\rangle\langle 2| + |2\rangle\langle 1|$ . Let us indicate the eigenstates of  $H_{\text{el}}$  in Eq.(1.67) with  $|X_1\rangle$  and  $|X_2\rangle$  and their corresponding eigenvalues with  $E_1$  and  $E_2$  (with  $E_1 > E_2$ ). As a result, the Hamiltonian in the exciton basis and its eigenvalues take the form:

$$H_{\text{exc}} = E\tilde{M} + \sum_{k=1}^2 E_k |X_k\rangle\langle X_k| \quad (1.68)$$

$$E_{1,2} = \pm V \sqrt{1 + \frac{\Delta\alpha^2}{4V^2}},$$

where  $E = (E_1 + E_2)/2$  is the average energy and  $\tilde{M} = |X_1\rangle\langle X_1| + |X_2\rangle\langle X_2|$ . Here, the ground state  $|G\rangle$  has been explicitly introduced in the electronic basis  $\{|G\rangle, |X_2\rangle, |X_1\rangle\}$ , with energy set to zero. The excitons  $|X_2\rangle$  and  $|X_1\rangle$  are symmetric and anti-symmetric linear combinations of the localized excited states:

$$\begin{pmatrix} |X_2\rangle \\ |X_1\rangle \end{pmatrix} = U \begin{pmatrix} |2\rangle \\ |1\rangle \end{pmatrix} \quad \text{with} \quad U = \begin{pmatrix} \cos\theta & \sin\theta \\ -\sin\theta & \cos\theta \end{pmatrix}, \quad (1.69)$$

where  $U$  is the unitary matrix that diagonalises the electronic Hamiltonian. The angle  $\theta$  is called ‘‘mixing angle’’ and is such that

$$\tan(2\theta) = \frac{2V}{\Delta\alpha} \implies \theta = \frac{1}{2} \arctan\left(\frac{2|V|}{\Delta\alpha}\right) \quad \text{with } 0 < \theta < \frac{\pi}{4}. \quad (1.70)$$

Therefore the exciton Hamiltonian assumes the form:

$$H_{\text{exc}} = E\tilde{M} + \frac{\Delta E}{2} \tilde{\sigma}_z, \quad (1.71)$$

where  $\tilde{\sigma}_z$  indicates that we are in the exciton basis, with  $\tilde{\sigma}_z = |X_1\rangle\langle X_1| - |X_2\rangle\langle X_2|$  and  $\Delta E = \sqrt{\Delta\alpha^2 + 4V^2}$  the energy difference between the eigenstates of the electronic Hamiltonian.

These concepts represent the formal explanation of the *first key quantum effect* in photosynthesis from Sec.1.2.3.

## 1.4.2 Vibrational Hamiltonian

We now focus our attention on Eq.(1.59). The position and momentum operators can be expressed in terms of creation and annihilation operators by using the following expressions:

$$\begin{aligned}\hat{x} &= \sqrt{\frac{\hbar}{2m\omega}} (\hat{d}^\dagger + \hat{d}), \\ \hat{p} &= i\sqrt{\frac{\hbar m\omega}{2}} (\hat{d}^\dagger - \hat{d}).\end{aligned}\tag{1.72}$$

Substituting in Eq.(1.59) and using the coordinate-momentum commutator identities, it is possible to rewrite the vibrational Hamiltonian as:

$$H_{\text{vib}} = \sum_{k=1}^N \omega_k \left( \hat{d}_k^\dagger \hat{d}_k + \frac{1}{2} \right),\tag{1.73}$$

in which  $\hbar = m = 1$ . The normal modes (phonons) represent the quantized vibrational motions of the chromophores themselves.

In presence of only two modes ( $N = 2$ ) with the same frequency  $\omega_1 = \omega_2 = \omega_{\text{vib}}$ , each coupled to one site, and neglecting the zero point energy, the equation above reads as:

$$H_{\text{vib}} = \omega_{\text{vib}}(d_1^\dagger d_1 + d_2^\dagger d_2).\tag{1.74}$$

where the symbol of operator has been omitted for sake of simplicity. In this case, it is possible to introduce the collective mode coordinates defined as

$$\begin{aligned}D_-^{(\dagger)} &= \frac{1}{\sqrt{2}} (d_1^{(\dagger)} - d_2^{(\dagger)}), \\ D_+^{(\dagger)} &= \frac{1}{\sqrt{2}} (d_1^{(\dagger)} + d_2^{(\dagger)}).\end{aligned}\tag{1.75}$$

They correspond to the relative displacement coordinates and to the mode centre of mass, respectively [22,80]. Neglecting the zero point energy, Eq.(1.73) can be rewritten as  $H_{\text{vib}} = \omega_{\text{vib}}(D_+^\dagger D_+ + D_-^\dagger D_-)$ . However, only the relative displacement mode  $D_-^{(\dagger)}$  couples to the excitonic system and, therefore, is relevant for the dynamics, leaving the vibrational Hamiltonian in the form:

$$H_{\text{vib}} = \omega_{\text{vib}} D_-^\dagger D_-.\tag{1.76}$$

The form of this Hamiltonian in the exciton basis does not change, since the matrix  $U$  in Eq.(1.69) does not affect it.

### 1.4.3 Interaction Hamiltonian

Finally, we focus the attention on the interaction Hamiltonian. As explained in Sec.1.2.3, the third key quantum effect in photosynthesis is related to the most relevant source of exciton localisation, which is the interaction between electronic degrees of freedom and vibrational modes. The excitons can be delocalised over several sites, thanks to the Coulomb interaction between them. In opposition, the coupling to the vibrational degrees of freedom tends to destroy phase relations between the electronic excitations over different chromophores and leads to more localised excitons over the sites.

The Hamiltonian describing this coupling between the electronic and vibrational parts (assuming  $\hbar = 1$ ) is given in Eq.(1.60). Replacing the expression for the position operator in Eq.(1.72), it becomes:

$$H_{\text{el-vib}} = \sum_{k=1}^N g_k |k\rangle\langle k| (d_k^\dagger + d_k), \quad (1.77)$$

where  $g_k = -\omega_k \sqrt{S_k} = -\sqrt{\omega_k \lambda_k}$  is the linear coupling strength between the excitation at site  $k$  and its phonon mode, which depends on the reorganisation energy. This interaction generates the so called “dynamic disorder” and causes a dynamical modulation of the electronic transition energies, shifting them in and out of equilibrium.

As already mentioned in Sec.1.2.3.3, the presence of the environment can have a twofold impact on the excitons, due to the nature of the vibrational motions. In fact, when the transitions time between the molecules is smaller than the intramolecular relaxation time,  $T_V < T_g$ , the electronic interactions are stronger than the coupling to the vibrational environment, namely  $V \gg \lambda$ . In this case *coherent* electronic energy transfer takes place and the excitation moves as a delocalised state through the aggregate. This implies that in thermal equilibrium the system is in a statistical mixture of electronic eigenstates: this regime is described by the Redfield model [87]. On the other hand, in the limit of weak electronic coupling,  $V \ll \lambda$ , the intermolecular transitions time is larger than the vibrational relaxation time,  $T_V > T_g$ . This condition induces *incoherent* electronic energy transfer and the excitonic states that diagonalise the density matrix in the steady state (vibronic states) are

more localised than the electronic eigenstates (the excitons). Such situation leads to the formation of polaritons, electronic states dressed by phonon modes. In thermal equilibrium, single sites are populated according to a Boltzmann distribution: this regime is described by the Forster theory [88].

All these arguments are related to the *second and third quantum key effects* in photosynthesis mentioned before.

In the simplest case of two sites with identical coupling to the modes (each coupled to one site), the interaction Hamiltonian is written as:

$$H_{\text{el-vib}} = \sum_{k=1}^2 g |k\rangle\langle k| (d_k^\dagger + d_k), \quad (1.78)$$

which, within the collective mode formulation, becomes:

$$H_{\text{el-vib}} = \frac{1}{\sqrt{2}} g \sigma_z (D_-^\dagger + D_-). \quad (1.79)$$

Here, the coupling related to the centre of mass term has been neglected, since it does not affect the dynamics of the system.

On the basis of the previous considerations, it is possible to use the unitary matrix  $U$  in Eq.(1.69) to obtain the interaction Hamiltonian in the exciton basis:

$$H_{\text{el-vib}}^{(e)} = U^\dagger H_{\text{el-vib}} U = \frac{1}{\sqrt{2}} g \left( \cos(2\theta) \tilde{\sigma}_z - \sin(2\theta) \tilde{\sigma}_x \right) (D_- + D_-^\dagger), \quad (1.80)$$

where  $\tilde{\sigma}_z$  has been defined before and  $\tilde{\sigma}_x = |X_1\rangle\langle X_2| + |X_2\rangle\langle X_1|$ . For sake of simplicity, we will omit the apex “e” (indicating the exciton basis) in the following.

#### 1.4.4 Full Hamiltonian

At this point we present the full Hamiltonian used in this thesis. The total Hamiltonian in the exciton basis, considering only two sites and the same vibrational frequency at each of them, can be written as:

$$H = E\tilde{M} + \frac{\Delta E}{2} \tilde{\sigma}_z + \omega_{\text{vib}} D_-^\dagger D_- + \frac{1}{\sqrt{2}} g \left( \cos(2\theta) \tilde{\sigma}_z - \sin(2\theta) \tilde{\sigma}_x \right) (D_- + D_-^\dagger). \quad (1.81)$$

Here, the coupling  $g/\sqrt{2} \cos(2\theta) \tilde{\sigma}_z (D_- + D_-^\dagger)$  causes transitions between vibrational

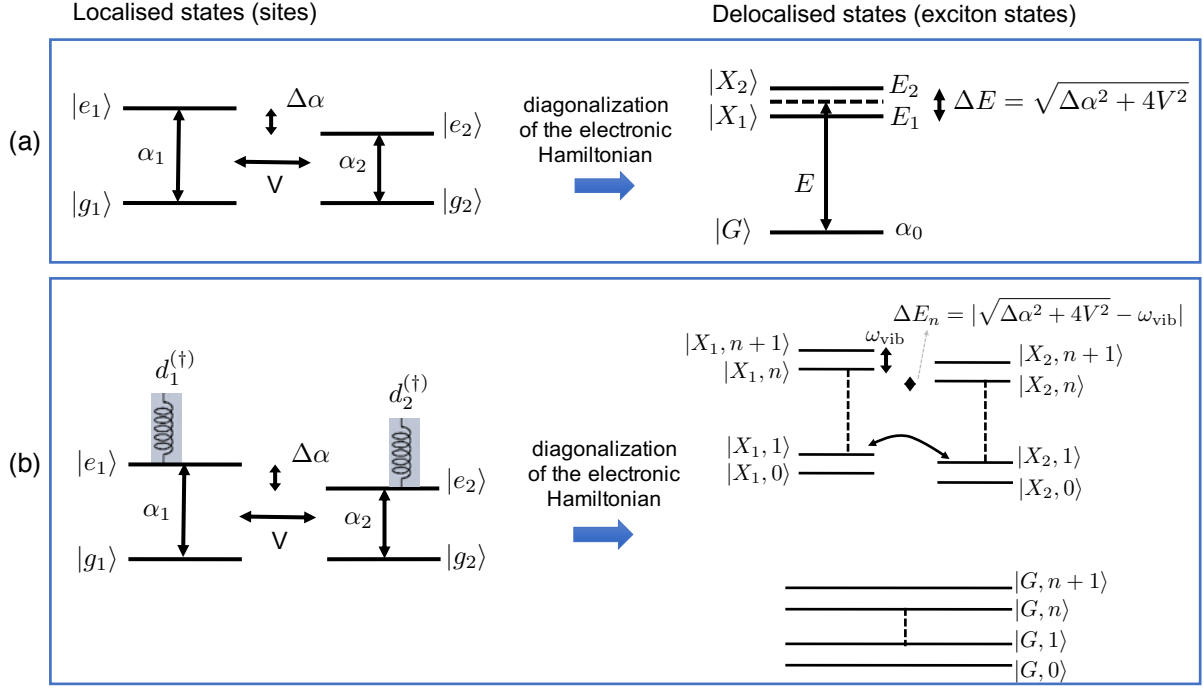


Figure 1.5: *The figure shows the system under study before and after diagonalising the electronic Hamiltonian, both for the electronic part only (a), and for the collective exciton-vibration description (b).*

states inside the same excitonic state  $|X_i, n\rangle \rightarrow |X_i, n+1\rangle$ , with  $i = 1, 2$ ; while the term  $g/\sqrt{2} \sin(2\theta)\tilde{\sigma}_x(D_- + D_-^\dagger)$  causes transitions between both exciton and vibrational states  $|X_1, n\rangle \rightarrow |X_2, n+1\rangle$  (Fig.1.5). In Eq. (1.81) it is interesting to notice that the bigger the mixing angle is, the more delocalisation the system experiences: in particular, for the limit case of an homodimer, where  $\Delta\alpha = 0$  and  $\theta = \pi/4$ , we recover the Jaynes-Cummings Hamiltonian. The opposite limit of  $\theta = 0$  gives excitons completely localised on the sites.

Since in Chap.4, we will use the Hamiltonian in the site basis, here we also report its expression in the case where only two sites are taken into account and without decoupling the mode centre of mass coordinates and the relative displacement coordinates. It can be obtained by combining together Eqs.(1.67), (1.74) and (1.78):

$$H = \alpha M + \frac{\Delta\alpha}{2} \sigma_z + V\sigma_x + \omega_{\text{vib}} \sum_{k=1}^2 d_k^\dagger d_k + \sum_{k=1}^2 g |k\rangle\langle k| (d_k^\dagger + d_k). \quad (1.82)$$

## 1.5 Probing quantum coherence

Witnessing quantum coherence is not a simple matter. Before explaining this concept, it is crucial to answer questions such as: “What is quantum coherence?”, “How is it possible to measure it?”. Once this will be clarified, it will be possible to understand the major issues hidden behind the concept of quantum photosynthesis and the main problems researchers are trying to deal with. Answering the questions above, from both a theoretical and experimental point of view, is the aim of the following sections.

### 1.5.1 Theoretical approach

Quantum coherences can be defined, in the simplest way, as the off-diagonal elements of the density matrix describing the system under study, which depends on the choice of the basis [56]. Let us consider the Hamiltonian eigenbasis, since this choice carries two simplifications. First of all, it links well with the spectroscopic procedures used to measure the transition energies: the populations in the density matrix depict the probability for the system to have a specific energy. Moreover, the Hamiltonian establishes the evolution of the quantum system, meaning that in the basis chosen the interpretation is quite simple. The equation of motion describing the system in any basis is given in Eq.(1.7), and written in the Hamiltonian eigenbasis becomes:

$$\frac{d}{dt}\rho_{ij} = -\frac{i}{\hbar}(E_i - E_j)\rho_{ij}, \quad (1.83)$$

where  $E_i$  is the energy of the  $i$ th eigenstate. This means that, under unitary evolution, populations ( $i = j$ ) are constant in time, whereas coherences ( $i \neq j$ ) oscillates in time as follows:

$$\rho_{ij}(t) = e^{-\frac{i}{\hbar}(E_i - E_j)t}\rho_{ij}(0). \quad (1.84)$$

Up to this point, it seems that the way to identify quantum coherence in the Hamiltonian eigenbasis is to observe oscillatory beating signals. This idea is also supported by the fact that such oscillations do not generally come from coherence in other basis: for instance, delocalisation (that is coherence in the site basis) can exist without showing any beating. Within the density matrix formalism, making an observation means to calculate the mean value of the corresponding operator. The first measurement one could think of is the energy of the system:

$$\langle E \rangle = \text{Tr}\{H\rho\} = \sum_i E_i \rho_{ii}. \quad (1.85)$$

However, notice that in Eq.(1.83), under unitary evolution, the energy of the system is conserved: it is independent of the coherences and, therefore, there are no oscillations. This implies that quantum coherences cannot be probed by measurements of energy. For this purpose, it is convenient to choose an operator that does not commute with the Hamiltonian: this guarantees that they do not have the same eigenvectors, hence the observable is not diagonal in the Hamiltonian eigenbasis. For the spectroscopic analysis, the dipole operator is the most suitable candidate, therefore we focus on this choice. This operator causes the transition between the ground and an excited state of a system after the interaction with light. In spectroscopic observations, the coherences of the dipole operator manifest as periodic oscillations in the intensity of the signal: these amplitudes are called quantum beats.

### 1.5.2 Experimental approach

One of the most used techniques to observe quantum coherence is ultra-fast multidimensional spectroscopy. For these experiments, the main methods more commonly used to perform measurements are pump-probe, two photon echo and two dimensional spectroscopy. They are all nonlinear methods of the third order polarization, used to study ultrafast electronic dynamics. The first two, in their simplest form, employ two laser pulses to measure either populations or coherences, while 2D spectroscopy involves the use of three lasers and it is considered the most powerful procedure, since it is able to investigate both populations and coherences [9, 89].

In a *pump-probe* scheme (Fig.1.6), a first laser “pump” pulse is used to excite the sample, generating a non-equilibrium state which is free to evolve. During this evolution the system undergoes both incoherent relaxation, because of the interaction with the environment, and coherent coupling with other excited states that facilitates energy transfer. These changes are monitored by a second “probe” pulse, following the first after a specific delay time. At this point, if the system was in an excited state, it will decay, otherwise it will populate.

The measurement of the fluorescence as a function of time delay between the pump and probe pulses yields information about the relaxation of electronic states in the system. More specifically, if coherent population transfer has happened in the dynamics, it will be witnessed by oscillations in the spectrum with frequency proportional to the coupling between the excited states and attenuated by the incoherent

relaxation.

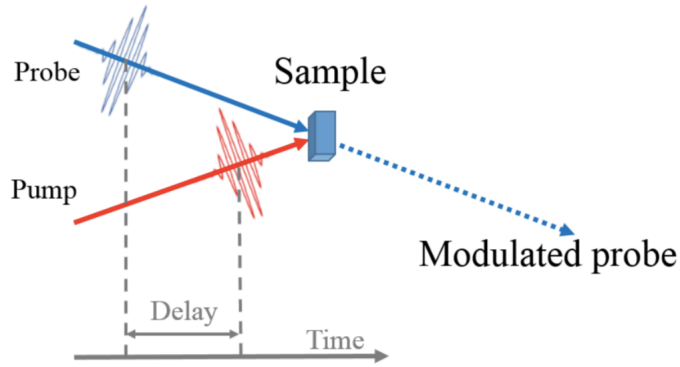


Figure 1.6: Representation of the pump-probe setup [90].

The first suggestion of possible coherence between excited states in a photosynthetic system (the Fenna-Matthews-Olson complex) came just from a pump-probe experiment performed in 1997 [91]. Here, measurements of anisotropy showed oscillations in the pump-probe signals, meaning that they had to be caused by quantum beatings between exciton levels, and not simply from coherent nuclear motion. However, this method measures coherences only indirectly, extrapolating the information about them from populations. As a result, it is very sensitive to any form of disorder, causing the laser pulse to go out of resonance and potentially introduce incoherent oscillations.

To directly measure coherence in the system, it is more convenient to use *photon-echo* spectroscopy [92]. In the simplest form, two pulses can be sent to the sample. The first laser pulse generates a phase rotation of  $\pi/2$  (see Fig.1.7), giving rise to a coherent superposition of excited states. The system is then free to evolve, but due to inhomogeneous disorder, the phases of the coherences will oscillate with slightly different frequencies (see Eq.(1.84)). To avoid this situation, a second pulse with phase  $\pi$  is sent on the system and, as a consequence, it flips the time evolution of the coherences (see Eq.(1.84)).

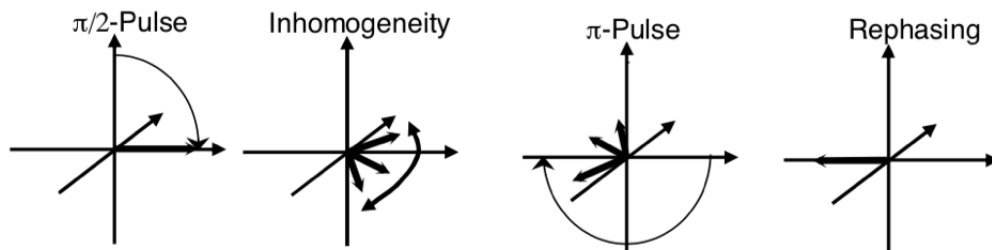


Figure 1.7: Representation of the geometry for a two-pulse photon echo experiment [93].

This phenomenon is called rephasing, since it recreates the same coherence in the

state that was obtained after the first pulse. More specifically, the system will be found in that state after a time equals to the time separation between the pulses. The signal emitted at this point contains information about the coherence created with the first pulse and this is the reason why it is called photon echo.

In addition, the interaction with the environment causes a relaxation of the system and, therefore, a decay of the coherences at a specific dephasing rate. This rate can be measured by varying the time between pulses, thus also acquiring information about the system-environment interaction.

One of the main advantages of this spectroscopic technique is that it is unaffected by inhomogeneous disorder. However, despite measuring coherence, this technique is unable to provide information about its origin: be it electronic, vibrational, or vibronic.

The most powerful method used nowadays to recover full information about the dynamics of the system is the *2D spectroscopy*. Indeed, the first direct probe of quantum coherence in biological system was obtained thanks to a 2D spectroscopic experiment in 2007 on the Fenna-Matthews-Olson complex [9].

In 2D spectroscopy three laser pulses interact with the sample, following the schematic representation in Fig.1.8.

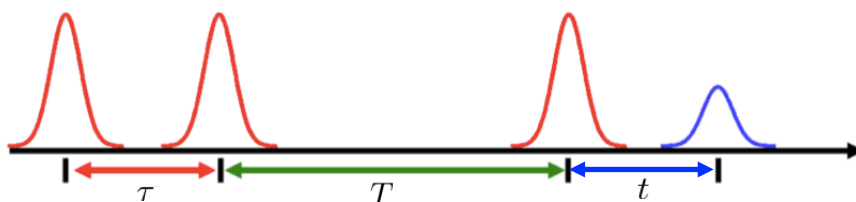


Figure 1.8: Representation of the scheme for a 2D spectroscopy experiment [94], where  $\tau$  corresponds to the coherence time passing until the first laser pulse,  $T$  is the waiting time between the second and third pulse, and  $t$  is the time delay with respect to the second pulse.

The first laser generates a coherent excited state. Such a coherence between the ground and the resonant excited states is free to evolve, undergoing dephasing and relaxation: this first time delay is called coherence time and is usually indicated with  $\tau$ . The second pulse changes the coherence into populations of both the excited and ground states, or in coherences between excited states. The latter occurs in presence of multi-chromophoric systems: the pulses, in fact, have a broad bandwidth, meaning that after the first excitation of a coherence between ground and excited state, the second pulse could interact with a different state, leaving a coherence and not a population. Such coherent evolution happens with phase equal to the energy

difference between the excitonic states. The time between the second and third pulse is called waiting time ( $T$ ). Last pulse causes rephasing in the system, the time delay with respect to the third one is called rephasing time ( $t$ ) and the signal emitted is a photon echo, as described in the previous method.

The main advantage of this technique is that it gives information about the energy levels in the system. More specifically, a 2D spectrum is actually a 3D figure where the intensity is function of two frequencies. However, in a 2D experiment the intensity is omitted and the dimensions of reference are the two frequencies. These are computed through the acquisition of two temporal functions (see Fig.1.8), then transformed in frequencies using the Fourier transform. As a consequence, the position and the intensity of the fluorescence peaks are different depending on the frequencies of the components excited in the system. This enables to distinguish the origin and the dynamics of these components [95]. Indeed, the use of 2D spectroscopy with different geometries of the laser pulses and detectors has found evidence of both electronic [11, 12, 25, 96] and vibrational coherences [97, 98], at low and ambient temperature. Thanks to two-dimensional spectroscopy, it has been experimentally proved that the interplay between the pigments and the protein environment allows quantum coherence to last longer [99]. Moreover, oscillations of excited-state population have been observed, implying that quantum energy transfer happens in photosynthetic complexes.

Although many steps forward have been made, the study of quantum photosynthesis is far from completed. The quantum interaction between electronic and vibrational degrees of freedom seems to be the reason behind the observed coherent dynamics. Some theoretical studies have shown non-classical fluctuations of collective chromophore motions [22]. The signature of this non-classicality lies in the negativity of the quasi-probability distribution of the collective mode coupled to the electronic degrees of freedom. However, alternative confirmations of these hypothesis are needed, using experimentally accessible techniques.

This is precisely the aim of this thesis: trying to provide tools which can be useful for the investigation of non-trivial quantum effects in the process of photosynthesis with alternative theoretical and experimental techniques. Our proposal relies on the theory of correlation functions: for this reason, in the next section, we will briefly outline the main concepts behind it and the basis of our idea.

## 1.6 Blind and coloured photon counting statistics

### 1.6.1 Blind correlation functions

One of the most common ways to investigate and define quantum properties of both light [38–41] and emitters [42–44], from a theoretical and experimental point of view, is the measurement of photon correlation functions. Any photon detection experiment requires the calculation of the correlation function of the field operators in normal- and time- order. The general average light intensity at a specific point  $\mathbf{r}$  and time  $t$  is [100]:

$$\langle I(\mathbf{r}, t) \rangle = \langle \hat{A}^\dagger(\mathbf{r}, t) \hat{A}(\mathbf{r}, t) \rangle, \quad (1.86)$$

where  $A^{(\dagger)}$  is the field operator with positive e negative frequencies, respectively:

$$\hat{A}(\mathbf{r}, t) = \sum_k \hat{\epsilon}_{\mathbf{k}} \mathcal{E}_{\mathbf{k}} a_{\mathbf{k}} e^{-i\nu_{\mathbf{k}}t + i\mathbf{k}\cdot\mathbf{r}}; \quad \hat{A}^\dagger(\mathbf{r}, t) = \sum_k \hat{\epsilon}_{\mathbf{k}} \mathcal{E}_{\mathbf{k}} a_{\mathbf{k}}^\dagger e^{i\nu_{\mathbf{k}}t - i\mathbf{k}\cdot\mathbf{r}}. \quad (1.87)$$

More specifically, the lowest order of these correlations (the second order) has been analysed as a tool to probe non-classical phenomena [39]. This second normally- and temporally-ordered correlation takes the following formal expression [101]:

$$g^{(2)}(t_1, t_2) = \frac{\langle \mathcal{T}_-[\hat{A}^\dagger(t_1)\hat{A}^\dagger(t_2)]\mathcal{T}_+[\hat{A}(t_2)\hat{A}(t_1)] \rangle}{\langle \hat{A}^\dagger(t_1)\hat{A}(t_1) \rangle \langle \hat{A}^\dagger(t_2)\hat{A}(t_2) \rangle}, \quad (1.88)$$

with  $\mathcal{T}_-$  and  $\mathcal{T}_+$  the time-ordering and antiordering superoperators needed to guarantee a physical description [101]. In particular,  $\mathcal{T}_-$  increases time arguments to the right in products of creation operators, while  $\mathcal{T}_+$  increases time arguments to the left in products of annihilation operators. The form of the equation above becomes easier if the radiation field consists of only a single mode:

$$g^{(2)}(\tau) = \frac{\langle a^\dagger(t) a^\dagger(t + \tau) a(t + \tau) a(t) \rangle}{\langle a^\dagger(t) a(t) \rangle \langle a^\dagger(t + \tau) a(t + \tau) \rangle}. \quad (1.89)$$

Based on the value of the zero and time dependent correlation function, it is possible to classify light in three different ways. The most common classification sees [102]:

- *coherent* light for which  $g^{(2)}(0) = 1$ . Perfectly coherent light has  $g^{(2)}(\tau) = 1$  for all values of  $\tau$  and it has a classical counterpart that is the coherent light with constant intensity. It has Poissonian photon statistics, with random time intervals between photons, hence the probability of detecting a photon is the same for all values of  $\tau$ .

- *bunched* light for which  $g^{(2)}(0) > 1$ . As the name suggests, it consists of a stream of photons, clumped together in bunches. This means that if we detect a photon at time  $t = 0$ , there is a higher probability of detecting another photon at short times than at long times, therefore  $g^{(2)}(\tau) > g^{(2)}(\infty)$ . Its classical description is the thermal or chaotic light, with a super-Poissonian distribution.
- *antibunched* light for which  $g^{(2)}(0) < 1$ . In this case, the probability of observing a photon counting event after detecting a photon is small for small values of  $\tau$  and then increases with  $\tau$ , so  $g^{(2)}(0) < g^{(2)}(\tau)$ . This kind of light is only possible in the photon interpretation and is thus a clear signature of the quantum nature of light. The antibunching is related to the sub-Poissonian distribution.

To calculate the correlation functions, a solution of the density matrix is not sufficient and the transition probability distribution is required. However, the *quantum regression theorem* allows to calculate a two-time correlation function from a single-time correlation function, under some conditions. The crucial assumption necessary for applying the theorem is the Markovian approximation, already explained in Sec.(1.3.3). This condition implies that the reservoir density matrix  $\rho_R(0)$  is uncoupled from the system density matrix  $\rho_S(0)$  at the initial time  $t = 0$ , meaning that  $\rho(0) = \rho_S(0) \otimes \rho_R(0)$ . A general statement of the quantum regression theorem is that if, for some operator  $\hat{O}$ , the single-time correlation function is known as

$$\langle \hat{O}(t + \tau) \rangle = \sum_j a_j(\tau) \langle \hat{O}_j(t) \rangle, \quad (1.90)$$

then it is easily possible to derive the two-time correlation function using the expression

$$\langle \hat{O}_i(t) \hat{O}(t + \tau) \hat{O}_k(t) \rangle = \sum_j a_j(\tau) \langle \hat{O}_i(t) \hat{O}_j(t) \hat{O}_k(t) \rangle. \quad (1.91)$$

In particular, it is possible to show that (for  $\tau \geq 0$ ) [103]:

$$\begin{aligned} \langle \hat{O}_1(t) \hat{O}_2(t + \tau) \rangle &= \text{Tr}_S \{ \hat{O}_2(0) e^{\mathcal{L}\tau} [\rho_S(t) \hat{O}_1(0)] \} \\ \langle \hat{O}_1(t + \tau) \hat{O}_2(t) \rangle &= \text{Tr}_S \{ \hat{O}_1(0) e^{\mathcal{L}\tau} [\hat{O}_2(0) \rho_S(t)] \}. \end{aligned} \quad (1.92)$$

The calculation of a correlation function between three operators,  $\langle \hat{O}_1(t) \hat{O}_2(t + \tau) \hat{O}_3(t) \rangle$ , for  $\tau \geq 0$ , occurs as follows:

$$\langle \hat{O}_1(t) \hat{O}_2(t + \tau) \hat{O}_3(t) \rangle = \text{Tr}_S \{ \hat{O}_2(0) e^{\mathcal{L}\tau} [\hat{O}_3(0) \rho_S(t) \hat{O}_1(0)] \}. \quad (1.93)$$

Having done this introduction, it is now possible to go back to the explanation of the motivation behind our work. We would like to investigate the quantum coherent interplay between electronic and vibrational degrees of freedom within a prototype photosynthetic complex, by analysing the photon counting statistics of the light emitted by the excitons. The biggest advantage of using this technique is the concrete possibility to investigate the problem experimentally. Until recently, the low fluorescence efficiency of light-harvesting complexes had impeded the study of individual molecules at room temperature. However, a recent paper [45] has demonstrated an over 500-fold fluorescence enhancement of a single molecule of light harvesting complex 2 (LH2). Therefore this is very promising for the project we aim to carry out, thanks to the realistic ability to measure eventual quantum effects in photosynthetic systems by using the second order correlation function.

### 1.6.2 Frequency-filtered correlation functions

In photodetection experiments, the light to be analysed often passes through a series of optical devices, such as spectral filters, before being registered by photodetectors [101]. In literature, the various authors who dealt with the problem of the frequency-filtered correlation function have given different names to this kind of correlation, such as “physical spectrum” [104], “time-resolved correlation spectrum” [105], “spectral time correlation function” [106], “frequency-filtered intensity correlation function” [107]. Despite the different names, the filtered two-time correlation function can be written as  $g_{F_1, F_2}^{(2)}(T_1, T_2)$  and is formally defined as in Eq.(1.88), but with the substitutions  $\hat{A}^{(\dagger)}(t_1) \rightarrow \hat{A}_{F_1}^{(\dagger)}(T_1)$  and  $\hat{A}^{(\dagger)}(t_2) \rightarrow \hat{A}_{F_2}^{(\dagger)}(T_2)$ , where

$$\begin{aligned} \hat{A}_F(t) &= \int_0^\infty F(t') \hat{A}(t - t') dt' \\ \hat{A}_F^\dagger(t) &= \int_0^\infty F(t') \hat{A}^\dagger(t - t') dt' \end{aligned} \quad (1.94)$$

are the filtered emission operators and  $F(t')$  is the time and space filter function

for each detector [101, 105, 107–109]. However, the calculation of these spectrally resolved correlations is not straightforward, because of the presence of a four dimensional integral. Higher-order correlations  $g_{F_1 \dots F_n}^{(n)}(T_1 \dots T_n)$  are similarly defined, but their theoretical computation becomes even more complicated.

When the spectral filters are Lorentzian, the general formula for the  $M$ th normally ordered correlation function is given by [101]:

$$\begin{aligned}
S_{\Gamma_1 \dots \Gamma_M}^{(M)}(\omega_1, T_1; \dots; \omega_M, T_M) &= \int_{-\infty}^{\infty} dt'_1 \int_{-\infty}^{\infty} dt'_{M+1} F_1^*(T_1 - t'_1) F_1(T_1 - t'_{M+1}) \\
&\dots \int_{-\infty}^{\infty} dt'_M \int_{-\infty}^{\infty} dt'_{2M} F_M^*(T_M - t'_M) F_M(T_M - t'_{2M}) \\
&\langle \mathcal{T}_- [a_1^{(+)}(t'_1) \dots a_M^{(+)}(t'_M)] \mathcal{T}_+ [a_1^{(-)}(t'_{M+1}) \dots a_M^{(-)}(t'_{2M})] \rangle,
\end{aligned} \tag{1.95}$$

where

$$F_m(t) = \theta(t) \frac{\Gamma_m}{2} e^{-(\Gamma_m/2 + i\omega_m)t}, \tag{1.96}$$

with  $\theta(t)$  the Heaviside function. This means that the spectral filter is replaced by a Lorentzian density of states of the probe system under the Markov decay process. Unfortunately, the computation of the  $M$ th order frequency-filtered correlation function in Eq.(1.95) is very complicated for  $M > 2$ , due to all the possible time orderings of the  $2M$  time correlators. Moreover, every correlator requires the application of the quantum regression theorem  $2M - 1$  times. On the contrary, the measure of this quantity is experimentally accessible thanks to devices such as streak cameras, that are able to detect photon clicks as a function of time and energy [110].

Given the difficulty of numerically calculating the multi-dimensional integrals in Eq.(1.95), some alternative methods have been recently developed to overcome the computational complexity of these integrals in the filtered photon correlations [46, 47, 111].

### 1.6.3 Sensor method for spectrally filtered photon correlations

The “sensor method” introduced in [46] is the inspiration for the new formalism we developed, which will fully be presented in Chap.2.

The sensor method is based on the use of sensors which are weakly coupled to the quantum emitter. The number of sensors depends on the statistical properties one is interested to investigate:  $M$  sensors are required to compute the  $M$ th order photon correlations. They are represented as two-level systems with annihilation

operator  $\varsigma_m = |0_m\rangle\langle 1_m|$  and transition frequency  $\omega_m$  that is matched to the emission frequency of the main system. The sensor Hamiltonian is then described as:

$$H_m = \omega_m \varsigma_m^\dagger \varsigma_m, \quad (1.97)$$

while the interaction Hamiltonian between the quantum emitter and the  $m$ -th sensor is given by:

$$H_{e,m} = \epsilon_m (a_m \varsigma_m^\dagger + a_m^\dagger \varsigma_m), \quad (1.98)$$

with the coupling strength  $\epsilon_m$  being small enough to justify that the dynamics of the system is not influenced by the presence of the sensors. The lifetime of each sensor  $1/\Gamma_m$  is the inverse detector linewidth. The condition of weak coupling implies that if  $\gamma_Q$  is the smallest transition rate within the open quantum system linked to the cavity mode, the couplings  $\epsilon_m$  to the sensors must satisfy the condition:

$$\epsilon_m \ll \sqrt{\frac{\Gamma_m \gamma_Q}{2}}, \quad (1.99)$$

meaning that losses into the sensors and their back action are negligible. In the limit of vanishing system-sensor coupling, the sensor population correlations are shown to quantify the photon correlations of interest.

It is worth noticing that the physical meaning of the sensor linewidth lies in the frequency-time uncertainty relation. The limit  $\Gamma \rightarrow 0$  describes the case of perfect detectors, with very high resolution in detecting frequencies, but complete indeterminacy in time, leading to averaging photons from all possible time delays. The opposite limit of  $\Gamma \rightarrow \infty$  corresponds to the case of blind detectors, with very high resolution in time, leading to photons detected at specific time delays but with complete indeterminate frequencies.

The main result of the paper [46], which is demonstrated in the Supplemental Material, is:

$$g_{\Gamma_1 \dots \Gamma_M}^{(M)}(\omega_1, t_1; \dots; \omega_M, t_M) = \lim_{\epsilon_1, \dots, \epsilon_M \rightarrow 0} \frac{\langle n_1(t_1) \dots n_M(t_M) \rangle}{\langle n_1(t_1) \rangle \dots \langle n_M(t_M) \rangle}, \quad (1.100)$$

where  $M$  is the order of the correlation function,  $\omega_m$  are the frequencies to correlate,  $\Gamma_m$  are the linewidths (inverse of the lifetime) of each transition,  $\langle n_m(t_m) \rangle = \langle \varsigma_m^\dagger(t_m) \varsigma_m(t_m) \rangle$  is the average population of the  $m$ -th sensor and it gives the probability of detecting a photon with frequency  $\omega_m$  at time  $t_m$  and  $\langle n_1(t_1) \dots n_M(t_M) \rangle$  is

the probability of detecting  $M$  photons, each at different time  $t_m$ . In Supplemental Material of [46], the authors prove that for open quantum systems described by Lindblad type master equations, the  $M$ -th frequency-filtered correlation function is given by:

$$S_{\Gamma_1 \dots \Gamma_M}^{(M)}(\omega_1, \dots, \omega_M; t_1, \dots, t_M) = \frac{\Gamma_1 \dots \Gamma_M}{(2\pi)^M \epsilon_1^2 \dots \epsilon_M^2} \langle n_1(t_1) \dots n_M(t_M) \rangle. \quad (1.101)$$

Eqs.(1.100) and (1.101) express the equivalence between the traditional integral approach in Eq.(1.95) and the sensor formalism to compute frequency-filtered and time-resolved photon correlations. This result reduces the complexity of computing  $g_{\Gamma_1 \dots \Gamma_M}^{(M)}(\omega_1, t_1; \dots; \omega_M, t_M)$  since no integral calculation is required and the quantum regression theorem has to be applied only  $M - 1$  times. It is also worth observing that, since the mathematical equivalence with the traditional integral approach has been proven through Eq.(1.95), the sensor method relies on the choice of Lorentzian filters.

One of the most peculiar aspects of Ref. [46] is that the result presented in Eq.(1.100), *apparently*, does not require the normal order of the sensor operators at arbitrary time delays. The apparent irrelevance of the normal order for any time delay seemed very surprising and was one of the points that brought our attention to this paper. In the initial discussion with the authors, they claimed that, indeed, the normal order of operators was not required to compute time-resolved correlation functions. This aspect is remarkable as it seemed that including the sensors in the analysis could surpass the non-commutativity of the field operators at different times. The proof presented in the supplementary information of the paper [46] is quite convoluted. Hence, to analyse the correctness of the claim, we aimed to reproduce their outcomes and check that we recovered physical results in all cases. Our general conclusion was that, while at zero time delay the operators of different sensors commute, and therefore normal order does not matter, this is not the case for finite time delay, where correlations between such operators emerge necessarily, leading to non-commutation at different times.

To illustrate the above points, we first consider the Jaynes-Cummings model, as it was done in Ref. [46], with  $H_0 = g(\sigma^\dagger a + a^\dagger \sigma)$ . The inclusion of the sensors results in the following Hamiltonian and master equation ( $\hbar = 1$ ):

$$\begin{aligned}
H &= g(\sigma^\dagger a + a^\dagger \sigma) + \sum_{m=1}^M \left( \omega_m \varsigma_m^\dagger \varsigma_m + \epsilon_m (a \varsigma_m^\dagger + a^\dagger \varsigma_m) \right) \\
\frac{\partial}{\partial t} \rho &= -i[H, \rho] + \left( \frac{\gamma_a}{2} \mathcal{L}_a(\rho) + \frac{\gamma_\sigma}{2} \mathcal{L}_\sigma(\rho) + \frac{P_\sigma}{2} \mathcal{L}_{\sigma^\dagger}(\rho) \right) + \sum_{m=1}^M \frac{\Gamma_m}{2} \mathcal{L}_{\varsigma_m}(\rho)
\end{aligned} \tag{1.102}$$

where  $\mathcal{L}_{c_i}(O) = (2c_i O c_i^\dagger - c_i^\dagger c_i O - O c_i^\dagger c_i)$ , for a system jump operator  $c_i$  and a relaxation process happening at rate  $\gamma_{c_i}$ .  $\gamma_a$  and  $\gamma_\sigma$  are the cavity and emitter decay rate, respectively, and  $P_\sigma$  is the incoherent pumping of the emitter.

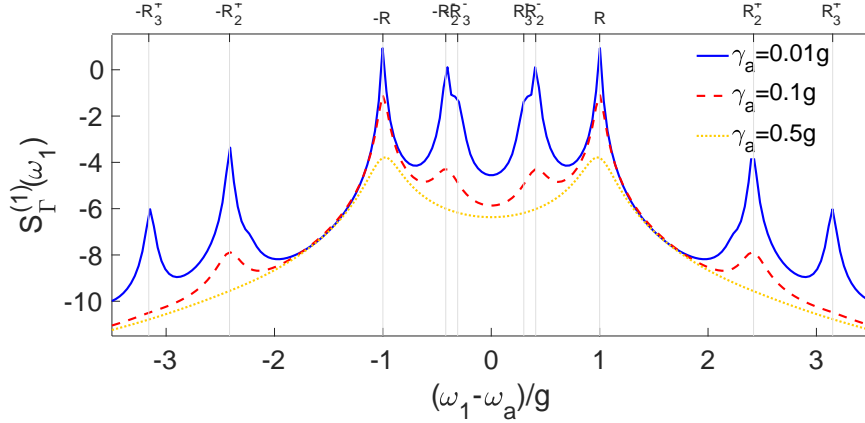


Figure 1.9: *Power spectra of emission probed by weak incoherent excitation ( $P_\sigma = \gamma_\sigma = 0.01g$ ) for three cavities of decreasing quality  $\gamma_a = 0.01g$  (solid line),  $\gamma_a = 0.1g$  (dashed) and  $\gamma_a = 0.5g$  (dotted). The values of the parameters are:  $g = 1$ ,  $\epsilon_1 = 10^{-5}$  and  $\Gamma = 0.001g$ . The figure is in semilog scale and it is plotted in arbitrary units.*

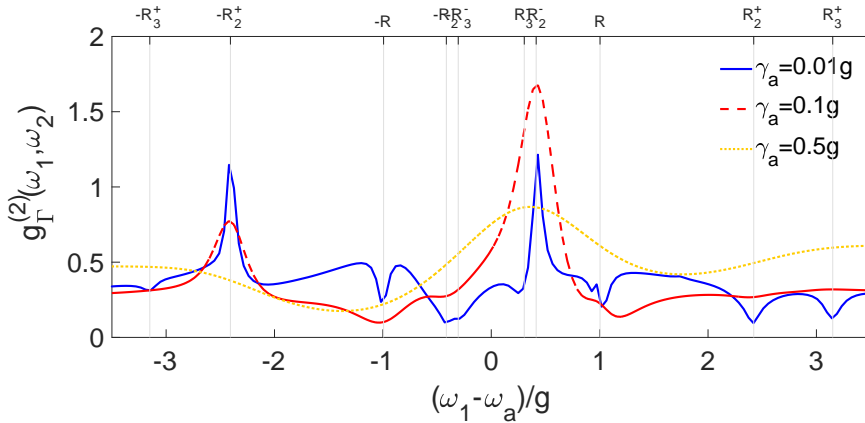


Figure 1.10: *Two-photon correlations at zero delay with  $\omega_2 = R$ . Same parameters as figure 1.9.*

We managed to obtain the results of the paper at all the configurations for zero time delay. As an example, figures 1.9 and 1.10 are the power spectrum and the

frequency-resolved second order correlation function at zero time delay, respectively. This assured that our setup was correct. However, we could not reproduce the results the article reported for the time-resolved second order correlation function. By following the main outcome they claimed, we obtained unphysical results, as shown in figure 1.11.

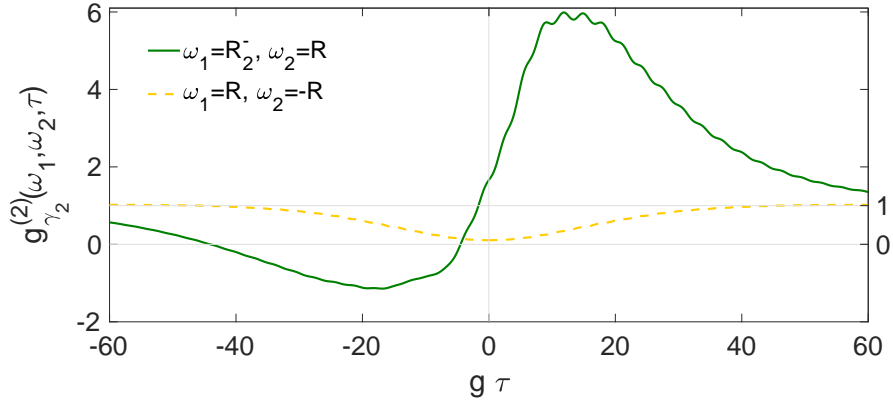


Figure 1.11: *Time-resolved correlation function without using the normal order of the sensor operators. Positive times correspond to detection of frequencies as reported in the legend, negative times to the opposite order.*

Our conclusion was that the normal order must be important in Eq.(1.100) and therefore we did the calculations with it: the use of the normal order guarantees physical results (figure 1.12).

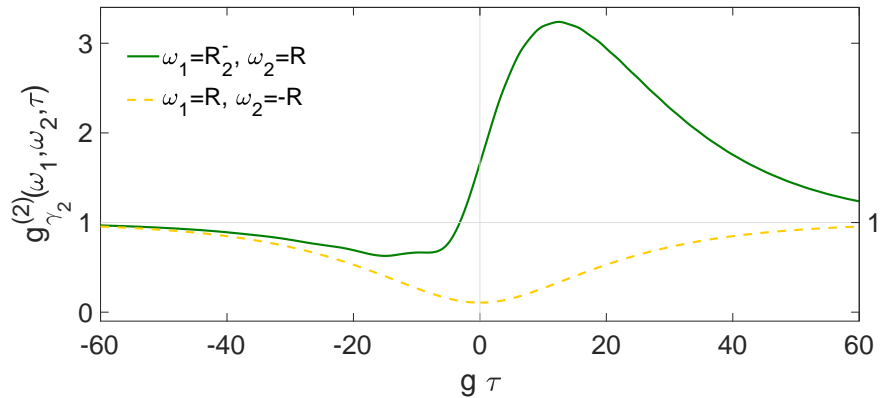


Figure 1.12: *Time-resolved second order correlation function. Positive times correspond to detection of frequencies as reported in the legend, negative times to the opposite order. Parameters:  $\Gamma = \gamma_2$  for both sensors,  $P_\sigma = \gamma_\sigma = 0.01g$ ,  $\gamma_a = 0.1g$ .*

After pointing this out to the authors, they indeed acknowledged that the figure they presented in the paper was actually computed with the normal order of the sensor operators, even though the theory claims the normal order was not necessary.

A following erratum to the initial paper was published in 2016 [47].

For clarity, we report here the correct forms of Eqs.(1.100) and (1.101) including the normal order of the sensor operators:

$$g_{\Gamma_1 \dots \Gamma_M}^{(M)}(\omega_1, T_1; \dots; \omega_M, T_M) = \lim_{\epsilon_1, \dots, \epsilon_M \rightarrow 0} \frac{\langle : n_1(T_1) \dots n_M(T_M) : \rangle}{\langle n_1(T_1) \rangle \dots \langle n_M(T_M) \rangle} \quad (1.103)$$

$$S_{\Gamma_1 \dots \Gamma_M}^{(M)}(\omega_1, \dots, \omega_M; t_1, \dots, t_M) = \frac{\Gamma_1 \dots \Gamma_M}{(2\pi)^M \epsilon_1^2 \dots \epsilon_M^2} \langle : n_1(t_1) \dots n_M(t_M) : \rangle. \quad (1.104)$$

Traditionally, equations include dots representing normal order. However, these were completely absent from Ref. [46] and also from its Supplemental Material. In particular, we identified that the following equation (Eq.(42) in the Supplemental Material of [46]) shows inconsistency:

$$\partial_\tau \langle n_1(0) n_2(\tau) \rangle = -\Gamma_2 \langle n_1(0) n_2(\tau) \rangle + 2 \Re \{ i \epsilon_2 \langle n_1(0) (s_2 a^\dagger)(\tau) \rangle \} \neq \partial_\tau \langle : n_1(0) n_2(\tau) : \rangle \quad (1.105)$$

Later on, the authors clarified that normal order, while omitted in the notation, was actually assumed throughout the proof and numerical calculations, as they indicate in the erratum of the paper [47]. We will go through more details of this issue in Chap.2.

Because of the inconsistency found in the paper [46] (and the time spent analysing it in detail), we were inspired to propose an alternative approach of this sensor method presented for the calculation of frequency-filtered and time-resolved photon correlations. Our method is based on the perturbative expansion of the steady state of the whole system (quantum emitter and sensors) with respect to the emitter-sensor coupling parameter  $\epsilon$ , as it will be explained more in detail in the next chapter.

## Chapter 2

# Perturbative method for computing frequency-filtered and time-resolved photon correlation

This chapter puts forward an alternative method of the sensor procedure proposed in [46,47] to compute frequency-filtered and time-resolved correlation functions. The new formalism relies on an algebraic expansion of the steady state of the whole quantum emitter-plus-sensors system with respect to the coupling parameter  $\epsilon$  between them. This procedure allows to express the photon correlations as a function of the dynamics of the emitting system only and it also guarantees the independence of the correlations on the specific choice of the coupling parameter. In addition, the use of the time-dependent perturbation theory to calculate the time-resolved photon correlation enables to define it as a sum of three contributions, which give insight into the physical processes dominating at different time scales. The outcomes obtained are applied to a bio-inspired toy model to show the agreement between the previous method and our formulation. The results obtained in this chapter are taken from Ref. [50] and represent the theoretical scaffolding on which the next chapters are built.

### 2.1 Introduction

One of the most powerful techniques used to analyse the quantum behaviour of a system is the study of the optical properties of the emitted light. Within this field,

the energy-time uncertainty relation plays a fundamental role: it implies that the arrival time of a photon and its frequency cannot be measured with precision simultaneously [104,112]. This uncertainty has not limited the research in the field, on the contrary it has presented an opportunity for new studies of quantum phenomena, both to identify new types of photon quantum correlations [46,47,113–115] and to develop new protocols for the preparation of entangled photons [48,116].

In particular, the impact of the spectral filtering of light signals in optical setups has become more and more relevant. Indeed, it is connected to the frequency and time resolution of detected light and, therefore, it has opened the way for the investigation of different phenomena in quantum optics [101,115,117–119]. Frequency-filtered and time-resolved correlation functions have also provided information about the dynamics of solid state systems [120] and complex molecular systems [49,121,122]. In the latter case, also the coherent multi-dimensional spectroscopy has contributed with important results [123], since in general ultrafast (femtoseconds) non-linear spectroscopy is a powerful method to analyse quantum coherence dynamics in many different biomolecular and chemical systems (see review [124]).

As presented in Sec.1.6.2, the traditional method of dealing with frequency-filtered and time-resolved photon counting statistics can be very overwhelming, since it requires the computation of multi-dimensional integrals. For this reason, the introduction of alternative techniques, able to overcome this computational complexity [46,47,111], has been greeted with enthusiasm by the community in the field.

Refs. [46,47] have been widely introduced in the first chapter (see Sec.1.6.2). Although the sensor method proposed by the authors does not need to explicitly compute the multi-dimensional integrals, one of its drawbacks is the requirement for computing the quantum dynamics of the whole system (including the sensors). This means that the dimensionality of the Hilbert space can become very big for quantum systems of large dimension and for higher order correlations.

This problem has been underlined and discussed in [111]. There the authors study the single-atom fluorescence and develop an interesting approach where filters are treated as black boxes connected to the output. They obtain higher orders of coloured correlation functions also resolved in time, where the expressions are defined in the Hilbert space of the atom only. Despite this formalism requiring the numerical solution of multi-dimensional integrals, some analytical solutions can be recovered under certain approximations.

The aim of our work is to propose an alternative formulation of the sensor method [46,47], able to examine the spectral filtered photon counting statistics of the system

under study, by focusing on the dynamics of the system only, and therefore reducing the dimension of the Hilbert space to operate on.

Our formalism relies on the algebraic expansion of the whole system-sensors state with respect to the weak coupling parameter between them. As a result, we find a hierarchy of auxiliary matrices related to the emitting system, from which it is possible to efficiently compute correlation functions of any order at zero time delay. Our approach recovers the analytical expressions presented in the Supplemental information of Ref. [46] and in Ref. [125] for the one- and two-photon spectrum, therefore showing full agreement between the methods. We also derive a solution for the second order time-resolved correlation function, using the time-dependent perturbation theory. We find that such photon correlation is the sum of three components, each of which is related to different physical processes happening during the emission dynamics at different time scales. The procedure can be generalised to higher order photon correlations, where only one sensor has a time delayed detection.

In the following we will first explain in more detail the motivation behind our work, then we will apply the perturbative method to the steady state and derive the photon correlations at zero time delay. After using time-dependent perturbation theory to analyse finite time delay correlations, we will apply the formalism to compute such quantities for a bio-inspired toy system. We will first show the agreement between our method and the one presented in [46, 47], then underlining the advantages of using filtered correlation functions to study quantum dynamics in biomolecular units.

## 2.2 Why an alternative sensor method?

The sensor method originally proposed in [46, 47] requires to solve the dynamics of a quantum emitter weakly coupled to  $M$  sensors, as explained in Sec.1.6.3.

For sake of generality, we have considered that the emission operators  $a_j$  coupled to each sensor can be different. This can occur in different situations, such as when in a multipartite quantum emitter it is possible to achieve local resolution or when emitted frequencies can be distinguished via fluorescence polarization detection. This is the case, for example, of single light-harvesting complexes [126], where the frequency filters are also polarizing filters: Fig.2.1(a) represents a possible experimental setup.

Under the hypothesis of Markovian decay processes for both the emitter and the sensors, the joint emitter-sensors density matrix  $\hat{\rho}$  satisfies the master equation in

Eq.(1.50), where the Liouvillian reads as ( $\hbar = 1$ ):

$$\mathcal{L}(\hat{\rho}) = \mathcal{L}_0(\hat{\rho}) + \sum_{m=1}^M (\mathcal{L}_m(\hat{\rho}) - i[H_{e,m}, \hat{\rho}]), \quad (2.1)$$

with

$$\mathcal{L}_0(\hat{\rho}) = -i[H_0, \hat{\rho}] + \sum_i \frac{\gamma_{c_i}}{2} \mathcal{L}_{c_i}(\hat{\rho}), \quad (2.2)$$

$$\mathcal{L}_m(\hat{\rho}) = -i[H_m, \hat{\rho}] + \frac{\Gamma_m}{2} \mathcal{L}_{s_m}(\hat{\rho}). \quad (2.3)$$

(where  $\mathcal{L}_0(\hat{\rho})$  is the Liouvillian describing the system only and every other term has been explained in Sec.1.6.3).

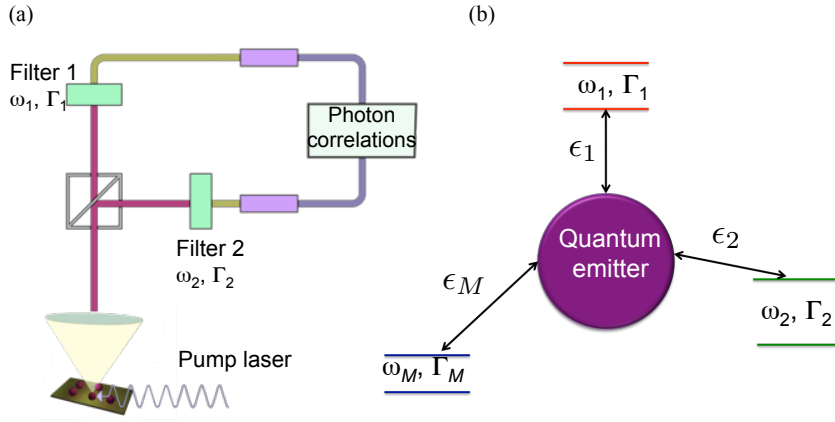


Figure 2.1: (a) Potential experimental setup to measure frequency-filtered and time-resolved correlation functions, similar to that used in Ref. [48]. (b) Diagram of the sensor method proposed in Ref. [46, 47] to compute frequency-filtered correlations. Each sensor is modelled as a two-level system coupled to the quantum emitter through the strength parameter  $\epsilon_m$ , with  $m = 1, \dots, M$ . Photon correlations are recovered in the limit of small coupling  $\epsilon_1, \dots, \epsilon_M \rightarrow 0$ .

In the limit of small  $\epsilon_m$ , satisfying  $\epsilon_m \ll \sqrt{\Gamma_m \gamma_Q / 2}$ , and sensor populations satisfying  $\langle n_m \rangle = \langle s_m^\dagger s_m \rangle \ll 1$ , intensity-intensity correlations of the form  $\langle : n_1 n_2 \dots n_M : \rangle$  are directly related to the  $M$ th order photon correlation functions in Eq.(1.101) as [46, 47]:

$$\langle : n_1(T_1) \dots n_M(T_M) : \rangle = \frac{\epsilon_1^2 \dots \epsilon_M^2}{\Gamma_1 \dots \Gamma_M} (2\pi)^M S_{\Gamma_1 \dots \Gamma_M}^{(M)}(\omega_1, T_1; \dots; \omega_M, T_M), \quad (2.4)$$

with  $S_{\Gamma_1 \dots \Gamma_M}^{(M)}(\omega_1, T_1; \dots; \omega_M, T_M)$  given in Eq.(1.95) for the case in which the filter

functions correspond to a Cauchy-Lorentz distribution Eq.(1.96). This situation can experimentally be realised through a Fabry-Perot interferometer with the reflection coefficients close to 1 [104]. We report a possible experimental setup in Fig.2.1(a) and the corresponding theoretical system used to compute the filtered photon counting statistics is presented in Fig.2.1(b).

The original presentation of Eqs.(1.100) and (1.101) in [46] did not contain the normal order of the sensor operators. However, its absence leads to unphysical results for a finite delay time, as shown in Sec.(1.6.3). In an Erratum [47] the authors clarified that normal order is implied through the proof of Eq.(1.100), nevertheless it is not necessary for correlations at zero time delay. Our approach is equivalent to the sensor method, considering the normal order of the sensor operators, therefore we have made a consistency check of the proof presented in the Supplemental Material of Ref. [46], which will be presented in Sec.2.5.

Although the formalism introduced in [46] is mathematically equivalent to the integral form of correlations, its computation involves some numerical challenges. Under the assumption that all the sensor couplings are the same,  $\epsilon_m = \epsilon$ , the numerical calculations of correlations depends on the choice of this small system-sensor coupling  $\epsilon$  that, at the same time, does not have to be *so* small that adding or subtracting terms of order  $\epsilon^{2M}$  to or from terms of order  $\epsilon^0$  causes problems within double arithmetic precision. This means that, in general, this approach requires to check convergence and stability of the numerical results for different values of  $\epsilon$ .

Even more relevant is the fact that to compute the correlation functions at zero time delay, it is necessary to numerically derive the zero eigenvalue of the Liouvillian superoperator associated to the whole system plus sensors state. As a result, the calculation of  $g_{\Gamma_1 \dots \Gamma_M}^{(M)}(\omega_1, T; \dots; \omega_M, T)$  when  $T \rightarrow \infty$ , involves the evaluation of the eigenvector with a zero eigenvalue of a matrix  $4^M$  times larger than that of the quantum emitter alone [113]. The same issue can raise for the calculation of the time-resolved correlations, as the calculation involves time propagation of the joint emitter-sensor state. This numerical problem becomes more demanding, the more the dimension of the system increases.

These issues provided sufficient motivation to develop a method which could overcome them. In the next section, we show that the algebraic expansion with respect to the coupling parameter  $\epsilon$  can both eliminate the explicit numerical dependence on  $\epsilon$  and reduce the dimensionality of the Hilbert space needed for computation.

## 2.3 Frequency-filtered spectrum and photon correlations at zero time delay

### 2.3.1 $M = 1$ : power spectrum

The assumption of weakly coupled sensors to the emitting system guarantees that they do not affect its dynamics. Based on this thought, we wanted to develop a procedure in which the filtered correlations depend only on the dynamics and operators of the system.

We start by deriving the expressions of the power spectrum, by considering the emitting system coupled to only one sensor. We indicate with  $\hat{\rho}_{ss}$  the steady state of the joint emitter-plus-sensor system. From Eq.(2.4), with  $M = 1$ , we can calculate the power spectrum as:

$$S_{\Gamma_1}^{(1)}(\omega_1) = \frac{\Gamma_1}{2\pi\epsilon^2} \langle n_1 \rangle = \frac{\Gamma_1}{2\pi\epsilon^2} \text{Tr} [n_1 \hat{\rho}_{ss}]. \quad (2.5)$$

The full steady state  $\hat{\rho}_{ss}$  can be obtained by using the identity operator in the sensor Hilbert space (that is  $\mathbb{1}_{s_1} = \sum_{j_1=0,1} |j_1\rangle\langle j_1|$ ) as follows:

$$\hat{\rho}_{ss} = \mathbb{1}_{s_1} \hat{\rho}_{ss} \mathbb{1}_{s_1} = \sum_{j_1, j'_1=0,1} \hat{\rho}_{j_1}^{j'_1} \otimes |j_1\rangle\langle j'_1|, \quad (2.6)$$

where the matrices  $\hat{\rho}_{j_1}^{j'_1} = \langle j_1 | \hat{\rho}_{ss} | j'_1 \rangle$  are traced over the sensor degrees of freedom, therefore depending only on the degrees of freedom of the quantum emitter. However, these matrices are conditioned on specific sensor states, hence they can be interpreted as “auxiliary conditional states”. The Hermitian conjugates are given by swapping the upper and lower indices. It is relevant to notice that each matrix  $\hat{\rho}_{j_1}^{j'_1}$  is of order  $\epsilon^{j_1+j'_1}$ . With this definition the power spectrum given in Eq.(2.5) becomes

$$S_{\Gamma_1}^{(1)}(\omega_1) = \frac{\Gamma_1}{2\pi\epsilon^2} \text{Tr} [\hat{\rho}_1^1]. \quad (2.7)$$

We now show how the matrix  $\hat{\rho}_1^1$  can be computed through a hierarchy of equations containing auxiliary matrices of lower order. These matrices bring information on the emission properties of the steady state probed at the specific sensor frequency  $\omega_1$ . The steady state of the whole system is calculated through the condition  $\mathcal{L}(\hat{\rho}_{ss}) = 0$ , where the Liouvillian in Eq.(2.1) ( $M = 1$ ) acts on every term in Eq.(2.6):

$$\mathcal{L}(\hat{\rho}_0^0 \otimes |0\rangle \langle 0|) = \mathcal{L}_0(\hat{\rho}_0^0 \otimes |0\rangle \langle 0|) \quad (2.8)$$

$$- i\epsilon(a_1 \hat{\rho}_0^0 \otimes |1\rangle \langle 0| - \hat{\rho}_0^0 a_1^\dagger \otimes |0\rangle \langle 1|),$$

$$\mathcal{L}(\hat{\rho}_1^0 \otimes |1\rangle \langle 0|) = (\mathcal{L}_0 - \Gamma_1/2 - i\omega_1)(\hat{\rho}_1^0 \otimes |1\rangle \langle 0|) \quad (2.9)$$

$$- i\epsilon(a_1^\dagger \hat{\rho}_1^0 \otimes |0\rangle \langle 0| - \hat{\rho}_1^0 a_1^\dagger \otimes |1\rangle \langle 1|),$$

$$\mathcal{L}(\hat{\rho}_1^1 \otimes |1\rangle \langle 1|) = (\mathcal{L}_0 - \Gamma_1)(\hat{\rho}_1^1 \otimes |1\rangle \langle 1|) \quad (2.10)$$

$$+ \Gamma_1 \hat{\rho}_1^1 \otimes |0\rangle \langle 0| - i\epsilon(a_1^\dagger \hat{\rho}_1^1 \otimes |0\rangle \langle 1| - \hat{\rho}_1^1 a_1 \otimes |1\rangle \langle 0|) .$$

Here, the expression for  $\mathcal{L}(\hat{\rho}_0^1 \otimes |0\rangle \langle 1|)$  is the complex conjugate of Eq.(2.9).

The sum of these expressions can be rewritten in a form similar to Eq.(2.6), associating together terms related to populations or coherences of the sensor:

$$\mathcal{L}(\hat{\rho}_{ss}) = \sum_{j_1, j_1' = 0, 1} \hat{B}_{j_1}^{j_1'} \otimes |j_1\rangle \langle j_1'| = \mathbf{0} , \quad (2.11a)$$

$$\hat{B}_{j_1}^{j_1'} = \mathbf{0}, \text{ For all } j_1, j_1' , \quad (2.11b)$$

At this point the solution of the problem can be found solving the set of coupled equations for  $\hat{\rho}_{j_1}^{j_1'}$ , such that the matrices  $\hat{B}_{j_1}^{j_1'}$  are equal to zero at every element. For instance, the equation  $\hat{B}_0^0 = \mathbf{0}$  contains terms coming from Eq.(2.8) (that is of zeroth order in  $\epsilon$ ) and from Eq.(2.9) and its complex conjugate: they give contributions of linear order in  $\epsilon$  as follows

$$\hat{B}_0^0 = \mathcal{L}_0(\hat{\rho}_0^0) - i\epsilon(a_1^\dagger \hat{\rho}_1^0 - \hat{\rho}_0^1 a_1) + \Gamma_1 \hat{\rho}_1^1 = \mathbf{0}. \quad (2.12)$$

The equation above shows that, for an arbitrary value of  $\epsilon$ ,  $\hat{\rho}_0^0$  depends on terms of higher orders in this coupling parameter. This means that the presence of the sensors actually affects the dynamics of the system and the set of equations in Eq.(2.11b) do not have a simple solution. However, in the limit of weak coupling  $\epsilon \ll 1$  we are assuming, sensor populations are very small, that is  $\langle n_1 \rangle = \text{Tr}[\hat{\rho}_1^1] \ll 1$ . This leads to neglect terms of the order of  $\epsilon^2$  in Eq.(2.12), hence the contribution of the terms  $\Gamma_1 \hat{\rho}_1^1$  and  $\|i\epsilon(a_1^\dagger \hat{\rho}_1^0 - \hat{\rho}_0^1 a_1)\|$  can be discarded. Similarly, the equation for  $\hat{B}_0^1$  reads like:

$$\hat{B}_0^1 = \left( \mathcal{L}_0 + i\omega - \frac{1}{2}\Gamma \right) \hat{\rho}_0^1 + i\epsilon \hat{\rho}_0^0 a_1^\dagger + i\epsilon a_1^\dagger \hat{\rho}_1^1 = \mathbf{0}. \quad (2.13)$$

but  $\|a_1^\dagger \hat{\rho}_1^1\| \ll \|\hat{\rho}_0^0 a_1^\dagger\|$ , therefore the term depending on  $\hat{\rho}_1^1$  can be neglected. These approximations apply to all the coupled equations and can be generalised saying that the matrices  $\hat{B}_{j_1}^{j_1'}$  receive contributions only from terms of the lower or same order in  $\epsilon$ , that is  $\hat{\rho}_\ell^{\ell'}$  with  $\ell + \ell' \leq j_1 + j_1'$ . This is equivalent to a formal expansion in  $\epsilon$ , since all the  $\hat{\rho}_\ell^{\ell'}$  matrices are of order  $\epsilon^{\ell+\ell'}$ . Following this thought, the equations for the steady state  $\hat{B}_{j_1}^{j_1'} = \mathbf{0}$  can be rewritten as:

$$\mathcal{L}_0(\hat{\rho}_0^0) \simeq 0 \quad (2.14a)$$

$$\mathcal{L}_0(\hat{\rho}_1^0) - (\Gamma_1/2 + i\omega_1)\hat{\rho}_1^0 - i\epsilon a_1 \hat{\rho}_0^0 \simeq 0 \quad (2.14b)$$

$$\mathcal{L}_0(\hat{\rho}_0^1) - (\Gamma_1/2 - i\omega_1)\hat{\rho}_0^1 + i\epsilon \hat{\rho}_0^0 a_1^\dagger \simeq 0 \quad (2.14c)$$

$$\mathcal{L}_0(\hat{\rho}_1^1) - \Gamma_1 \hat{\rho}_1^1 - i\epsilon(a_1 \hat{\rho}_0^1 - \hat{\rho}_1^0 a_1^\dagger) = 0. \quad (2.14d)$$

Notice that Eq.(2.14d) has an equality, because all terms are of the same order, therefore they all contribute. At this point, it is possible to solve these equations starting with  $\hat{\rho}_0^0$  from top and proceeding to bottom.

Since the problem is solved numerically, it is easier to reformulate it within the Liouville space, where  $|\hat{\rho}_0^0\rangle\rangle$  is the zero eigenvector of the (square) matrix  $\mathcal{L}_0$ , which therefore corresponds to steady state of the system without any sensor. The remaining equations can be solved as:

$$|\hat{\rho}_1^0\rangle\rangle \sim \frac{i\epsilon a_1 |\hat{\rho}_0^0\rangle\rangle}{\mathcal{L}_0 - (\Gamma_1/2 + i\omega_1)\mathbb{1}} \quad (2.15a)$$

$$|\hat{\rho}_1^1\rangle\rangle = \frac{i\epsilon (a_1 |\hat{\rho}_0^1\rangle\rangle - |\hat{\rho}_1^0\rangle\rangle a_1^\dagger)}{\mathcal{L}_0 - \Gamma_1 \mathbb{1}}, \quad (2.15b)$$

where  $a_1$  and  $a_1^\dagger$  are written in the Liouville space form, and  $\mathbb{1}$  is the identity operator in the emitter Hilbert space. There is no need to solve for  $\hat{\rho}_0^1$  since it is equal to  $\hat{\rho}_1^0 \dagger$ . In Eq.(2.15)  $\hat{\rho}_1^0$  depends on  $\epsilon$  and  $\hat{\rho}_1^1$  on  $\epsilon^2$ . As the power spectrum in Eq.(2.7) has a prefactor  $1/\epsilon^2$ , in this expression the dependence on  $\epsilon$  disappears algebraically, so the numerical computation does not rely on the value of the coupling parameter. In principle, this numerical calculation of the matrices given by Eqs.(2.15) could be evaluated using a small value for  $\epsilon$ . However, this could lead to numerical instabilities due to the smallness of  $\epsilon$ . With our procedure, instead, such instabilities do not occur thanks to the re-scaled matrices  $\tilde{\rho}_{j_1}^{j_1'} = \hat{\rho}_{j_1}^{j_1'}/\epsilon^{j_1+j_1'}$  (such that  $\tilde{\rho}_1^0 = \hat{\rho}_1^0/\epsilon$  and  $\tilde{\rho}_1^1 = \hat{\rho}_1^1/\epsilon^2$ ), which are now  $\epsilon$ -independent system operators.

The power spectrum is finally given by:

$$S_{\Gamma_1}(\omega_1) = \frac{\Gamma_1}{2\pi} \text{Tr}[\tilde{\rho}_1^1], \quad (2.16)$$

where  $\tilde{\rho}_{j_1}^{j_1'} = \hat{\rho}_{j_1}^{j_1'} / \epsilon^{j_1+j_1'}$ .

The substitution of Eq.(2.15) in Eq.(2.16) gives a semi-analytical expression comparable to that obtained in Ref. [125] for the one-photon spectrum, but in our case it is generalised to any open quantum system dynamics described by a superoperator  $\mathcal{L}_0$ . In addition, the hierarchical set of equations in Eq.(2.15) provides some physical insight on how the sensors are able to measure statistical properties of the light emitted by the system in the steady state  $\hat{\rho}_0^0$ . Indeed, the emission operator  $a_1$  ( $a_1^\dagger$ ) acts on an ‘‘auxiliary state’’  $\hat{\rho}_0^1(\hat{\rho}_1^0)$ , which in turn contains information about the emitted transitions filtered at frequency  $\omega_1$ .

### 2.3.2 $M = 2$ : zero-delay correlations

We now focus our attention to the zero time delay second order correlation function ( $M = 2$ ), which is given by:

$$g_{\Gamma_1\Gamma_2}^{(2)}(\omega_1, \omega_2) = \frac{S_{\Gamma_1, \Gamma_2}^{(2)}(\omega_1, \omega_2)}{S_{\Gamma_1}^{(1)}(\omega_1) S_{\Gamma_2}^{(1)}(\omega_2)}, \quad (2.17)$$

where  $S_{\Gamma_1}(\omega_1)$  and  $S_{\Gamma_2}(\omega_2)$  are the mean count rates for the two sensors, as given in Eq.(2.16), and

$$S_{\Gamma_1, \Gamma_2}^{(2)}(\omega_1, \omega_2) = \frac{\Gamma_1 \Gamma_2}{(2\pi)^2 \epsilon^4} \langle : n_1 n_2 : \rangle. \quad (2.18)$$

When the photon correlations do not depend on time, the sensor operators  $n_j$  commute, meaning that normal order in Eq.(2.18) is not necessary. Proceeding as we did before, this time including two sensors, the steady state density matrix can be written as:

$$\hat{\rho}_{ss} = \sum_{j_1, j_2, j_1', j_2'=0,1} \hat{\rho}_{j_1, j_2}^{j_1', j_2'} \otimes |j_1\rangle \langle j_1'| \otimes |j_2\rangle \langle j_2'|, \quad (2.19)$$

where  $\{j_1, j_1'\}$  and  $\{j_2, j_2'\}$  are counters over the states of sensor 1 and sensor 2, respectively. Again, the matrices  $\hat{\rho}_{j_1, j_2}^{j_1', j_2'} = \langle j_1 j_2 | \hat{\rho}_{ss} | j_1' j_2' \rangle$  are defined in the Hilbert space of the emitting system only. This definition leads to the following form of the second-order photon coincidence:

$$S_{\Gamma_1, \Gamma_2}^{(2)}(\omega_1, \omega_2) = \frac{\Gamma_1 \Gamma_2}{(2\pi)^2} \text{Tr} \left[ \tilde{\rho}_{1,1}^{1,1} \right], \quad (2.20)$$

with the power spectrum given by

$$S_{\Gamma_1}^{(1)}(\omega_1) = \frac{\Gamma_1}{2\pi} \text{Tr}[\tilde{\rho}_{1,0}^{1,0}] \quad , \quad S_{\Gamma_2}^{(1)}(\omega_2) = \frac{\Gamma_2}{2\pi} \text{Tr}[\tilde{\rho}_{0,1}^{0,1}], \quad (2.21)$$

where  $\tilde{\rho}_{j_1, j_2}^{j'_1, j'_2} = \hat{\rho}_{j_1, j_2}^{j'_1, j'_2} / \epsilon^{j_1 + j'_1 + j_2 + j'_2}$ . To compute the matrices  $\tilde{\rho}_{j_1, j_2}^{j'_1, j'_2}$ , we need to solve the equation for the steady state  $\mathcal{L}(\hat{\rho}_{ss}) = 0$  with two sensors. Again, the prefactor for  $|j_1\rangle \langle j'_1| \otimes |j_2\rangle \langle j'_2|$  includes only terms  $\hat{\rho}_{\ell_1, \ell_2}^{\ell'_1, \ell'_2}$  such that  $\ell_1 + \ell_2 + \ell'_1 + \ell'_2 \leq j_1 + j_2 + j'_1 + j'_2$ . This means we discard matrices depending on powers of  $\epsilon$  higher than those in the matrix in question. The hierarchical set of linearly dependent equations, not including those that are Hermitian conjugates of others, results:

$$\mathcal{L}_0(\tilde{\rho}_{0,0}^{0,0}) \simeq 0 \quad (2.22a)$$

$$[\mathcal{L}_0 - \frac{\Gamma_1}{2} - i\omega_1](\tilde{\rho}_{1,0}^{0,0}) \simeq ia_1 \tilde{\rho}_{0,0}^{0,0} \quad (2.22b)$$

$$[\mathcal{L}_0 - \frac{\Gamma_2}{2} - i\omega_2](\tilde{\rho}_{0,1}^{0,0}) \simeq ia_2 \tilde{\rho}_{0,0}^{0,0} \quad (2.22c)$$

$$[\mathcal{L}_0 - \Gamma_1](\tilde{\rho}_{1,0}^{1,0}) \simeq i(a_1 \tilde{\rho}_{0,0}^{1,0} - \tilde{\rho}_{1,0}^{0,0} a_1^\dagger) \quad (2.22d)$$

$$[\mathcal{L}_0 - \Gamma_2](\tilde{\rho}_{0,1}^{0,1}) \simeq i(a_2 \tilde{\rho}_{0,0}^{0,1} - \tilde{\rho}_{0,1}^{0,0} a_2^\dagger) \quad (2.22e)$$

$$[\mathcal{L}_0 - \frac{\Gamma_2 + \Gamma_1}{2} - i(\omega_1 + \omega_2)](\tilde{\rho}_{1,1}^{0,0}) \simeq i(a_1 \tilde{\rho}_{0,1}^{0,0} + a_2 \tilde{\rho}_{1,0}^{0,0}) \quad (2.22f)$$

$$[\mathcal{L}_0 - \frac{\Gamma_2 + \Gamma_1}{2} - i(\omega_1 - \omega_2)](\tilde{\rho}_{1,0}^{0,1}) \simeq i(a_1 \tilde{\rho}_{0,0}^{0,1} - \tilde{\rho}_{1,0}^{0,0} a_2^\dagger) \quad (2.22g)$$

$$[\mathcal{L}_0 - (\frac{\Gamma_1}{2} + \Gamma_2) - i\omega_1](\tilde{\rho}_{1,1}^{0,1}) \simeq i(a_1 \tilde{\rho}_{0,1}^{0,1} + a_2 \tilde{\rho}_{1,0}^{0,1} - \tilde{\rho}_{1,1}^{0,0} a_2^\dagger) \quad (2.22h)$$

$$[\mathcal{L}_0 - (\frac{\Gamma_2}{2} + \Gamma_1) - i\omega_2](\tilde{\rho}_{1,1}^{1,0}) \simeq i(a_1 \tilde{\rho}_{0,1}^{1,0} - \tilde{\rho}_{1,1}^{0,0} a_1^\dagger + a_2 \tilde{\rho}_{1,0}^{1,0}) \quad (2.22i)$$

$$[\mathcal{L}_0 - (\Gamma_1 + \Gamma_2)](\tilde{\rho}_{1,1}^{1,1}) = i(a_1 \tilde{\rho}_{0,1}^{1,1} - \tilde{\rho}_{1,1}^{0,1} a_1^\dagger + a_2 \tilde{\rho}_{1,0}^{1,1} - \tilde{\rho}_{1,1}^{0,0} a_2^\dagger). \quad (2.22j)$$

In a similar way,  $|\tilde{\rho}_{0,0}^{0,0}\rangle\rangle$  is the eigenvector with zero eigenvalue for  $\mathcal{L}_0$  and corresponds to the steady state of the system without any coupling to the sensors. The solutions

for the matrices, in analogy to those in Eq.(2.15), are the following:

$$|\tilde{\rho}_{1,0}^{0,0}\rangle\rangle \simeq \frac{ia_1|\tilde{\rho}_{0,0}^{0,0}\rangle\rangle}{\mathcal{L}_0 - (i\omega_1 + \Gamma_1/2)\mathbb{1}}, \quad (2.23a)$$

$$|\tilde{\rho}_{0,1}^{0,0}\rangle\rangle \simeq \frac{ia_2|\tilde{\rho}_{0,0}^{0,0}\rangle\rangle}{\mathcal{L}_0 - (i\omega_2 + \Gamma_2/2)\mathbb{1}}, \quad (2.23b)$$

$$|\tilde{\rho}_{1,0}^{1,0}\rangle\rangle \simeq \frac{i(a_1|\tilde{\rho}_{0,0}^{1,0}\rangle\rangle - |\tilde{\rho}_{1,0}^{0,0}\rangle\rangle a_1^\dagger)}{\mathcal{L}_0 - \Gamma_1\mathbb{1}}, \quad (2.23c)$$

$$|\tilde{\rho}_{0,1}^{0,1}\rangle\rangle \simeq \frac{i(a_2|\tilde{\rho}_{0,0}^{0,1}\rangle\rangle - |\tilde{\rho}_{0,1}^{0,0}\rangle\rangle a_2^\dagger)}{\mathcal{L}_0 - \Gamma_2\mathbb{1}}, \quad (2.23d)$$

$$|\tilde{\rho}_{1,1}^{0,0}\rangle\rangle \simeq \frac{i(a_1|\tilde{\rho}_{0,1}^{0,0}\rangle\rangle - a_2|\tilde{\rho}_{1,0}^{0,0}\rangle\rangle)}{\mathcal{L}_0 - (i\omega_1 + i\omega_2 + \Gamma_1/2 + \Gamma_2/2)\mathbb{1}}, \quad (2.23e)$$

$$|\tilde{\rho}_{1,0}^{0,1}\rangle\rangle \simeq \frac{i(a_1|\tilde{\rho}_{0,0}^{0,1}\rangle\rangle - |\tilde{\rho}_{1,0}^{0,0}\rangle\rangle a_2^\dagger)}{\mathcal{L}_0 - (i\omega_1 - i\omega_2 + \Gamma_1/2 + \Gamma_2/2)\mathbb{1}}, \quad (2.23f)$$

$$|\tilde{\rho}_{1,1}^{0,1}\rangle\rangle \simeq \frac{i(a_1|\tilde{\rho}_{0,1}^{0,1}\rangle\rangle + a_2|\tilde{\rho}_{1,0}^{0,1}\rangle\rangle - |\tilde{\rho}_{1,1}^{0,0}\rangle\rangle a_2^\dagger)}{\mathcal{L}_0 - (i\omega_1 + \Gamma_1/2 + \Gamma_2)\mathbb{1}}, \quad (2.23g)$$

$$|\tilde{\rho}_{1,1}^{1,0}\rangle\rangle \simeq \frac{i(a_1|\tilde{\rho}_{0,1}^{1,0}\rangle\rangle - |\tilde{\rho}_{1,1}^{0,0}\rangle\rangle a_1^\dagger + a_2|\tilde{\rho}_{1,0}^{1,0}\rangle\rangle)}{\mathcal{L}_0 - (i\omega_2 + \Gamma_2/2 + \Gamma_1)\mathbb{1}}, \quad (2.23h)$$

$$|\tilde{\rho}_{1,1}^{1,1}\rangle\rangle = \frac{i(a_1|\tilde{\rho}_{0,1}^{1,1}\rangle\rangle - |\tilde{\rho}_{1,1}^{0,1}\rangle\rangle a_1^\dagger + a_2|\tilde{\rho}_{1,0}^{1,1}\rangle\rangle - |\tilde{\rho}_{1,1}^{1,0}\rangle\rangle a_2^\dagger)}{\mathcal{L}_0 - (\Gamma_1 + \Gamma_2)\mathbb{1}}. \quad (2.23i)$$

Our derivation agrees with previous results [125], in fact, if we replace Eqs.(2.23i) in Eq.(2.20), it is possible to find an analytical expression comparable to that presented in [125] for the two-photon spectrum at zero time delay.

The coupled set of equations in Eq.(2.23) and, in particular, the compact form obtained for the relevant matrix  $\tilde{\rho}_{1,1}^{1,1}$  in Eq.(2.23i), give some insight into the physical meaning of measuring the second order correlations through the sensors weakly coupled to the system. The sensors populations (given by  $\text{Tr}[\tilde{\rho}_{1,1}^{1,1}]$ ) contain the action of the emission operators on “auxiliary conditional states”, in particular  $a_1$  on  $\tilde{\rho}_{0,1}^{1,1}$  and  $a_2$  on  $\tilde{\rho}_{1,0}^{1,1}$ . These “auxiliary conditional states” carry information about the correlations between the transitions of the system steady state  $\tilde{\rho}_{0,0}^{0,0}$ , probed at frequencies  $\omega_1$  and  $\omega_2$ .

### 2.3.3 $M > 2$ : numerical procedure to compute zero time delay correlations at higher orders

Our method allows also to compute photon correlations at zero time delay of orders higher than the second, providing a compact form of the hierarchical set of equations. The first step is to write the general steady state for the system-plus-sensors in an

analogous form of Eqs. (2.6) and (2.19):

$$\hat{\rho}_{ss} = \sum_{j_1, j'_1, \dots, j_M, j'_M=0,1} \hat{\rho}_{j_1 \dots j_m \dots j_M}^{j'_1 \dots j'_m \dots j'_M} \otimes |j_1\rangle \langle j'_1| \otimes \dots \otimes |j_M\rangle \langle j'_M|. \quad (2.24)$$

where  $\{j_m, j'_m\}$  are counters over the state of sensor  $m$  and

$$\hat{\rho}_{j_1 \dots j_m \dots j_M}^{j'_1 \dots j'_m \dots j'_M} = \langle j_1 \dots j_m \dots j_M | \hat{\rho}_{ss} | j'_1 \dots j'_m \dots j'_M \rangle.$$

The  $M$ th order photon-coincidence at  $\tau = 0$  is given in terms of the trace of matrix with  $j_m = j'_m = 1$  for all  $m$  as follows:

$$S_{\Gamma_1 \dots \Gamma_M}^{(M)}(\omega_1, \dots, \omega_M) = \frac{\Gamma_1 \dots \Gamma_m \dots \Gamma_M}{(2\pi)^M} \text{Tr} \left[ \tilde{\rho}_{1 \dots 1 \dots 1}^{1 \dots 1 \dots 1} \right]. \quad (2.25)$$

The power spectrum for each sensor  $m$ , instead, is given by the trace of the matrix with  $j_m = j'_m = 1$  for  $m$  and  $j_y = j'_y = 0$  from  $y \neq m$ :

$$S_{\Gamma_m}^{(1)}(\omega_m) = \frac{\Gamma_m}{2\pi} \text{Tr} \left[ \tilde{\rho}_{0 \dots 1 \dots 0}^{0 \dots 1 \dots 0} \right], \quad (2.26)$$

where  $\tilde{\rho}_{j_1 \dots j_m \dots j_M}^{j'_1 \dots j'_m \dots j'_M} = \hat{\rho}_{j_1 \dots j_m \dots j_M}^{j'_1 \dots j'_m \dots j'_M} / e^{j_1 + j'_1 + \dots + j_m + j'_m + \dots + j_M + j'_M}$ . The matrices  $\tilde{\rho}_{j_1 \dots j_m \dots j_M}^{j'_1 \dots j'_m \dots j'_M}$  satisfy the following general equation in the steady state  $\mathcal{L}(\hat{\rho}_{ss}) = 0$ :

$$\left[ \mathcal{L}_0 - \sum_{m=1}^M \left\{ (j_m + j'_m) \Gamma_m / 2 + (j_m - j'_m) i \omega_m \right\} \right] \tilde{\rho}_{j_1 \dots j_m \dots j_M}^{j'_1 \dots j'_m \dots j'_M} = i \sum_{m=1}^M \left[ \delta_{j_m, 1} a_m \tilde{\rho}_{j_1 \dots j_m(1-\delta_{j_m,1}) \dots j_M}^{j'_1 \dots j'_m \dots j'_M} - \delta_{j'_m, 1} \tilde{\rho}_{j_1 \dots j_m \dots j_M}^{j'_1 \dots j'_m(1-\delta_{j'_m,1}) \dots j'_M} a_m^\dagger \right], \quad (2.27)$$

where  $\delta_{u,v}$  is the Kronecker delta function, equal to zero if  $u \neq v$  or 1 if  $u = v$ . The starting point to derive Eq.(2.27) is to see that in Eq.(2.24), the  $M$ th order photon correlation at zero time delay for the emitter-plus- $M$  sensors system depends on the rescaled matrix  $\tilde{\rho}_{1 \dots 1}^{1 \dots 1} = \langle 1_1, \dots, 1_M | \hat{\rho}_{ss} | 1_1, \dots, 1_M \rangle$ . This matrix can be obtained solving the equation for the steady state  $\mathcal{L}(\hat{\rho}_{ss}) = 0$  which can be written in analogy to Eq.(2.11):

$$\mathcal{L}(\hat{\rho}_{ss}) = \sum_{j_1, j'_1, \dots, j_M, j'_M} \hat{B}_{j_1 \dots j_m \dots j_M}^{j'_1 \dots j'_m \dots j'_M} \otimes |j_1\rangle \langle j'_1| \dots \otimes |j_m\rangle \langle j'_m| \dots \otimes |j_M\rangle \langle j'_M| = 0. \quad (2.28)$$

The hierarchy of equations satisfying  $\hat{B}_{j_1 \dots j_m \dots j_M}^{j'_1 \dots j'_m \dots j'_M} = \mathbf{0}$  can be derived using the approximation that neglects the down coupling, as previously explained. This leads to a set satisfied by the matrices  $\tilde{\rho}_{j_1 \dots j_m \dots j_M}^{j'_1 \dots j'_m \dots j'_M}$ . A careful look at the expressions in Eq.(2.14) and Eq.(2.22) allows to derive a general form for such a set. Let us indicate with  $J = j_1 + j'_1 + \dots + j_m + j'_m \dots + j_M + j'_M$  the sum of all matrix indices. For  $J = 0$  the solution is simply given by  $\mathcal{L}_0 \left( \tilde{\rho}_{0, \dots, 0}^{0, \dots, 0} \right) \sim 0$ . More in general, the form for the left hand side terms for each equation is given by

$$\left[ \mathcal{L}_0 - \sum_{m=1}^M \{ (j_m + j'_m) \Gamma_m / 2 + (j_m - j'_m) i \omega_m \} \right] \tilde{\rho}_{j_1 \dots j_m \dots j_M}^{j'_1 \dots j'_m \dots j'_M}. \quad (2.29)$$

This term represents the evolution under the Liouvillian of the emitter and the decay and phase evolution of the sensors. Each matrix with  $J \geq 1$  is coupled only to matrices with  $J - 1$ . Therefore the solution of the  $J = 2M$  matrix  $\tilde{\rho}_{1, \dots, 1}^{1, \dots, 1}$  contains only matrices with  $J = 2M - 1$  and so on (cf. Eq.(2.22)). The total number of tier-below matrices required equals  $J$  and each of these matrices differs only in one index  $j_m$  or  $j'_m$ , which will be 0 rather than unity. Let us call this tier-below matrices  $\tilde{\rho}_{\ell_1 \dots \ell_m \dots \ell_M}^{\ell'_1 \dots \ell'_m \dots \ell'_M}$ . The matrix that differs in the  $m$ th component such that  $j_m = 1$  and  $\ell_m = 0$ , with all others equal, will add a term of the form  $i a_m \tilde{\rho}_{j_1 \dots j_m=0 \dots j_M}^{j'_1 \dots j'_m \dots j'_M}$ . Likewise, if  $j'_m = 1$  but  $\ell'_m = 0$  and  $\ell'_y = j'_y$  and  $\ell_y = j_y$  for  $y \neq m$ , we have a contribution of the form  $-i \tilde{\rho}_{j_1 \dots j_m \dots j_M}^{j'_1 \dots j'_m=0 \dots j'_M} a_m^\dagger$ . Therefore, the right-hand side term, to which Eq.(2.29) is approximated to, will be of the form:

$$i \sum_{m=1}^M \left[ \delta_{j_m, 1} a_m \tilde{\rho}_{j_1 \dots j_m(1-\delta_{j_m, 1}) \dots j_M}^{j'_1 \dots j'_m \dots j'_M} - \delta_{j'_m, 1} \tilde{\rho}_{j_1 \dots j_m \dots j_M}^{j'_1 \dots j'_m(1-\delta_{j'_m, 1}) \dots j'_M} a_m^\dagger \right] \quad (2.30)$$

where  $\delta_{u,v}$  is the Kronecker delta function, equal to zero if  $u \neq v$  or unity if  $u = v$ .

The importance of this result lies in the fact that it depends only on the Liouvillian  $\mathcal{L}_0$  of the emitting system and, therefore, allows for computation of the frequency-filtered multi-photon correlations that scale efficiently with the dimension of the emitter Hilbert space. This represents an important advantage for quantum emitters where the dimension of the Hilbert space is large, such as multi-chromophoric complexes [45]. Moreover, although we have supposed a Lindblad form for  $\mathcal{L}_0$  (see Eq.(2.2)), the expression in Eq.(2.27) does not explicitly depend on this assumption. In the Supplemental Material of [46] it was shown the equivalence between the sensor method and the integral method within systems undergoing

Markovian dynamics, where the quantum regression theorem is applicable. However, a proof of this equivalence beyond the Markovian and quantum regression restriction would allow to use our result in Eq.(2.27) for open quantum systems undergoing non-Markovian dynamics.

## 2.4 Frequency-filtered correlations at finite delay time

For the calculation of the photon correlation functions at finite time delay we will use time-dependent perturbation theory, focusing on the second order correlation  $g_{\Gamma_1\Gamma_2}^{(2)}(\omega_1, T; \omega_2, T + \tau)$ . In the steady state  $\hat{\rho}_{ss}$  there is no explicit dependence on time  $T$ , hence the photon correlation can be rewritten as  $g_{\Gamma_1\Gamma_2}^{(2)}(\omega_1, \omega_2, \tau)$ . In terms of the sensor operators, it becomes

$$g_{\Gamma_1\Gamma_2}^{(2)}(\omega_1, \omega_2, \tau) = \frac{S_{\Gamma_1, \Gamma_2}^{(2)}(\omega_1, \omega_2, \tau)}{S_{\Gamma_1}^{(1)}(\omega_1) S_{\Gamma_2}^{(1)}(\omega_2)}, \quad (2.31)$$

where the numerator has the form

$$S_{\Gamma_1, \Gamma_2}^{(2)}(\omega_1, \omega_2, \tau) = \frac{\Gamma_1 \Gamma_2}{(2\pi)^2 \epsilon^4} \langle \varsigma_1^\dagger \varsigma_2^\dagger(\tau) \varsigma_2(\tau) \varsigma_1 \rangle \quad (2.32)$$

and the functions in the denominator are given in Eq.(2.21). To obtain our result, we start from correlations in Eq.(2.32) at positive times  $\tau > 0$ , meaning that sensor 1 records the first detection, followed by sensor 2 that does the same after a time  $\tau$ . Here the normal time ordering is of crucial importance as the sensor operators do not commute at different times. Correlations for negative times  $\tau < 0$  can be recovered by exchanging  $\varsigma_1 \rightarrow \varsigma_2$  and  $\varsigma_2(\tau) \rightarrow \varsigma_1(\tau)$ . In Liouville space the correlation function in Eq.(2.32) can be expressed as

$$\begin{aligned} \langle \varsigma_1^\dagger \varsigma_2^\dagger(\tau) \varsigma_2(\tau) \varsigma_1 \rangle &= \text{Tr}\{\varsigma_2^\dagger \varsigma_2 \mathcal{G}(\tau) \varsigma_1 \hat{\rho}_{ss} \varsigma_1^\dagger\} \\ &\equiv \langle\langle \varsigma_2^\dagger \varsigma_2 | \mathcal{G}(\tau) \varsigma_1 \hat{\rho}_{ss} \varsigma_1^\dagger \rangle\rangle, \end{aligned} \quad (2.33)$$

where  $\mathcal{G}(\tau) = \exp(\mathcal{L}\tau)$  is the time propagator operator for the entire system including the sensors, and  $\mathcal{L}$  is given in Eq.(2.1). The term  $\varsigma_1 \hat{\rho}_{ss} \varsigma_1^\dagger$  represents the initial condition, where sensor 1 detects a photon, decaying then to its ground state and leaving the emitter and sensor 2 in a joint “conditional state” of the form:

$$\hat{\rho}(0) = \varsigma_1 \hat{\rho}_{ss} \varsigma_1^\dagger = \sum_{j_2, j'_2=0,1} \hat{\rho}_{1,j_2}^{1,j'_2} \otimes |j_2\rangle \langle j'_2| \otimes |0_1\rangle \langle 0_1|. \quad (2.34)$$

Notice that  $\hat{\rho}(0)$  is not normalised but has a trace equal to  $\langle \varsigma_1^\dagger \varsigma_1 \rangle$ . We can define

$$|\hat{\rho}(\tau)\rangle\rangle = \mathcal{G}(\tau)|\hat{\rho}(0)\rangle\rangle \quad (2.35)$$

with initial condition  $|\hat{\rho}(0)\rangle\rangle = |\varsigma_1 \hat{\rho}_{ss} \varsigma_1^\dagger\rangle\rangle$ . In principle, it would be possible to compute this explicit time-propagation. As sensor 1 is in the ground state, only the interaction Hamiltonian with sensor 2,  $H_{e,2} = \epsilon (a_2 \varsigma_2^\dagger + a_2^\dagger \varsigma_2)$ , affects the dynamics of the whole system, requiring in any case a test for convergence in  $\epsilon$ . However, since the regime under study considers a small value of the coupling parameter  $\epsilon$ , it is possible to analyse such dynamics by using time-dependent perturbation theory with respect to  $H_{e,2}$ . Therefore, we expand  $|\hat{\rho}(\tau)\rangle\rangle$  as in [92]

$$|\hat{\rho}(\tau)\rangle\rangle = |\hat{\rho}^{(0)}(\tau)\rangle\rangle + |\hat{\rho}^{(1)}(\tau)\rangle\rangle + |\hat{\rho}^{(2)}(\tau)\rangle\rangle + \dots \quad (2.36)$$

The zeroth order term corresponds to the dynamics where no interactions happen, that is:

$$|\hat{\rho}^{(0)}(\tau)\rangle\rangle = \mathcal{G}_0(t)|\hat{\rho}(0)\rangle\rangle, \quad (2.37)$$

with  $\mathcal{G}_0(t) = \exp([\mathcal{L}_0 + \mathcal{L}_1 + \mathcal{L}_2]t)$  and  $\mathcal{L}_0, \mathcal{L}_1$  and  $\mathcal{L}_2$  as in Eqs. (2.2) and (2.3). Given the initial condition expressed above, sensor 1 (2) does not contribute to the dynamics for  $\tau > 0$  ( $\tau < 0$ ), hence can be traced over. The  $k$ th order solution implies  $k$  interactions with  $H_{e,2}$ , but time propagation occurs only in terms of  $\mathcal{G}_0(t)$ :

$$|\hat{\rho}^{(k)}(\tau)\rangle\rangle = -i \int_0^\tau dt H_{e,2}^\times \mathcal{G}_0(\tau - t) |\hat{\rho}^{(k-1)}(t)\rangle\rangle, \quad (2.38)$$

where  $H_{e,2}^\times |\rho\rangle\rangle \equiv [H_{e,2}, \rho]$  indicates a commutator in Liouville space. At this point it is appropriate to notice that the initial condition  $\hat{\rho}(0)$  contains  $\hat{\rho}_{1,j_2}^{1,j'_2}$  which has terms of order  $\epsilon^{2+j_2+j'_2}$ , that is, from  $\epsilon^2$  up to  $\epsilon^4$ . This leads to the conclusion that for the computation of the second order correlation function it is sufficient to consider only terms up to second order in the perturbation theory, because two

interactions will bring terms of order  $\epsilon^4$  or higher. In fact, third order perturbation theory would produce terms of order  $\epsilon^5$  or higher, which are negligible by our weak coupling assumption. To clarify even more, for example, to compute the 3rd order correlation function in a three sensors system,  $\hat{\rho}(0)$  would have terms of order  $\epsilon^2$  up to order  $\epsilon^6$ , hence we would need to go up to the 4th order in the time dependent perturbation theory, in order to have four interactions carrying a factor  $\epsilon^4$ .

The time-resolved photon correlation can thus be written as

$$\langle \varsigma_1^\dagger \varsigma_2^\dagger(\tau) \varsigma_2(\tau) \varsigma_1 \rangle = \langle \langle \varsigma_2^\dagger \varsigma_2 | \hat{\rho}(\tau) \rangle \rangle = I_0(\tau) + I_1(\tau) + I_2(\tau), \quad (2.39)$$

where  $I_k(\tau) = \langle \langle \varsigma_2^\dagger \varsigma_2 | \hat{\rho}^{(k)}(\tau) \rangle \rangle = \text{Tr}\{\varsigma_2^\dagger \varsigma_2 \hat{\rho}^{(k)}(\tau)\}$ .

The *zeroth order* term becomes:

$$I_0(\tau) = \langle \langle n_2 | \mathcal{G}_0(\tau) \hat{\rho}(0) \rangle \rangle = e^{-\Gamma_2 \tau} \text{Tr} \left[ \hat{\rho}_{1,1}^{1,1} \right], \quad (2.40)$$

which simplifies to  $I_0(\tau) = \exp(-\Gamma_2 \tau) \langle n_2 n_1 \rangle$ . It is peculiar to observe that this term contains the same information as  $g_{\Gamma_1 \Gamma_2}^{(2)}(0)$  at zero time delay (see Eqs.(2.17) and (2.20)), while the exponential function is connected to the uncertainty in detection time and does not give any information about the emitting system dynamics.

The following term, coming from the *first order* perturbation theory, reads as:

$$I_1(\tau) = -i \int_0^\tau dt_1 \langle \langle n_2 | \mathcal{G}_0(\tau - t_1) H_{e,2}^\times \mathcal{G}_0(t_1) \hat{\rho}(0) \rangle \rangle. \quad (2.41)$$

We proceed considering first the action of  $\mathcal{G}_0(\tau - t_1)$  to the left, which gives  $\langle \langle n_2 | \mathcal{G}_0(\tau - t_1) \rangle \rangle = \langle \langle n_2 | \exp[-\Gamma_2(\tau - t_1)] \rangle \rangle$ . To the right the elements that give contribution are  $a_2 \hat{\rho}_{1,0}^{1,1}(t_1) \exp[-(\Gamma_2/2 + i\omega_2)t_1]$  and  $\hat{\rho}_{1,1}^{1,0}(t_1) a_2^\dagger \exp[-(\Gamma_2/2 - i\omega_2)t_1]$ , with

$$|\hat{\rho}_{1,j_2}^{1,j_2'}(t)\rangle \equiv \Theta[t] \exp(\mathcal{L}_0 t) |\hat{\rho}_{1,j_2}^{1,j_2'}(0)\rangle$$

defined through the evolution of the system only. But these two terms are complex conjugates, therefore it is possible to express them in the form:

$$I_1(\tau) = 2\epsilon \text{Im} \left( \int_0^\tau dt_1 e^{-\Gamma_2(\tau - t_1/2) + i\omega_2 t_1} \text{Tr}[a_2 \hat{\rho}_{1,0}^{1,1}(t_1)] \right). \quad (2.42)$$

This is essentially a finite time Laplace transform of a complex number. Here the density matrix  $\hat{\rho}_{1,0}^{1,1}(t_1)$  evolves under the action of Liouvillian  $\mathcal{L}_0$ .

Finally, the *second order* term,  $I_2(\tau)$ , takes the form:

$$I_2(\tau) = - \int_0^\tau dt_2 \int_0^{t_2} dt_1 \langle\langle n_2 | \mathcal{G}_0(\tau - t_2) H_{e,2}^\times \mathcal{G}_0(t_2 - t_1) H_{e,2}^\times \mathcal{G}_0(t_1) | \hat{\rho}(0) \rangle\rangle. \quad (2.43)$$

Since there are two interactions involved, both  $\hat{\rho}_{1,0}^{1,0} \otimes |0_2\rangle \langle 0_2|$  and  $\hat{\rho}_{1,1}^{1,1} \otimes |1_2\rangle \langle 1_2|$  terms can contribute. However,  $\text{Tr}[\hat{\rho}_{1,1}^{1,1}] \ll \text{Tr}[\hat{\rho}_{1,0}^{1,0}]$ , therefore we have to consider only  $\hat{\rho}_{1,0}^{1,0} \otimes |0_2\rangle \langle 0_2|$  in our initial condition. The second order contribution therefore becomes:

$$\begin{aligned} I_2(\tau) &= -\epsilon^2 \int_0^\tau dt_2 \int_0^{t_2} dt_1 e^{-\Gamma_2(\tau-t_2)} \langle\langle n_2 | a_2 \overleftarrow{S}_2^\dagger \mathcal{G}_0(t_2 - t_1) a_2^\dagger \overleftarrow{S}_2 \mathcal{G}_0(t_1) | \rho(0) \rangle\rangle + h.c. \\ &= -2\epsilon^2 \text{Re} \int_{t_1}^\tau dt_2 \int_0^{t_2} dt_1 e^{-\Gamma_2[\tau-(t_2+t_1)/2] + i\omega_2(t_2-t_1)} \text{Tr}\{a_2(t_2 - t_1) \hat{\rho}_{1,0}^{1,0}(t_1) a_2^\dagger\}, \end{aligned} \quad (2.44)$$

where *h.c.* indicates the Hermitian conjugate,  $\overrightarrow{O}|\rho\rangle\rangle \equiv \hat{O}\hat{\rho}$  and  $\overleftarrow{O}|\rho\rangle\rangle \equiv \hat{\rho}\hat{O}$ .  $a_2(t)$  is written in the Heisenberg picture and represents the time dependent operator, evolving through the adjoint of  $\mathcal{L}_0$ . The double integral is numerically more complex but can be solved.

Eq.(2.32) for the time-resolved photon correlations becomes

$$S_{\Gamma_1, \Gamma_2}^{(2)}(\omega_1, \omega_2, \tau > 0) = \frac{\Gamma_1 \Gamma_2}{(2\pi)^2 \epsilon^4} [I_0(\tau) + I_1(\tau) + I_2(\tau)]. \quad (2.45)$$

Notice that  $I_0(\tau)$ ,  $I_1(\tau)$  and  $I_2(\tau)$  will all feature a prefactor  $\epsilon^4$ . Therefore, the  $\epsilon$  dependence in Eq.(2.45) cancels out algebraically, as expected. The time-resolved photon-coincidence can therefore be written as:

$$S_{\Gamma_1, \Gamma_2}^{(2)}(\omega_1, \omega_2, \tau > 0) = \frac{\Gamma_1 \Gamma_2}{(2\pi)^2} [\tilde{I}_0(\tau) + \tilde{I}_1(\tau) + \tilde{I}_2(\tau)], \quad (2.46)$$

with  $\tilde{I}_k(\tau) = \epsilon^{-4} I_k(\tau)$  the  $k$ th order term, which requires  $k$  interactions with the coupling Hamiltonian  $H_{e,2}$ . The final expression for the second-order correlation at a finite time delay reads:

$$g_{\Gamma_1\Gamma_2}^{(2)}(\omega_1, \omega_2, \tau > 0) = \frac{\tilde{I}_0(\tau) + \tilde{I}_1(\tau) + \tilde{I}_2(\tau)}{\langle \tilde{n}_1 \rangle \langle \tilde{n}_2 \rangle} \quad (2.47)$$

with  $\langle \tilde{n}_1 \rangle = \text{Tr} [\tilde{\rho}_{1,0}^{1,0}]$  and  $\langle \tilde{n}_2 \rangle = \text{Tr} [\tilde{\rho}_{0,1}^{0,1}]$ .

The correlation for  $\tau < 0$  is obtained by taking  $\hat{\rho}(0) = \varsigma_2 \hat{\rho}_{ss} \varsigma_2^\dagger$  and doing time-dependent perturbation theory with respect to  $H_{e,1}$ . This results in making the replacements  $\Gamma_2 \rightarrow \Gamma_1$ ,  $\omega_2 \rightarrow \omega_1$ ,  $a_2 \rightarrow a_1$ ,  $\hat{\rho}_{1,0}^{1,1}(t_1) \rightarrow \hat{\rho}_{0,1}^{1,1}(t_1)$ , and  $\hat{\rho}_{1,0}^{1,0}(t_1) \rightarrow \hat{\rho}_{0,1}^{0,1}(t_1)$  in Eqs.(2.40), (2.42) and (2.44).

At this point it is relevant to underline that, in general, the time-resolved two-photon coincidence can show time asymmetry if the two frequencies detected are different from each other ( $\omega_1 \neq \omega_2$ ), even in the case  $a_1 = a_2$ . This can be seen in the definition of  $I_1$  in Eq.(2.42) and  $I_2$  in Eq.(2.44): both contributions have exponentials in their integrands, depending on  $\omega_2$  or  $\omega_1$  for positive or negative times, respectively. Instead, symmetric time-resolved correlation functions are expected whenever we are in presence of identical system emission operators ( $a_1 = a_2$ ), identical frequencies ( $\omega_1 = \omega_2$ ) and identical sensor decay rates ( $\Gamma_1 = \Gamma_2$ ).

Finally, we want to bring to the attention that the perturbative method used to obtain the second order time-dependent correlation can also be applied in the calculation of higher-order photon correlations when only one sensor has a time delayed detection, i.e.  $g_{\Gamma_1, \dots, \Gamma_m, \dots, \Gamma_M}^{(M)}(\omega_1, \dots, \omega_m, \tau, \dots, \omega_M)$ . However, the generalisation to multiple time delays is more complex. For instance, computation of the 3rd order correlations for different delay times implies the application of second-order perturbation theory with respect to the interactions with sensors 2 and 3,  $H_{e,2}$  and  $H_{e,3}$  respectively, but at different times during the evolution. This implies to solve a four dimensional numerical integration. In this case it is more efficient to compute the auxiliary matrices that define the steady state (see Eq.(2.27)) and propagate in time without perturbation.

### 2.4.1 Behaviours at short time delays

Now we want to analyse the behaviour at short time delay regime. Regarding the first order contribution, as mentioned above, we have:

$$\tilde{I}_0(\tau) \propto e^{-\Gamma_2 \tau} \quad \text{for all } \tau \geq 0 \quad (2.48)$$

meaning that the time dependence simply captures the uncertainty in the detection.

As for the other two contributions, when  $\tau$  is smaller than any relevant system timescale, to lowest order, we obtain:

$$\begin{aligned}\tilde{I}_1(\tau) &\sim 2\tau \operatorname{Im}(\operatorname{Tr}[a_2\tilde{\rho}_{1,0}^{1,1}]) \\ \tilde{I}_2(\tau) &\sim \tau^2 \operatorname{Re}(\operatorname{Tr}[a_2\tilde{\rho}_{1,0}^{1,0}a_2^\dagger])\end{aligned}\tag{2.49}$$

for  $\tau \geq 0$ . Here, the most interesting information is given by the short time behaviour of  $\tilde{I}_2(\tau)$ . In this term, after a first iteration with  $H_{e,2}$  (see Eq.(2.43)), the system evolves in time, thus its short-time behaviour can involve contributions from coherent dynamics inside the excited manifold of the system under scrutiny. Indeed, the proportionality of  $\tilde{I}_2(\tau)$  to  $\tau^2$  hints that quantum speed-up processes can be captured by this function [127].

For  $\tau < 0$ , sensors detect photons in the opposite way (sensor 2 detects the first photon, followed by the detection of an another photon from sensor 1 after a time  $\tau$ ), then we have:

$$\begin{aligned}\tilde{I}_1(\tau) &\sim 2\tau \operatorname{Im}(\operatorname{Tr}\{a_1\tilde{\rho}_{0,1}^{1,1}\}) \\ \tilde{I}_2(\tau) &\sim \tau^2 \operatorname{Re}(\operatorname{Tr}\{a_1\tilde{\rho}_{0,1}^{0,1}a_1^\dagger\})\end{aligned}\tag{2.50}$$

Generally,  $\operatorname{Re}(\operatorname{Tr}\{a_1\tilde{\rho}_{0,1}^{0,1}a_1^\dagger\}) \neq \operatorname{Re}(\operatorname{Tr}\{a_2\tilde{\rho}_{1,0}^{1,0}a_2^\dagger\})$  and analogously  $\operatorname{Im}(\operatorname{Tr}\{a_2\tilde{\rho}_{1,0}^{1,1}\}) \neq \operatorname{Im}(\operatorname{Tr}\{a_1\tilde{\rho}_{0,1}^{1,1}\})$ . Therefore, we expect an asymmetry in  $g_{\Gamma_1, \Gamma_2}^{(2)}(\omega_1, \omega_2, \tau)$  for positive and negative  $\tau$ , even when  $a_1 = a_2$ .

## 2.4.2 Behaviours at large time delays

We now examine the contributions  $\tilde{I}_1(\tau)$  and  $\tilde{I}_2(\tau)$  in the case of  $\tau$  large with respect to the emitter or sensor linewidth timescales. We indicate with  $\gamma_{sys}$  the largest emitter decay rate linked to the field operator  $a_2$ .

In the regime of  $\gamma_{sys} \gg \Gamma_2$  and  $\tau\gamma_{sys} \gg 1$ , we can make the approximation

$$\tilde{I}_1(\tau) \sim 2e^{-\Gamma_2\tau} \operatorname{Im} \left( \int_0^\infty dt_1 e^{+\Gamma_2 t_1/2 + i\omega_2 t_1} \operatorname{Tr}[a_2\tilde{\rho}_{1,0}^{1,1}(t_1)] \right).\tag{2.51}$$

This integral is now independent of  $\tau$  and can be identified as the infinite Laplace transform  $F(s)$  of  $\operatorname{Tr}[a_2\tilde{\rho}_{1,0}^{1,1}(t_1)]$  and  $s = \Gamma_2/2 + i\omega_2$ , i.e.  $\tilde{I}_1(\tau) \sim 2e^{-\Gamma_2\tau} \operatorname{Im}\{F(\Gamma_2/2 + i\omega_2)\}$ , thus time dependence is only due to uncertainty in the detection time. Since  $I_1(0) = 0$ , the contribution  $\tilde{I}_2(\tau)$  undergoes an initial rise, followed by an exponential decay.

On the other hand, if  $\gamma_{sys} \ll \Gamma_2$ ,  $\tilde{\rho}_{1,0}^{1,1}(t)$  can be approximated as having a single dominant coherent transition frequency  $\omega_{sys}$ , namely  $\tilde{\rho}_{1,0}^{1,1}(t) \simeq \exp(+\gamma_{sys}t - i\omega_{sys}t) \tilde{\rho}_{1,0}^{1,1}(0)$ , and slowly varying. Defining  $\tilde{t}_1 = \tau - t_1$ , it is possible to write

$$\tilde{I}_1(\tau) = 2 \operatorname{Im} \left( \int_0^\tau d\tilde{t}_1 e^{-\Gamma_2(\tilde{t}_1+\tau)/2 + i\omega_2(\tilde{t}_1-\tau)} \operatorname{Tr}[a_2 \tilde{\rho}_{1,0}^{1,1}(\tau - \tilde{t}_1)] \right) \quad (2.52)$$

$$\simeq 2 \operatorname{Im} \left( \frac{e^{-(\Gamma_2+\gamma_{sys})\tau/2 - i(\omega_{sys}-\omega_2)\tau} - e^{-\Gamma_2\tau}}{(\Gamma_2 - \gamma_{sys})/2 + i(\omega_2 - \omega_{sys})} \operatorname{Tr}[a_2 \tilde{\rho}_{1,0}^{1,1}(\tau)] \right), \quad (2.53)$$

where, by assumption, the dominant term is the numerator of the fraction resulting in a damped oscillatory function. The approximation of a single frequency cannot be applied when the sensor linewidth is smaller than the emission spectrum.

We expect  $g_{\Gamma_1, \Gamma_2}^{(2)}(\omega_1, \omega_2, \tau) \rightarrow 1$  when  $\Gamma_2\tau \gg 1$  and  $\gamma_{sys}\tau \gg 1$ . Since  $\tilde{I}_0(\tau)$  and  $\tilde{I}_1(\tau)$  decay exponentially in this regime,  $\tilde{I}_2(\tau)$  has to tend to a constant value. To see this, it is possible to rewrite  $\tilde{I}_2$  in terms of  $\tilde{t}_1 = \tau - (t_2 + t_1)/2$  and  $\tilde{t}_2 = t_2 - t_1$  as

$$\tilde{I}_2(\tau) = 2\operatorname{Re} \int_0^\tau d\tilde{t}_2 \int_0^{\tau-\tilde{t}_2/2} d\tilde{t}_1 e^{-\Gamma_2\tilde{t}_1 + i\omega_2\tilde{t}_2} \operatorname{Tr}[a_2(\tilde{t}_2) \tilde{\rho}_{1,0}^{1,0}(\tau - \tilde{t}_1 - \tilde{t}_2/2) a_2^\dagger]. \quad (2.54)$$

As  $\tau \rightarrow \infty$ ,  $\tilde{\rho}_{1,0}^{1,0}(\tau)$  will approach the form of the original steady state for the emitter, therefore it is possible to write  $\tilde{\rho}_{1,0}^{1,0}(\tau - \tilde{t}_1/2 - \tilde{t}_2) \rightarrow \langle \tilde{n}_1 \rangle [\tilde{\rho}_{0,0}^{0,0} - \Delta\tilde{\rho}_{ss}(\tau - \tilde{t}_1/2 - \tilde{t}_2)]$ . The trace of the difference term  $\Delta\rho_{ss}$  is expected to be exponentially small when  $\tau \rightarrow \infty$ , and the variation in terms of  $\tilde{t}_1$  and  $\tilde{t}_2$  to be slow enough to be neglected. Therefore the integral over  $\tilde{t}_1$  can be taken to obtain

$$\tilde{I}_2(\tau) \sim \frac{2\langle \tilde{n}_1 \rangle}{\Gamma_2} \operatorname{Re} \int_0^\tau d\tilde{t}_2 \left( 1 - e^{-\Gamma_2(\tau-\tilde{t}_2/2)} \right) e^{+i\omega_2\tilde{t}_2} \operatorname{Tr} \left[ a_2(\tilde{t}_2) \{ \tilde{\rho}_{0,0}^{0,0} - \Delta\tilde{\rho}_{ss}(\tau - \tilde{t}_2/2) \} a_2^\dagger \right]. \quad (2.55)$$

Taking the integral over  $\tilde{t}_2$  to infinity (assuming  $\gamma_{sys}\tau \gg 1$ ), the term dependent on  $\tilde{\rho}_{0,0}^{0,0}$  will tend to  $\langle \tilde{n}_1 \rangle \langle \tilde{n}_2 \rangle$  and the remainder term, which is a function of  $\Delta\tilde{\rho}_{ss}(\tau - \tilde{t}_2/2)$ , will tend to zero, giving  $g_{\Gamma_1, \Gamma_2}^{(2)}(\omega_1, \omega_2, \tau) \rightarrow 1$ . Assuming  $\Delta\tilde{\rho}_{ss}(t)$  does not have rapidly oscillating components, we expect Eq.(2.55) to be a good general approximation for a wide range of  $\tau$ .

## 2.5 Consistency check about the equivalence of the sensor and the integral methods

As part of this project, we also wanted to carry out a consistency check concerning the equivalence between the original sensor method and the integral method. Therefore, before applying our procedure to compute frequency-filtered and time-resolved photon correlations to a biological toy model, we wish to underline the reasons why the normal and time ordering in Eq.(2.32) are essential to guarantee physical results.

We start considering Eq.(42) in the Supplemental Material of Ref. [46, 47]:

$$\partial_\tau \langle n_1(0)n_2(\tau) \rangle = -\Gamma_2 \langle n_1(0)n_2(\tau) \rangle + 2\text{Re}[i\epsilon_2 \langle n_1(0)(c_2 a^\dagger)(\tau) \rangle], \quad (2.56)$$

where  $n_j = \varsigma_j^\dagger \varsigma_j$  is the sensor number operator and  $\langle n_1(0)n_2(\tau) \rangle \equiv \text{Tr}[n_2(\tau)\hat{\rho}_{ss}n_1]$ . The equation written in this way does not contain the normal order of the operators, leading to implausible results, such as negative values in  $g_{\Gamma_1\Gamma_2}^{(2)}(\omega_1, \omega_2, \tau)$ . To see this, we write the steady state density matrix for the whole emitter-plus-sensors system as in Eq.(2.19). In this way the difference between using or not normally ordered operators becomes immediately evident:

$$\varsigma_1 \hat{\rho}_{ss} \varsigma_1^\dagger = \sum_{j_2, j_2'=0,1} \hat{\rho}_{1,j_2}^{1,j_2'} \otimes |j_2\rangle \langle j_2'| \otimes |0_1\rangle \langle 0_1| \quad (2.57)$$

$$\hat{\rho}_{ss} \varsigma_1^\dagger \varsigma_1 = \sum_{j_2, j_2'=0,1} |j_2\rangle \langle j_2'| \otimes \left( \hat{\rho}_{1,j_2}^{1,j_2'} \otimes |1_1\rangle \langle 1_1| + \hat{\rho}_{0,j_2}^{1,j_2'} \otimes |0_1\rangle \langle 1_1| \right). \quad (2.58)$$

First of all, it is worth to mention that, even if the two expressions above are different, they have equal traces, i.e.  $\text{Tr}[n_2 \hat{\rho}_{ss} n_1] = \text{Tr}[n_2 \varsigma_1 \hat{\rho}_{ss} \varsigma_1^\dagger]$ , implying that at  $\tau = 0$  the normal order for computation of the second-order photon counting statistics is not necessary. However, the difference in these expressions does affect the correlations at finite delay times  $\tau \neq 0$ . The second expression, which does not involve the normal order, has the term  $\hat{\rho}_{1,j_2}^{1,j_2'} \otimes |1_1\rangle \langle 1_1|$  rather than  $\hat{\rho}_{1,j_2}^{1,j_2'} \otimes |0_1\rangle \langle 0_1|$  in the first one. It also contains an additional term  $\hat{\rho}_{0,j_2}^{1,j_2'} \otimes |0_1\rangle \langle 1_1|$ , which makes the expression not Hermitian (the Hermitian conjugate term with  $|1_1\rangle \langle 0_1|$  vanishes due to the action of  $n_1$ ).

The effect of this difference appears more visible when we consider the mean value  $\langle n_1(0)n_2(\tau) \rangle \equiv \text{Tr}[n_2(\hat{\rho}_{ss}n_1)(\tau)]$ . Indeed, this equation shows that the population of sensor 1 decays exponentially in time with a rate  $\Gamma_1$ . In terms of derivatives in  $\tau$  this implies that the term  $\hat{\rho}_{1,j_2}^{1,j_2'} \otimes |j_2\rangle \langle j_2'|$  in  $(\hat{\rho}_{ss} \varsigma_1^\dagger \varsigma_1)(\tau)$  receives an extra factor  $-\Gamma_1$  when compared to those in  $(\varsigma_1 \hat{\rho}_{ss} \varsigma_1^\dagger)(\tau)$ , which is not included in Eq.(2.56). This already disproves Eq.(2.56).

On the other hand, a similar equation that involves the use of the normal order is valid:

$$\partial_\tau \langle \varsigma_1^\dagger(0) n_2(\tau) \varsigma_1(0) \rangle = -\Gamma_2 \langle \varsigma_1^\dagger(0) n_2(\tau) \varsigma_1(0) \rangle + 2\text{Re}[i\epsilon_2 \langle \varsigma_1^\dagger(0) (\varsigma_2 a^\dagger)(\tau) \varsigma_1(0) \rangle] + O(\epsilon_1^2, \epsilon_2^2). \quad (2.59)$$

The solution of this normally ordered derivative in  $\tau$  can be obtained starting from a vector similar to  $\mathbf{w}'[11, \mu_2 \nu_2](\tau)$  given in Eq.(43) in the Supplemental Material of [46, 47] but that carries the normal order:

$$\tilde{\mathbf{w}}[11, \mu_2 \nu_2](\tau) = \begin{bmatrix} \langle \varsigma_1^\dagger (\varsigma_2^{\dagger, \mu_2} \varsigma_2^{\nu_2}) (\tau) \varsigma_1 \rangle \\ \langle \varsigma_1^\dagger (\varsigma_2^{\dagger, \mu_2} \varsigma_2^{\nu_2} a) (\tau) \varsigma_1 \rangle \\ \langle \varsigma_1^\dagger (\varsigma_2^{\dagger, \mu_2} \varsigma_2^{\nu_2} a^\dagger) (\tau) \varsigma_1 \rangle \\ \langle \varsigma_1^\dagger (\varsigma_2^{\dagger, \mu_2} \varsigma_2^{\nu_2} a^\dagger a) (\tau) \varsigma_1 \rangle \\ \vdots \end{bmatrix}. \quad (2.60)$$

The time derivatives of the elements in  $\tilde{\mathbf{w}}[11, \mu_2 \nu_2](\tau)$  are of the form

$$\partial_\tau \langle \varsigma_1^\dagger (\varsigma_2^{\dagger, \mu_2} \varsigma_2^{\nu_2} a^{\dagger \nu} a^{\nu'}) (\tau) \varsigma_1 \rangle = \text{Tr}\{(\varsigma_2^{\dagger, \mu_2} \varsigma_2^{\nu_2} a^{\dagger \nu} a^{\nu'}) (\tau) \mathcal{L}(\varsigma_1 \rho_{ss} \varsigma_1^\dagger)\}, \quad (2.61)$$

where the Liouvillian is defined as previously in Eq.(2.1). More specifically, we would like to obtain an equation when  $\mu_2 = 0$  and  $\nu_2 = 1$ .

Applying the procedure described in the supplemental material of [46, 47] or our alternative time-dependent perturbation approach, it is possible to prove that, in the limit  $\langle n_{1(2)} \rangle \ll 1$ , the solution for the normally ordered correlation is formally identical to Eq. (44) in the Supplemental Material in Ref. [46, 47]:

$$\partial_\tau \tilde{\mathbf{w}}[11, 01](\tau) = [\mathbf{M} - (i\omega_2 + \Gamma_2/2)\mathbb{1}] \tilde{\mathbf{w}}[11, 01](\tau) - i\epsilon_2 \mathcal{T}_- \tilde{\mathbf{w}}[11, 00](\tau), \quad (2.62)$$

where  $\mathbf{M}$  is the matrix that controls the dynamics of the emitting system. This means that the normally ordered vector  $\tilde{\mathbf{w}}[11, \mu_2 \nu_2](\tau)$  (in Eq.(2.60)) obeys exactly the same equations given in the proof in the Supplemental Material [46], according to the clarification presented in the Erratum [47].

## 2.6 Comparison between results obtained with new and original formalism

At this point we compare the results given by our new formalism with the previous method involving the sensors. To follow this purpose, we consider a prototype biological system, formed of a dimer coupled to a collective vibrational mode, as in Refs [22, 34, 128]. Our motivation arises from the measurements conducted at ambient temperature that have shown anti-bunching effects in photon counting statistics experiments, both in bichromophoric [129, 130] and multi-chromophoric systems [45].

The toy model considered is described by the electronic Hamiltonian given in Eq.(1.61) with  $N = 2$ , where the two sites are also coupled to two vibrational modes of the same frequency, whose Hamiltonian is expressed in Eq.(1.74). This linear coupling between the electronic and vibrational degrees of freedom is given in Eq.(1.78). The introduction of the collective coordinates and the transformation into the exciton basis (explained in detail in Sec.1.4), lead to the form of the Hamiltonian expressed in Eq.(1.81) and here reported for clarity:

$$H_0 = E \tilde{M} + \frac{\Delta E}{2} \tilde{\sigma}_z + \omega_{\text{vib}} D^\dagger D + \frac{g}{\sqrt{2}} \left( \cos(2\theta) \tilde{\sigma}_z - \sin(2\theta) \tilde{\sigma}_x \right) (D + D^\dagger). \quad (2.63)$$

All the other operators in the equation above have been previously specified in Sec.1.4.

At this point, following the procedure presented in Sec.1.3.3.2, we consider energy transfer dynamics assuming generators of the Lindblad form as in Eq.(1.50) to describe the system of interest.

Since a light-harvesting complex is formed of pigments organised in protein scaffolds, the coupling between them and the surrounding vibrational protein environment has to be taken into account in the dissipation processes. Therefore, as first decoherent term in Eq.(1.50) ( $\mu = 1$ ), we choose a pure dephasing model in the site basis to describe such interaction [131]. We assume that the bath fluctuations at different sites are uncorrelated and that the correlations in the protein environment are independent on the sites, meaning that each chromophore undergoes the same coupling strength  $\gamma_{pd}$  to the bath [16]. Therefore, looking at Eq.(1.50), each site is subject to pure dephasing at a rate  $\gamma_{c_1} = \gamma_{pd}$ , with jump operator  $c_1 = A_k = |k\rangle\langle k|$ , with  $k = 1, 2$ . This term alone would lead to exponential decay of coherences in the density matrix and to an equalisation of populations at long times, corresponding then

to the limit of high temperatures [56]. The simulations here presented were also performed using the Redfield master equation, with dissipator in Eq.(1.34). Since the results obtained were qualitatively very similar to those obtained using the pure dephasing model, we chose to perform all the simulations with this simpler model. Another dissipator term we take into account in the phenomenological master equation Eq.(1.50) has to do with the phonon modes. Considering the collective mode, one can assume it experiences thermal relaxation with emission ( $\mu = 2$  in Eq.(1.50)) and absorption ( $\mu = 3$ ) rates  $\gamma_{c_2} = \Gamma_{th}(\eta(\omega_{vib}) + 1)$  and  $\gamma_{c_3} = \Gamma_{th}\eta(\omega_{vib})$ , respectively, and corresponding to jump operators  $c_2 = D$  and  $c_3 = D^\dagger$ . Here  $\eta(\omega_{vib}) = (e^{\beta\omega_{vib}} - 1)^{-1}$  is the mean phonon number for the vibrational mode and  $\beta = 1/K_B T$  is the thermal energy scale.

Due to the interactions with the zero point fluctuations, the excited vibronic states are characterised by radiative decay processes ( $\mu = 4$  in Eq.(1.50)) to the ground state at rate  $\gamma_{c_4} = \gamma$ . To define the form of the jump operator, we denote the vibrational eigenstates of the collective mode operators  $D^\dagger D$  as  $|l\rangle$ , where  $l = 0, 1, \dots, L$ , with  $L$  the maximum number set in the numerical simulation. As a result, the ground electronic-vibrational eigenstates of  $H$  (in Eq.(1.81)) can be written as  $|G, l\rangle \equiv |G\rangle \otimes |l\rangle$ . The excited vibronic eigenstates are indicated as  $|F_v\rangle$  and expressed as quantum superpositions of states  $|X_i, l\rangle \equiv |X_i\rangle \otimes |l\rangle$  i.e.  $|F_v\rangle = \sum_{l=0}^L \sum_{i=1,2} C_{il}(v) |X_i, l\rangle$ . The jump operator describing the emission from the vibronic states takes then the form  $c_4 = \sigma_{vl} = |G, l\rangle \langle F_v|$ , where  $v = 1, \dots, 2L$  and  $l = 1 \dots L$ .

Finally, the highest energy exciton  $|X_1\rangle$  experiences incoherent pumping, which drives the steady state of the system out of equilibrium. The jump operator describing such process is  $c_5 = \sigma_{X_1}^\dagger = |X_1\rangle \langle G|$  and it occurs at rate  $\gamma_{c_5} = P_{X_1}$ .

These considerations lead to the following form of the Linblad master equation:

$$\begin{aligned} \mathcal{L}_0(\hat{\rho}) = & -i[H_0, \hat{\rho}] + \sum_{k=1,2} \frac{\gamma_{pd}}{2} \mathcal{L}_{A_k}(\hat{\rho}) + \frac{\Gamma_{th}(\eta(\omega_{vib}) + 1)}{2} \mathcal{L}_D(\hat{\rho}) \\ & + \frac{\Gamma_{th}\eta(\omega_{vib})}{2} \mathcal{L}_{D^\dagger}(\hat{\rho}) + \frac{\gamma}{2} \sum_{v=1}^{2L} \sum_{l=1}^L \mathcal{L}_{\sigma_{vl}}(\hat{\rho}) + \frac{P_{X_1}}{2} \mathcal{L}_{\sigma_{X_1}^\dagger}(\hat{\rho}), \end{aligned} \quad (2.64)$$

We now introduce the sensors in the formalism: their bare Hamiltonian is given by Eq.(1.97), while their coupling to the emitting system has the form of Eq.(1.98). Since we couple the sensors to the excitons, we have  $a = \sigma_{X_1} + \sigma_{X_2}$ :

$$H_{e,m} = \epsilon[(\sigma_{X_1} + \sigma_{X_2})\varsigma_m^\dagger + (\sigma_{X_1}^\dagger + \sigma_{X_2}^\dagger)\varsigma_m], \quad (2.65)$$

where we have assumed that each sensor is coupled to the emitting system with equal strength  $\epsilon$ . In addition, we suppose they have identical linewidths  $\Gamma$ , so that the second term for the Liouvillian superoperator in Eq.(2.1) is given by:

$$\mathcal{L}_I(\hat{\rho}) = \sum_{m=1}^M \left( \frac{\Gamma}{2} \mathcal{L}_{\varsigma_m}(\hat{\rho}) - i[H_m + H_{e,m}, \hat{\rho}] \right). \quad (2.66)$$

In the right-hand side of Eqs.(2.64) and (2.66),  $\mathcal{L}_{c_\mu}(\rho)$  has the expression given in Eq.(1.51).

We analyse a bio-inspired toy model with parameters in Refs. [22, 132], where the energy difference between the sites is  $\Delta\alpha = 1,042 \text{ cm}^{-1}$ , while the electronic coupling has value  $V = 92 \text{ cm}^{-1}$  [22]. The average energy of the two excitons is  $E = 18000 \text{ cm}^{-1}$  [132], while the energy difference between them is  $\Delta E = 1,058.2 \text{ cm}^{-1}$ . This energy splitting is of the same order of the vibrational frequency  $\omega_{\text{vib}} = 1,111 \text{ cm}^{-1}$ , whilst the thermal energy  $K_B T = 200 \text{ cm}^{-1}$  is comparable to the coupling between the electronic and vibrational degrees of freedom  $g = 267.1 \text{ cm}^{-1}$ , but much smaller than  $\omega_{\text{vib}}$ . This means that a number of  $L = 4$  vibrational levels in the collective mode is sufficient to guarantee converged results. Note that in our numerical simulations all wavenumbers are multiplied by  $2\pi c$ , where  $c$  is the speed of light. The value of the electronic pure dephasing is  $\gamma_{pd} = [1 \text{ ps}]^{-1}$ . We also consider an enhanced radiative decay rate of  $\gamma = [0.5 \text{ ns}]^{-1}$  and a pumping rate  $P_{X_1} = [0.6 \text{ ns}]^{-1}$ . The thermal damping  $\Gamma_{\text{th}}$  is equal to the sensor linewidth  $\Gamma$ , such that  $\Gamma_{\text{th}} = \Gamma = [4.8 \text{ ps}]^{-1}$ .

All the computations in this chapter and in the following have been performed using the Matlab software. Fig.2.2 presents the power spectra  $S_\Gamma(\omega_1)$  for the vibronic dimer, comparing our formalism and the previous method, with different values of  $\epsilon$  satisfying  $\epsilon \ll \sqrt{\Gamma\gamma_Q/2} \sim 10^{-1} \text{ cm}^{-1}$ . The highest peak can be observed at frequency  $\omega_1 = R_3 = 17455 \text{ cm}^{-1}$  and includes transitions from the excited vibronic states mainly localised on the lowest exciton  $|X_2, l\rangle$  to the ground state with the same vibrational quanta  $|G, l\rangle$ . It captures also transitions from excited states with bigger amplitude on the highest exciton  $|X_1, l\rangle \rightarrow |G, l+1\rangle$ . The peak at  $\omega_1 = R_4 = 18515 \text{ cm}^{-1}$  accounts for transitions from excited vibronic states quasi-localised on  $|X_1, l\rangle \rightarrow |G, l\rangle$ , as well as transitions from states quasi-localised on  $|X_2, l\rangle \rightarrow$

$|G, l - 1\rangle$ .

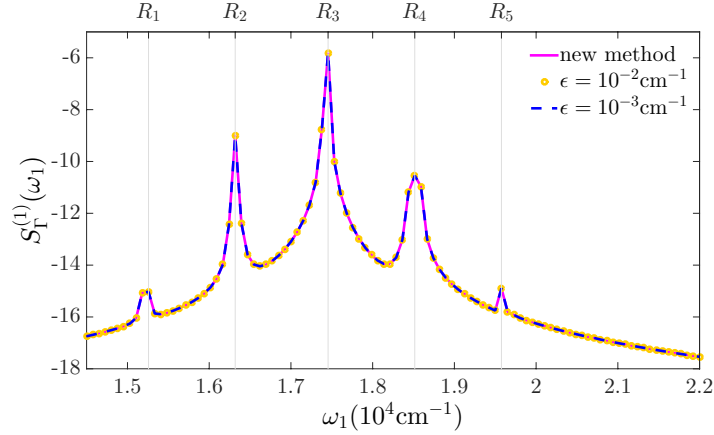


Figure 2.2: Power spectra  $S_{\Gamma}(\omega_1)$  for the system under study as a function of the frequency  $\omega_1$ . The figure is in log scale and compares the results with the new proposed method and the original sensor method.

In Fig.2.3 (a) it can be seen that the original  $\epsilon$ -dependent method tends to slightly underestimate the spectrum, with differences of the order of  $\epsilon$ . The results converge for  $\epsilon \sim 10^{-3} \text{cm}^{-1}$ .

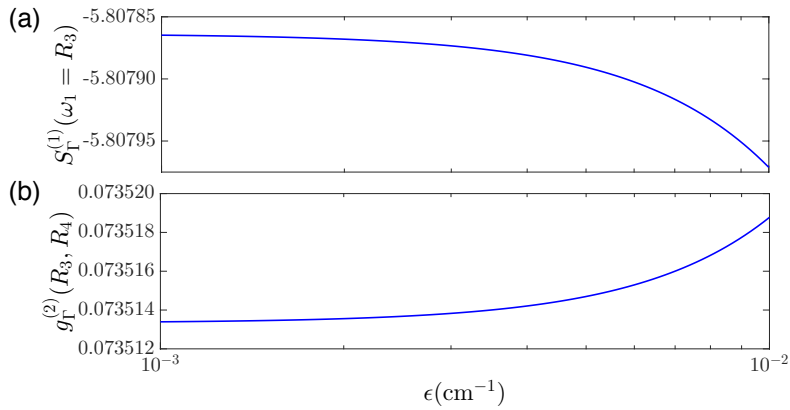


Figure 2.3: (a) Intensity of power spectrum at a fixed frequency,  $S_{\Gamma}(\omega_1 = R_3)$  in log-log scale, and (b) zero-delay time second-order correlation  $g_{\Gamma}^{(2)}(R_4, R_3)$  in semilog scale, as functions of  $\epsilon$ . Both functions are calculated with the  $\epsilon$ -dependent method for our vibronic dimer.

Fig.2.4(a) represents the second order correlation function at zero time delay  $g_{\Gamma}^{(2)}(\omega_1, \omega_2)$ : here, one frequency has been fixed ( $\omega_2 = R_3$ ), while the other ( $\omega_1$ ) scans over the whole spectrum. We observe anti-bunching over the full regime of frequencies, with a bigger offset from zero for the pair of frequencies  $(R_5, R_3)$ , meaning that transitions between states with these energies are weakly correlated.

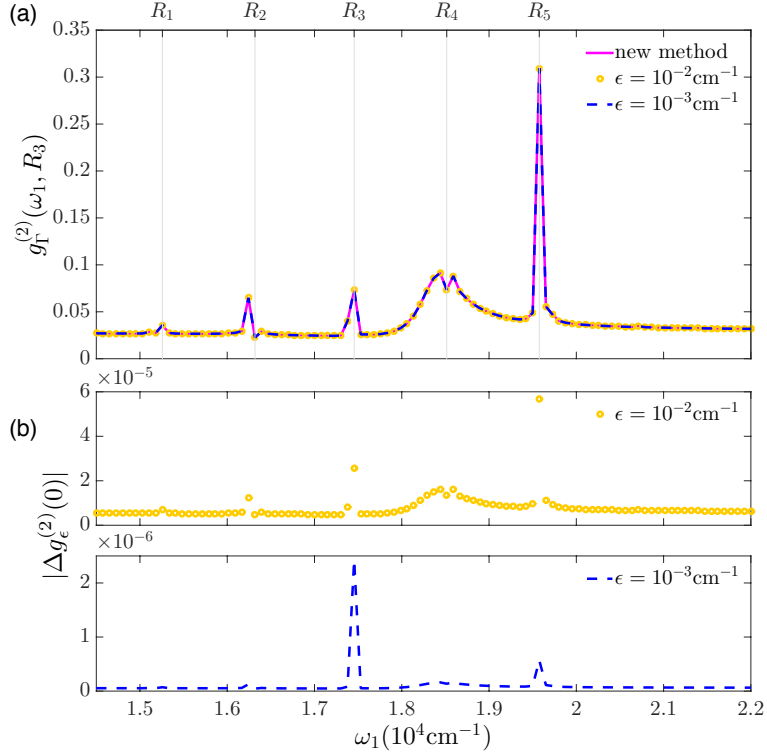


Figure 2.4: (a) Comparison between the second order photon correlations at zero time delay  $g_{\Gamma}^{(2)}(\omega_1, R_3)$  versus  $\omega_1$  computed with the new method and the  $\epsilon$ -dependent sensor method for different values of  $\epsilon$ . (b)  $|\Delta g_{\epsilon}^{(2)}(0)|$ , the absolute difference value between the predictions of the two methods, versus  $\omega_1$  for two values of  $\epsilon$ .

The results with the two methods agree up to differences that scale with  $\epsilon^2$ , as it can be noted in Fig.2.4(b). This figure plots  $|\Delta g_{\epsilon}^{(2)}(0)|$ , that is the absolute value of the difference between the values obtained with our formalism (solving Eq.(2.22)) and the original  $\epsilon$ -dependent method. The latter tends to overestimate the second order photon correlations as shown in Fig.2.3(b), which plots  $g_{\Gamma}^{(2)}(R_4, R_3)$  as function of  $\epsilon$ .

We now focus the attention to the function  $g_{\Gamma}^{(2)}(R_4, R_3, \tau)$  computed in Figs. 2.5(a) and (b), which depict the photon correlations between the frequencies  $\omega_1 = R_4$  and  $\omega_2 = R_3$ , as a function of the delay time. We perform the computation of this time-resolved correlations in two ways. First of all, we compute the numerical integration for the contributions  $\tilde{I}_0(\tau)$ ,  $\tilde{I}_1(\tau)$  and  $\tilde{I}_2(\tau)$  in Eq.(2.47) and add them together (Fig.2.5(a)). Secondly, we follow the  $\epsilon$ -dependent method (Fig.2.5(b)). The two approaches show agreement for both short-time (main panels) and long-time regimes (inset (ii) in Fig.2.5(a) and inset in Fig.2.5(b)).

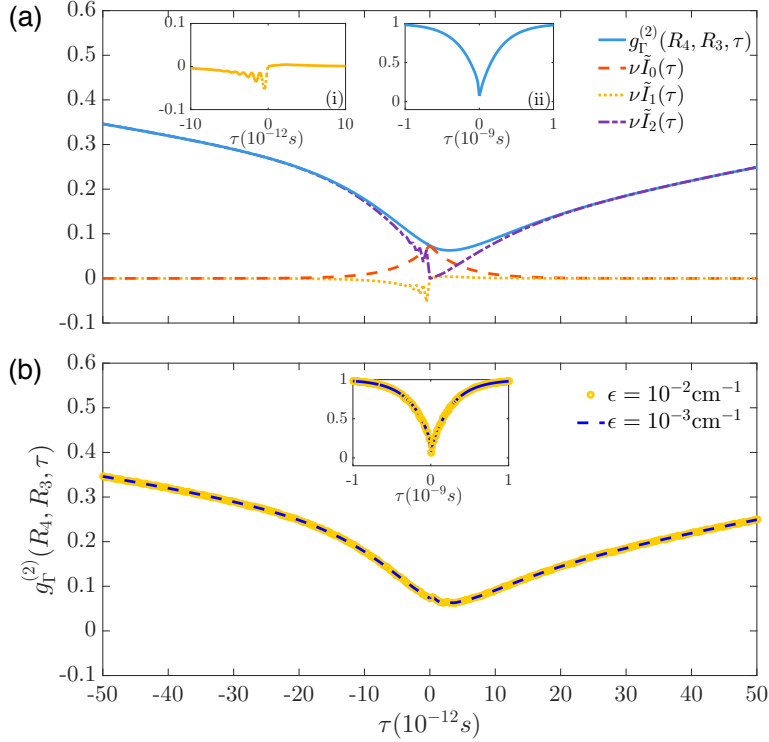


Figure 2.5: Frequency- and time-resolved correlation function  $g_{\Gamma}^{(2)}(R_4, R_3, \tau)$  versus  $\tau$  predicted with (a) the perturbative method and (b) the  $\epsilon$ -dependent method. Inset (i) in panel (a) depicts the short time behaviour of  $\nu\tilde{I}_0(\tau)$  as defined in the text. Inset (ii) in (a) and inset in (b) report long time regime of  $g_{\Gamma}^{(2)}(\omega_1, \omega_2, \tau)$ .

The figures put in evidence the asymmetry of  $g_{\Gamma}^{(2)}(R_4, R_3, \tau)$  with respect to  $\tau$ , which appears in the time scale of the vibronic decoherence in our model (set mainly by  $\Gamma_{th}$ ). The components  $\nu\tilde{I}_k(\tau)$  ( $k = 0, 1, 2$ ), with  $\nu = [\langle\tilde{n}_1\rangle\langle\tilde{n}_2\rangle]^{-1}$ , are also plotted in Fig.2.5(a). As predicted,  $\tilde{I}_0(\tau)$  decays exponentially from the initial value set by  $g_{\Gamma}^{(2)}(R_4, R_3, \tau = 0)$ .  $\tilde{I}_1(\tau)$  is linear in  $\tau$  in the short time regime and becomes negative for bigger times (see inset (i) in Fig.2.5(a)). This reflects an overdamped oscillation that decays to zero in the long-time regime, in agreement with the behaviours discussed in Section 2.4.2. Even if  $\tilde{I}_1(\tau)$  takes negative values at some times, they are counteracted by  $\tilde{I}_0(\tau)$  and  $\tilde{I}_2(\tau)$ , so that  $g_{\Gamma}^{(2)}(R_4, R_3, \tau)$  has always physical meaning. Fig.2.5 also highlights that the short-time asymmetry in  $g_{\Gamma}^{(2)}(R_4, R_3, \tau)$  is related to  $\tilde{I}_1(\tau)$  and  $\tilde{I}_2(\tau)$ , meaning that the correlation function is capturing coherent processes in this time scale. Depending on which frequency is probed first, such coherent processes set a different rate for approaching the uncorrelated steady-state emission at large times (see inset (ii) in Fig.2.5(a)).

In summary, we have shown that the formalism we proposed is equivalent to the  $\epsilon$ -dependent sensor method to compute frequency-filtered correlation functions.

However, within our method there is no dependence of correlation functions on  $\epsilon$ , hence it does not need to test the convergence of results for different values of  $\epsilon$ , and it avoids possible numerical instabilities associated to the smallness of this factor. An eventual identification of possible instabilities with the  $\epsilon$ -dependent method can be difficult, since it depends on the system analysed.

## 2.7 Conclusion

Using the sensor method, we have presented an alternative approach for the calculation of the frequency-filtered and time-resolved correlation functions, both at zero time delay and at finite delay time. Our main results are summarised by Eqs. (2.25)-(2.27) and Eq.(2.47).

The formulation is based on the perturbation theory and allows to solve the problem of computing photon correlations using a series of auxiliary matrices defined in the Hilbert space of the emitter only. This set of matrices gives some insight into the physical processes involved in the measure of photon correlations through the weak coupling to the sensors. We recover some analytical results previously obtained for the power spectrum and the zero time delay second order correlation function [46, 47, 113, 125], which confirm the validity of our approach.

In addition, in Refs. [46, 47] the quantum regression theorem was at the basis of the proof for the equivalence between the sensor and integral methods to calculate  $M$ -photon correlations. Instead, our relations in Eqs.(2.25)-(2.27) and Eq.(2.47), in principle, are valid for a general non-Markovian, non-perturbative open quantum dynamics of the emitter.

Another advantage of our method is that the numerical computation of the photon correlations does not depend explicitly on the choice of the small coupling parameter  $\epsilon$ , therefore there is no need to check the convergence and the stability of the results.

Recently, it has been demonstrated the equivalence between the results obtained with the weak and coherent coupling to the sensors in Refs. [46, 47] and a cascaded incoherent coupling of finite strength between the emitter and the sensors [133, 134]. This represents another way to compute photon correlations and implies equivalence also with our approach.

Our formulation to evaluate time-resolved correlations uses the time-dependent perturbation theory to obtain the equation of the second-order correlation function  $g_{\Gamma_1\Gamma_2}^{(2)}(\omega_1, \omega_2, \tau)$  in Eq.(2.47). It is expressed as a sum of three components  $\tilde{I}_0$ ,  $\tilde{I}_1$  and  $\tilde{I}_2$ , each giving an idea of the physical processes ruling the correlations at different

timescales. It is important to notice that the theoretical approach here developed recovers the limit of  $g_{\Gamma_1\Gamma_2}^{(2)}(\omega_1, \omega_2, \tau) \rightarrow 1$  for large times, as seen in Sec.2.4.2. The computation of two of these components needs numerical integration of single and double integrals.

This formalism can be extended to higher-order but when there is delay in only one of the detectors. The generalisation to multiple time delays is more complicated. In this case, it could be best to compute the auxiliary matrices given in Eq.(2.27) and then propagate in time without perturbation, therefore combining the main advantages of both our method and the previous sensor formalism.

We also showed the agreement between the two methods comparing the outcomes for the frequency-filtered and time-resolved photon correlations of a bio-inspired prototype system, simulating a light-harvesting vibronic dimer.

Our goal, at this point, was to prove the equivalence between the predictions of the two formalisms, therefore we did not provide a detailed analysis of the physics behind the system under consideration. However, it is important to highlight that the results obtained suggest that frequency-filtered and time-resolved photon-counting statistics can offer a powerful tool to measure coherent contributions to the emission dynamics in biomolecular complexes [45]. A more detailed analysis of the frequency-filtered photon counting statistics for this bio-inspired toy model will be displayed in the following chapters.

## Chapter 3

# Frequency-filtered and time-resolved photon counting statistics of prototype light harvesting dimers

We now apply the theoretical setup developed in Chap.2 to compute frequency-filtered and time-resolved correlation functions for the light emitted by prototype photosynthetic complexes in free space. The aim is to assess the extent to which these frequency-filtered photon correlations allow to probe the quantum interactions between electronic and vibrational degrees of freedom in prototype light-harvesting units. In particular, we assess whether such photon correlations carry out a signature of steady-state quantum coherence within the excited state manifold.

### 3.1 Introduction

Two-photon correlations are one of the most widely used tools to observe quantum behaviour in photon detection processes [100, 102, 135]. In particular, a value of the correlation function less than 1 implies that the system under study is subject to sub-Poissonian statistics, which can usually be related to antibunching effects [136, 137]. The presence of this property has enabled identification of the quantum interplay of composite systems in different scenarios which include cavity [138–140] and circuit [141, 142] quantum electrodynamics and optomechanics [143].

More recently, it has also been applied in the field of quantum biology to measure photon antibunching of a single light-harvesting complex [122, 144]. Within

this area, researchers have been looking for tools that could unequivocally prove the presence of non-trivial quantum effects in certain biomolecular processes. In the last decade ultrafast two-dimensional spectroscopy techniques have been able to show oscillatory behaviour in the electronic dynamics of photosynthetic complexes, lasting several picoseconds [9, 12, 25, 29, 30]. It has been suggested that the coherent dynamics happening within these photosynthetic systems witnesses the interaction between the electronic and vibrational degrees of freedom [1, 22, 29–35]. Nevertheless, this hypothesis requires further confirmation with different approaches, since there are some controversial debates in the community about this matter [36].

Multidimensional spectroscopy, indeed, presents some challenges due to both the difficulty of investigating individual molecules and on the unambiguous understanding of the origin of the beating patterns observed in the coherent dynamics of light harvesting systems.

From a theoretical perspective, the quantum coherent dynamics involving this vibronic mechanism has been argued to lead to truly non-trivial quantum behaviour, such as non-classical fluctuations of collective molecular motions [22]. Photon correlations of the light emitted by single systems could test such theoretical predictions [45].

In this context, it is interesting to see whether or not second order correlation functions can complement and confirm the presence of coherent dynamics suggested by ultrafast two-dimensional spectroscopy [49, 121]. The aim of this work is to find complementary experimental signatures of this quantum interaction between electronic and vibrational degrees of freedom, by analysing the photon counting statistics of the light emitted by the excitons of two different prototype dimers. The biggest advantage of using this technique is the concrete possibility to investigate the problem experimentally.

Experiments on individual molecules of light-harvesting complexes at room temperature had shown until recently very low fluorescence emission. However, in [45], a single molecule of light harvesting complex 2 (LH2) has been weakly coupled to a gold nanoantenna, giving raise to an over 500-fold fluorescence enhancement. Therefore this is very promising thanks to the tangible possibility to probe quantum effects in photosynthetic systems by measuring frequency-filtered and time-resolved second order correlation functions.

In photodetection experiments the light under study usually passes through filters which select specific frequencies relevant to understand particular spectral properties of the system. The effects of the filters have been studied both from a theoretic-

cal and experimental point of view [46,47,109,111,115,133]. In one of the formalisms recently developed [50] these filters are replaced by sensors weakly coupled to the system under scrutiny. This method is based on time dependent perturbation theory up to the order of the correlation one wants to compute: it has been described in Chap.2 and it is the approach we will follow for the analysis of the two prototype models of interest.

We will proceed as follows. In Sec.3.2 we describe the system: a prototype vibronic dimer within two different regimes, one with the excitons quasi-localised over the sites and the other exhibiting more delocalised excitons. Sec.3.3 analyses the dynamics of the two configurations. Then, Secs.3.4 and 3.5 present the investigation of the related counting statistics. Finally, Sec.3.6 is devoted to concluding remarks.

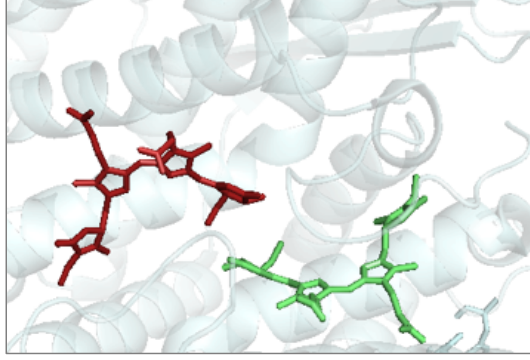
## 3.2 Model in free space

We focus our analysis on a prototype vibronic dimer [22,34,128] within two slightly different regimes. The choice of the dimer is due to the fact that it is the minimal unit needed to observe such effects. In addition, this choice has been pushed forward by experimental measurements of correlation functions in similar bichromophoric systems [129,130] and multi-chromophoric systems [45] that have shown anti-bunching at room temperature.

The system under study is a dimer where each chromophore has an excited electronic state  $|k\rangle$  with energy  $\alpha_k$  ( $k = 1, 2$ ), and the electronic Coulomb interaction is given by  $V_{kk'}$ . As already explained in Sec.1.2.3.1, under normal light conditions, the flux of photons is very low with respect to its transport time through the aggregate, meaning that the dynamics of the system can be studied in the single excitation manifold [76]. Each site is individually coupled to a quantised vibrational mode of frequency  $\omega_{vib}$  much larger than the thermal energy scale  $K_B T$ , with coupling strength  $g$ . The vibrational modes are described by the operators  $d_k$  and  $d_k^\dagger$ , which annihilates and creates, respectively, a phonon of the vibrational mode of chromophore  $k$ . Following the rationale in Chap.1 (Sec.1.4), introducing the collective mode and transforming into the exciton basis, the effective Hamiltonian for the prototype dimer takes the form of a generalised quantum Rabi model [145], as shown in Eq.(1.81) and here reported for clarity:

$$H = E\tilde{M} + \frac{\Delta E}{2} \tilde{\sigma}_z + \omega_{vib} D_-^\dagger D_- + \frac{1}{\sqrt{2}} g \left( \cos(2\theta) \tilde{\sigma}_z - \sin(2\theta) \tilde{\sigma}_x \right) (D_- + D_-^\dagger) \quad (3.1)$$

The size of the mixing angle  $\theta$  determines the degree of localisation of the excitons over the sites. In particular, here, we analyse two different situations close to the limit cases: “dimer 1”, that is the standard central dimer in PE545 cryptophyte antenna (illustrated in Fig.3.1(a)) quasi-localised on the sites and “dimer 2”, which undergoes a slightly bigger delocalisation.



(a)

General parameters	
$\Delta E = 1058.2 \text{ cm}^{-1}$	$\gamma = (0.5 \text{ ns})^{-1}$
$E = 18000 \text{ cm}^{-1}$	$\gamma_{pd} = (1 \text{ ps})^{-1}$
$\omega_{\text{vib}} = 1111 \text{ cm}^{-1}$	$P_{X_1} = (0.6 \text{ ns})^{-1}$
$g = 267.1 \text{ cm}^{-1}$	$\Gamma_{th} = (1 \text{ ps})^{-1}$
$\beta = (K_B T)^{-1} = 0.0048 \text{ cm}$	$\Gamma = (4.8 \text{ ps})^{-1}$

(b)

Dimer 1	Dimer 2
$g > V_1$	$g \sim V_2$
$\zeta_1 = \frac{2V_1}{\Delta\alpha_1} = 0.1$	$\zeta_2 = \frac{2V_2}{\Delta\alpha_2} = 0.5$
$V_1 = 92 \text{ cm}^{-1}$	$V_2 = 236.6 \text{ cm}^{-1}$
$\Delta\alpha_1 = 1042 \text{ cm}^{-1}$	$\Delta\alpha_2 = 946.5 \text{ cm}^{-1}$

(c)

Figure 3.1: Picture (a) represents the dimer under study and is based on the protein structure of PE545. Table (b) reports the set of parameters common to both the regimes analysed, while table (c) indicates the parameters for the two specific configurations.

Table in Fig.3.1(b) shows the values of parameters characterising both configura-

tions, while the table in Fig.3.1(c) highlights the differences between them. (For clarity, in our numerical calculations all wavenumbers given in the tables are multiplied by  $2\pi c$ , where  $c$  is the speed of light.) More specifically, the two regimes present different degrees of delocalisation of the excitons over the sites, that we indicate with:

$$\zeta_i = \tan(2\theta_i) = \frac{2V_i}{\Delta\alpha_i} \quad \text{with: } i = 1, 2 \quad (3.2)$$

For the first model (dimer 1), we have chosen parameters inspired by the central dimer in the cryptophyte antennae PE545 [22, 132] (see table in Fig.3.1(c)): in this case the degree of delocalisation is  $\zeta_1 = 0.1$ .

We build the model for dimer 2 maintaining the same resonance condition between the exciton energy splitting and the vibrational energy ( $\Delta E_1 = \Delta E_2 = \Delta E$ ) and fixing the degree of delocalisation at the value  $\zeta_2 = 0.5$ . Given these conditions, the coupling between the sites in dimer 2 becomes  $V_2 = \zeta_2 \Delta E / \left(2\sqrt{1 + \zeta_2^2}\right)$  and the energy splitting between them  $\Delta\alpha_2 = \Delta E / \sqrt{1 + \zeta_2^2}$ .

The interaction between the chromophores and the environment (protein and solvent) involves many degrees of freedom, which makes the exact solution challenging. Here, we address the problem by accounting, at a Hamiltonian level, for the relevant exciton-vibration interactions, while including dephasing and relaxation channels in a phenomenological manner as described in Sec.1.3.3.2. Under the hypothesis of weak system-bath coupling, the interaction between the electronic and vibrational degrees of freedom leads to dynamics characterised by dephasing and relaxation. In addition, the energy transfer dynamics of the system only is described by generators of the Linblad form expressed in Eq.(2.64) and here reported for clarity:

$$\begin{aligned} \mathcal{L}_0(\hat{\rho}) = & -i [H_0, \hat{\rho}] + \sum_{k=1,2} \frac{\gamma_{pd}}{2} \mathcal{L}_{A_k}(\hat{\rho}) + \frac{\Gamma_{th}(\eta(\omega_{vib}) + 1)}{2} \mathcal{L}_D(\hat{\rho}) \\ & + \frac{\Gamma_{th}\eta(\omega_{vib})}{2} \mathcal{L}_{D^\dagger}(\hat{\rho}) + \frac{\gamma}{2} \sum_{v=1}^{2L} \sum_{l=1}^L \mathcal{L}_{\sigma_{vl}}(\hat{\rho}) + \frac{P_{X_1}}{2} \mathcal{L}_{\sigma_{X_1}^\dagger}(\hat{\rho}). \end{aligned} \quad (3.3)$$

The sensors and their decoherent terms in the master equation are described by Eqs. (1.97), (1.98) and (2.66), respectively, and rewritten here for clarity:

$$H_m + H_{em} = \omega_m \zeta_m^\dagger \zeta_m + \epsilon_m (a_m \zeta_m^\dagger + a_m^\dagger \zeta_m) \quad (3.4)$$

$$\mathcal{L}_I(\hat{\rho}) = \sum_{m=1}^M \left( \frac{\Gamma}{2} \mathcal{L}_{s_m}(\hat{\rho}) - i [H_m + H_{e,m}, \hat{\rho}] \right). \quad (3.5)$$

### 3.3 Dynamics

For our analysis we have chosen bio-inspired dimers that satisfy the condition  $\Delta E \sim \omega_{\text{vib}} \gg K_B T$ , meaning that the intramolecular mode of interest has energy comparable to the energy difference between the excitons, but much larger than the thermal energy scale (cf. the table in Fig.3.1(b)). In such a case the effects of underdamped high-energy vibrational motions are expected to be the most important [31, 146]. In nature many light-harvesting complexes comprise pairs of chromophores which fall in this regime. Two examples are the central dimer PEB<sub>50c</sub>-PEB<sub>50d</sub> in the cryptophyte antennae PE545 [147], and the Chl<sub>b601</sub>-Chl<sub>a602</sub> pair in the light-harvesting complex II (LH II) of higher plants [147].

The dynamics and non-classical features of these systems have previously been investigated [22] and spectroscopy of photosynthetic complexes, including such a prototype, has revealed long-lived quantum beating signals [12].

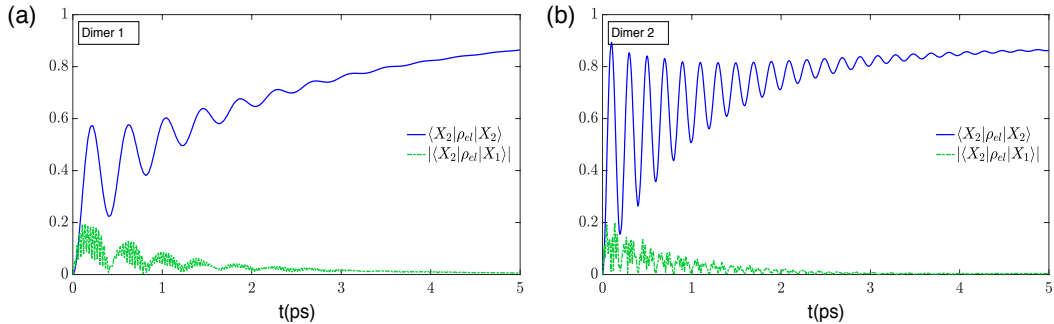


Figure 3.2: *Dynamics (populations and coherences) of the electronic system only without the sensors: (a) for dimer 1 (quasi-localised model) and (b) dimer 2 (more delocalised model), with parameters in Fig.3.1(b) and 3.1(c) and  $\rho_{el} = \text{Tr}_{\text{vib}}\{\rho(t)\}$ .*

Fig.3.2 shows the dynamics of the electronic degrees of freedom for the two regimes of dimer 1 (a) and dimer 2 (b). For both models, the initial condition chosen for the electronic part is the exciton with highest energy, namely  $\rho_{el}(0) = |X_1\rangle\langle X_1|$ . The initial state considered for the vibrational part, instead, is a thermal distribution  $\rho_{\text{vib}}(0) = \rho_{\text{th}} = \sum_{n=0}^{\infty} P(n) |n\rangle\langle n|$ , where  $n$  denotes the phonon occupation number of the relative displacement mode coupled with the exciton dynamics, while  $P(n)$  is the thermal occupation of the  $n$ th level given by  $P(n) = \left(1 - e^{-\frac{\hbar\omega}{K_B T}}\right) e^{-\frac{\hbar\omega n}{K_B T}}$ .

Therefore, the total initial state reads:

$$\rho_{tot}(0) = \sum_{n=0}^{\infty} P(n) |X_1\rangle\langle X_1| \otimes |n\rangle\langle n|. \quad (3.6)$$

The plots depict both the population of the lowest exciton and the coherence between the two excitons, with  $\rho_{el} = \text{Tr}_{\text{vib}}\{\rho(t)\}$ . As we can see in Fig.3.2, both populations and coherences oscillate with a frequency related to the electronic interaction  $V$  ( $\sim (0.4\text{ps})^{-1}$  for dimer 1 and  $\sim (0.2\text{ps})^{-1}$  for dimer 2). The smallest value of the period of oscillation for dimer 2 (see Fig.3.2(b)) is related to the fact that in this configuration the excitons are more delocalised over the sites. Coherences, instead, are also modulated by a higher frequency of the order of the energy difference between the excitons  $\Delta E$  ( $\sim (0.03\text{ps})^{-1}$ ), which is the same for both dimers. In addition, it can be noticed that for dimer 2 populations oscillate with a larger amplitude, meaning that more coherent energy transfer happens in this more delocalised configuration.

It is also worth mentioning that the oscillations in both populations and coherences of the order of  $V$  are observed because the value of the pure dephasing rate has been set at  $\gamma_{pd} = (1\text{ps})^{-1}$ . Increasing this value would destroy such oscillations, bringing the system to the equilibrium faster and making the coherences decay in shorter time [31].

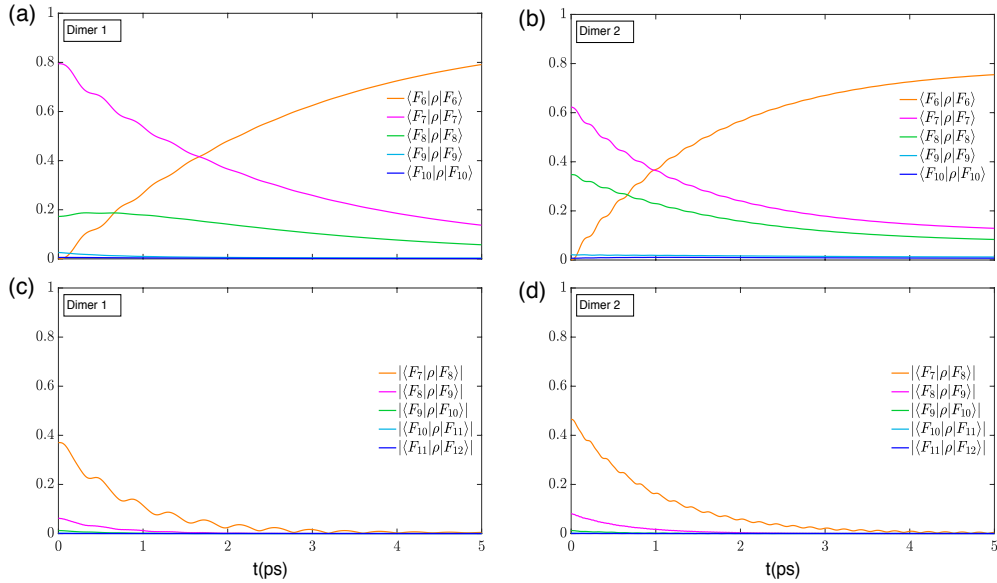


Figure 3.3: *Vibronic dynamics of the system without the sensors. The figure represents some populations (a) and coherences (c) for dimer 1 (quasi-localised model) and for dimer 2 (b) and (d) (more delocalised model), with parameters in Fig.3.1(b) and 3.1(c).*

As a further analysis, we also present the vibronic populations and coherences in Figs. 3.3(a)(b) and 3.3(c)(d), respectively. In this case the amplitude of oscillations for both populations and coherences is much smaller, though their frequencies are similar, as expected. This is due to the fact that every eigenstate of the vibronic system  $|F_\nu\rangle$  is a linear superposition of the exciton-vibrational states  $|X_i, l\rangle$ . Therefore, when we calculate, for example, the population  $\langle F_\nu | \rho | F_\nu \rangle$  and expand  $|F_\nu\rangle$  in terms of  $|X_i, l\rangle$ , we obtain different terms oscillating with different frequencies, that almost cancel out. The same considerations apply to the coherences. It can also be noticed that, within configuration 1, coherences decay faster (lasting up to 3 ps) than in configuration 2, where they last up to 4 ps (cf. Figs. 3.3(c) and 3.3(d)).

Converged results have been obtained restricting the vibrational Hilbert space to  $L = 4$ . However, even using only two excitations in the collective vibrational mode ( $L = 2$ ) gives results for the statistics qualitatively and quantitatively very close to those that converge, as shown in Appendix A.

## 3.4 Counting statistics in free space

We now focus on the computation of the frequency-filtered and time-resolved photon correlations using the formalism presented in Chap.2.

### 3.4.1 First order correlations

First of all, we compute the power spectra according to Eq.(2.16). Fig.3.4 shows the frequencies emitted by the system of interest for both configurations. In the case of dimer 1 (Fig.3.4(a)) the frequencies emitted by the system are:  $R_1 = 15220 \text{ cm}^{-1}$ ,  $R_2 = 16330 \text{ cm}^{-1}$  and  $R_3 = 17450 \text{ cm}^{-1}$ ,  $R_4 = 18480 \text{ cm}^{-1}$ ,  $R_5 = 19600 \text{ cm}^{-1}$ . We concentrate our attention on the peaks at frequencies  $R_3$  and  $R_4$ , because they correspond to the highest frequencies emitted and, for this reason, they were chosen for the further analysis of frequency-filtered and time-resolved correlation functions. The highest peak at frequency  $R_3$  is mainly due to the transitions  $|X_2, 0\rangle \rightarrow |G, 0\rangle$  and  $|X_1, 0\rangle \rightarrow |G, 1\rangle$ , but it also includes contributions deriving from all the transitions with the same energy, such as  $|X_2, l\rangle \rightarrow |G, l\rangle$  or  $|X_1, l\rangle \rightarrow |G, l+1\rangle$ . One of the other relevant peaks can be seen at frequency  $R_4$  and it is related to the transitions  $|X_1, 0\rangle \rightarrow |G, 0\rangle$  and  $|X_2, 1\rangle \rightarrow |G, 0\rangle$ , plus other contributions from transitions with the same energy.

The examination of the model with more delocalisation of the excitons (dimer 2) leads to the power spectrum in Fig.3.4(b), which exhibits peaks at the same fre-

quencies as dimer 1, but with more splittings in some of them, due to enhanced delocalisation over the sites.

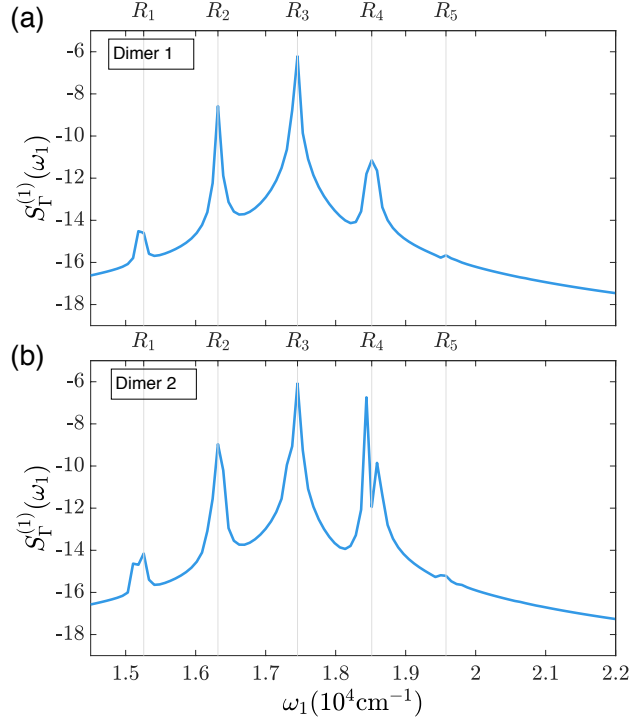


Figure 3.4: Power spectra of the exciton emission for: (a) dimer 1 (quasi-localised model) and (b) dimer 2 (more delocalised model), with parameters in Fig.3.1(b) and 3.1(c). The figure is in log scale.

### 3.4.2 Second order correlations: zero time delay

To compute the frequency-filtered correlation function at zero time delay, we fixed the frequency at the peak  $\omega_2 = R_3$  (the highest peak in both power spectra in Fig.3.4), whereas the other photon has variable frequency  $\omega_1$  which scans the spectral range. The results in Fig.3.5 seem to suggest that one would observe antibunching for all emitting states within the pure dephasing model, however we will provide a deeper analysis later on, which will not necessarily lead to this conclusion.

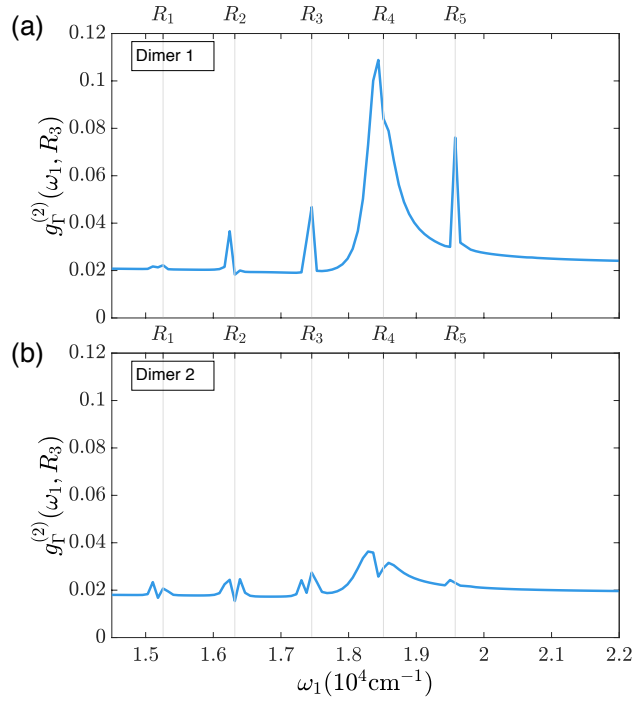


Figure 3.5: Two color-photon correlations at zero time delay for (a) dimer 1 (quasi-localised model) and (b) dimer 2 (more delocalised model), with parameters in Fig.3.1(b) and 3.1(c). The figure is in semilog scale.

### 3.4.3 Second order correlations: finite time delay

We now present the results for the computation of the time-resolved second order correlation function at finite time delay, for both the auto-correlations  $R_4 - R_4$  and the cross-correlations  $R_4 - R_3$ , again within both regimes.

First of all, we computed the standard  $g^{(2)}(\tau)$ , to see what kind of information it could provide. In the simulation presented in Fig.3.6 the emission operator considered are the exciton operators  $(\sigma_{X_1} + \sigma_{X_2})$ . As it can be noticed, the blind detectors analysis of these models gives the standard behaviour of  $g^{(2)}(\tau)$  for a single quantum system emitting photons of any frequency, as presented in Fig.3.6. This implies that the blind photon correlations are not able to distinguish among different regimes. Notice that  $g^{(2)}(\tau)$  is identical for the two situations. This is because the approach of  $g^{(2)}(\tau)$  to the uncorrelated emission unit is dominated by the radiative decay mechanism over a time scale which is the same for both systems.

To confirm this, we also investigated the standard  $g^{(2)}(\tau)$  for a third configuration: the central dimer in PC645 algae. In this case the energy gap between the excitons is different from that in the two dimers under study, since  $\Delta E = 645\text{cm}^{-1}$ . However, the two-photon correlation exhibits exactly the same behaviour seen in the two

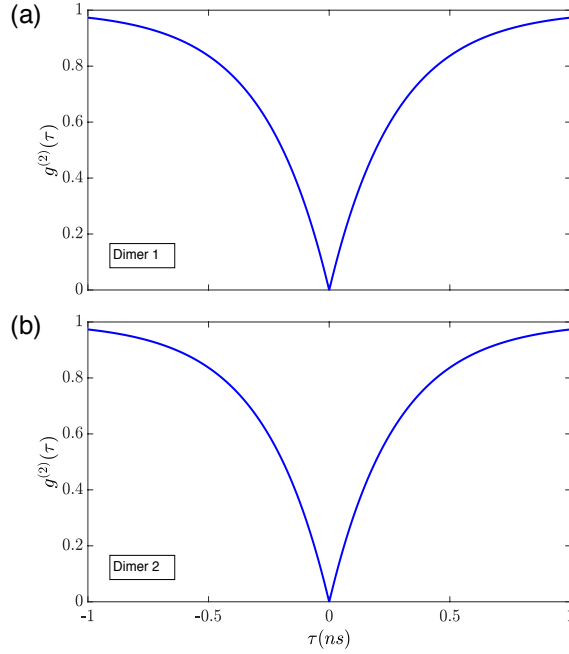


Figure 3.6: *Blind two-photon correlations at finite time delay for (a) dimer 1 (quasi-localised model) and (b) dimer 2 (more delocalised model), with parameters in Fig.3.1(b) and 3.1(c).*

previous regimes (this is the reason why the plot has not been reported here). This behaviour is due to the fact that in all three regimes the exciton lifetime is of the order of 1ns and the standard  $g^{(2)}(\tau)$  reaches uncorrelated emission just in that time scale. Therefore, we can conclude that such color blind analysis of the second order correlation function is not able to capture the differences between two configurations exhibiting a different degree of exciton delocalisation.

In contrast, the time-resolved second order correlation function, reveals specific features for the two dimers, as depicted in Figs.3.7 and 3.8. They show the dependence of the correlations both at positive and negative delay times. The statistics describing the system under study is sub-Poissonian, since  $g_{\Gamma}^{(2)}(\tau) < 1$ , but interpreting the nature of the light emitted in this case requires more analysis.

Photon antibunching is signified by a normalised two-time correlation function that increases from the initial value at  $\tau = 0$ , namely  $g^{(2)}(t, t + \tau) > g^{(2)}(t, t)$ . Equivalently, its characterisation for a well behaved function  $g^{(2)}(t, t + \tau)$  (continuous and with derivatives at every order), relies on having positive derivative at  $\tau = 0$  [148]. However, these definitions are ambiguous when  $g^{(2)}(t)$  shows oscillatory or structured features [149–151] and deducing the nature of the light emitted in these cases requires more analysis.

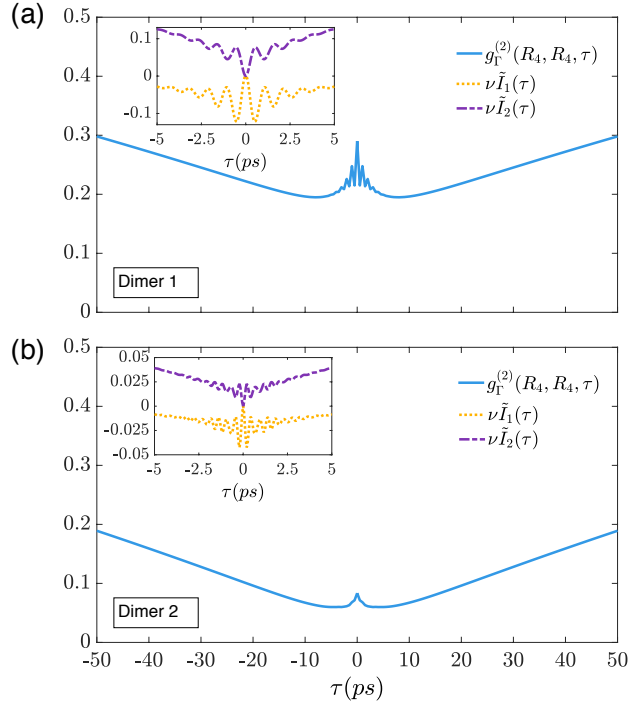


Figure 3.7: Frequency- and time-resolved auto-correlation function  $g_{\Gamma}^{(2)}(R_4, R_4, \tau)$  versus  $\tau$  predicted for (a) dimer 1 (quasi-localised model) and (b) dimer 2 (more delocalised model), with parameters in Fig.3.1(b) and 3.1(c). The inserts in panels (a) and (b) show the short time behaviour of  $\nu \tilde{I}_1(\tau)$  and  $\nu \tilde{I}_2(\tau)$  (with  $\nu = [\langle \tilde{n}_1 \tilde{n}_2 \rangle]^{-1}$ ).

The auto-correlations shown in Fig.3.7 fall precisely in this situation: they do not exhibit anti-bunching within either model, independently on the degree of delocalisation of the excitons. In fact, there are periods where  $g_{\Gamma}^{(2)}(0) > g_{\Gamma}^{(2)}(\tau)$ , meaning that the light is not necessarily antibunched [137, 152], despite showing sub-Poissonian statistics. To be able to establish this, investigation of higher order correlations are needed [152], but they are beyond the scope of this work.

As expected, given that we are detecting the same frequency  $R_4$ , the photon correlation is symmetric for positive and negative times. In addition, Fig.3.7(a) witnesses a peculiar behaviour given by the oscillations observed around  $\tau = 0$ : this kind of oscillations has also been observed in other systems [133]. The frequency of these oscillations is  $\omega = (1\text{ps})^{-1}$ , but they cannot be directly related to the dynamics observed in Figs.3.2 and 3.3. Those figures, indeed, describe ultrafast dynamics with initial state given in Eq.(3.6), which is different from the steady state that represents the initial condition in the counting statistics analysis. These oscillations, more evident in Fig.3.7(a), have to do with internal coherent dynamics, but with current technologies they cannot be resolved experimentally.

What Fig.3.7 seems to suggest is that the frequency-filtered and time-resolved auto-

correlations could give information about the degree of delocalisation of the system. Indeed, the oscillations around  $\tau = 0$  quickly average to zero for dimer 2, that experiences more delocalisation.

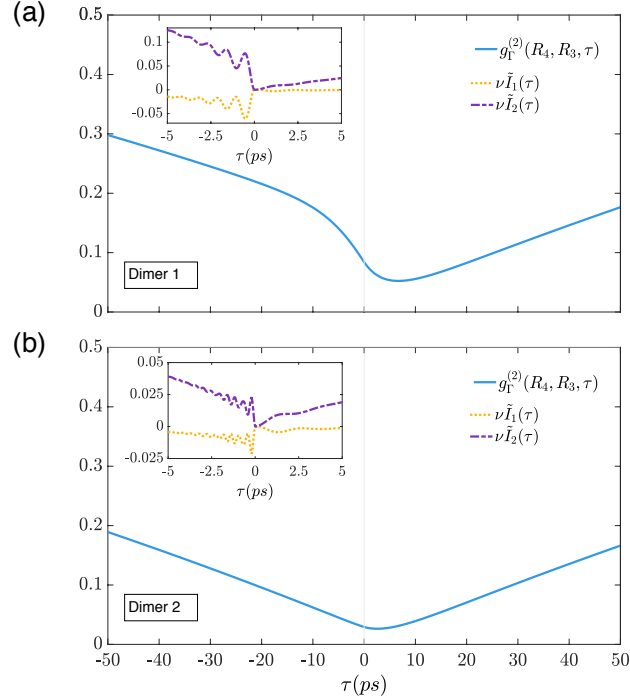


Figure 3.8: Frequency- and time-resolved cross-correlation function  $g_{\Gamma}^{(2)}(R_4, R_3, \tau)$  for (a) dimer 1 (quasi-localised model) and (b) dimer 2 (more delocalised model), with parameters in Fig.3.1(b) and 3.1(c). The inserts in panels (a) and (b) show the short time behaviour of  $\nu \tilde{I}_1(\tau)$  and  $\nu \tilde{I}_2(\tau)$ .

Fig.3.8 represents the second-order, time delayed cross-correlations. The dip in the time-resolved  $g_{\Gamma}^{(2)}(R_4, R_3, \tau)$  does not go to zero, while it does in the condition of colour blind filters (Fig.3.6). This off-set is related to the loss of time resolution due to the presence of the filters. Even more importantly, it is possible to notice that the minimum of the correlation function is not at  $\tau = 0$  ns: again the system is characterised by sub-Poissonian statistics, but it is not possible to assert that the light is antibunched without further analysis.

The most remarkable aspect displayed in Fig.3.8 is the asymmetry between positive and negative times, contrary to what is shown for auto-correlations. Therefore we are interested in quantifying the asymmetry of the correlation function with respect to the y-axis. We define the function:

$$f_- = \| f(x) - f(-x) \| . \quad (3.7)$$

If  $f_- = 0$ , the function is fully symmetric, while if  $f_- > 0$ , the function is not

symmetric. In our case  $f(x)$  corresponds to the values of  $g_{\Gamma}^{(2)}(R_4, R_3, \tau)$  for positive times  $\tau > 0$ , namely when the frequency  $R_4$  is detected before than  $R_3$ . Viceversa,  $f(-x)$  corresponds to the values of  $g_{\Gamma}^{(2)}(R_4, R_3, \tau)$  for negative times  $\tau < 0$ , that is when the first frequency detected is  $R_3$ . The norm used is the functional norm given by  $\|f_{-}\| = \sqrt{h \sum_k |f_{-k}|^2}$ , where  $h = (\tau_{\max} - \tau_{\min})/N_{\text{points}}$ . Here  $\tau_{\max}$  and  $\tau_{\min}$  are the maximum and minimum of the time interval considered in Fig.3.8, and  $N_{\text{points}}$  is the number of points in the numerical vector  $g_{\Gamma}^{(2)}(R_4, R_3, \tau)$ . This analysis gives  $f_{-} = 0.6$  for the correlation function describing the quasi-localised excitons model, and  $f_{-} = 0.11$  for the more delocalised configuration. Hence, dimer 1 exhibits more asymmetry than dimer 2.

These results highlight an important feature: the asymmetry of the correlation function is an indication of the emission dynamics being dependent on which photon is detected first. This feature results to be more notorious in the system where the vibronic mechanism involves quasi-localised excitons.

We now investigate whether  $g_{\Gamma}^{(2)}(R_4, R_3, \tau)$  witnesses coherence in the excited state by analysing the specific processes that  $I_1$  and  $I_2$  capture (their formal expressions are given in Eqs.(2.42) and (2.44)). Regarding the contribution  $I_1$  given in Eq.(2.42), within the approximation of  $t_2 - t_1 \simeq 0$ , we can write:

$$\text{Tr}[a_2 \tilde{\rho}_{1,0}^{1,1}(t_1)] = \sum_{i=1}^2 \sum_{l=0}^L \langle X_i, l | \tilde{\rho}_{1,0}^{1,1}(t_1) | G, l \rangle, \quad (3.8)$$

meaning that this contribution is related to the interference of coherence elements between the ground and the excited states. Notice also that  $I_1$  tends to zero in the intermediate-time regime, as shown in our numerical results presented in Fig.3.8 (a) and (b) (insets). This means that in the intermediate- to long-time regimes, the frequency-filtered and time-resolved correlations are dominated by  $I_2$ . This has important consequences in using this technique to witness excited-state coherences as we analyse below.

For very small times ( $t_2 - t_1 \simeq 0$ ), the trace that appears in  $I_2$  (cf. Eq.(2.44)) can be approximated as:

$$\text{Tr}[a_2(t_2 - t_1) \tilde{\rho}_{1,0}^{1,0}(t_1) a_2^{\dagger}] \simeq \sum_{i=1}^2 \sum_{j=1}^2 \sum_{l=0}^L \langle X_i, l | \tilde{\rho}_{1,0}^{1,0}(t_1) | X_j, l \rangle. \quad (3.9)$$

This result indicates that  $I_2$  tracks superpositions of excited states which arise only when the excitonic states are subjected to quantum coherent dynamics. Notice also that the oscillatory pattern, both in  $I_1$  and  $I_2$ , changes from dimer 1 to dimer 2, indicating that this must come from coherent vibronic evolution rather than solely from coherent vibrational dynamics.

The above analysis shows that frequency- and time-resolved photon correlations are sensitive to the exciton-vibration interactions and that these correlation functions witness coherences within the excited state manifold of the systems under study. To support this hypothesis, we have also performed a simulation with the same parameters in Fig.3.8(a), but decreasing the coupling to the effective vibrational mode ( $g = (33\text{ps})^{-1} = 1\text{cm}^{-1}$ ). The dotted plot in Fig.3.9 shows a behaviour closer to the perfect quantum emitter, with a smaller asymmetry  $f_- = 0.54$ . This result suggests that the statistics is affected by the vibronic dynamics.

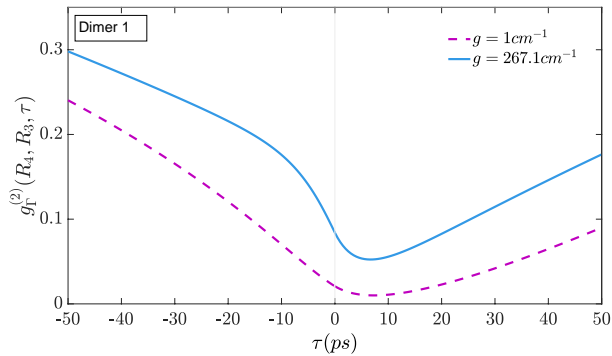


Figure 3.9: Frequency- and time-resolved cross-correlation functions  $g_{\Gamma}^{(2)}(R_4, R_3, \tau)$  for dimer 1 comparing different couplings  $g$  to the phonon bath (other parameters in Fig.3.1(b) and 3.1(c)).

The asymmetry observed in Fig.3.8 has also another non-trivial implication. In general, time symmetry of the cross-correlations of two different state variables around equilibrium are a fundamental aspect bringing to the Onsager relations [153]. The symmetry comes from the microscopic reversibility (two different state variables are assumed to be symmetric under time-reversal), and, very importantly, it requires that the detailed balance is respected. This means that transitions between any two states take place with equal frequency in either direction at equilibrium. In a Markovian process, this further implies that the equilibrium probability current vanishes [154]. On the other hand, in open quantum systems, one is usually interested in the steady state out of equilibrium. Here, correlation functions of the light emitted by an open system are probed with different detection techniques, which is the situation studied in this Chapter. Generally, in all these cases, the fluctuations around the steady state may have a specific time order, thus breaking the symmetry and the detailed balance. Nonetheless, even if the detailed balance is not guaranteed to hold out of equilibrium [155], there are several cases where the particular boundary conditions and the symmetry of the problem allow it still to

hold [156–160]. Therefore, it is not trivial when we find a situation in which there is a breakdown of the detailed balance. In our case, the steady state system is out of equilibrium because of the incoherent pumping of the highest exciton. Furthermore, we have observed that the correlation function is asymmetric, thus reporting the breakdown of the detailed balance. In the situation analysed, the asymmetry can be traced back to the particular form of the contribution  $I_2$  in Eq.(2.44), which has two different frequencies,  $\omega_2$  and  $\omega_1$  in the exponential factor for positive or negative times, respectively.

### 3.5 Relations between coherent contribution dynamics and filtering analysis

To gain a better understanding of the features shown by the study of the frequency-filtered and time-resolved correlation functions, we now present the plots for different pumping rates  $P = (0.3, 0.6, 0.9\text{ns})^{-1}$  of the highest exciton (Figs. 3.10 and 3.11) and for different values of the thermal damping of the collective mode  $\Gamma_{th} = (1, 3, 6.7\text{ps})^{-1}$  (Figs. 3.12 and 3.13). In nature this damping rate has a fixed value, however, it is possible to change it within superconducting circuits [161].

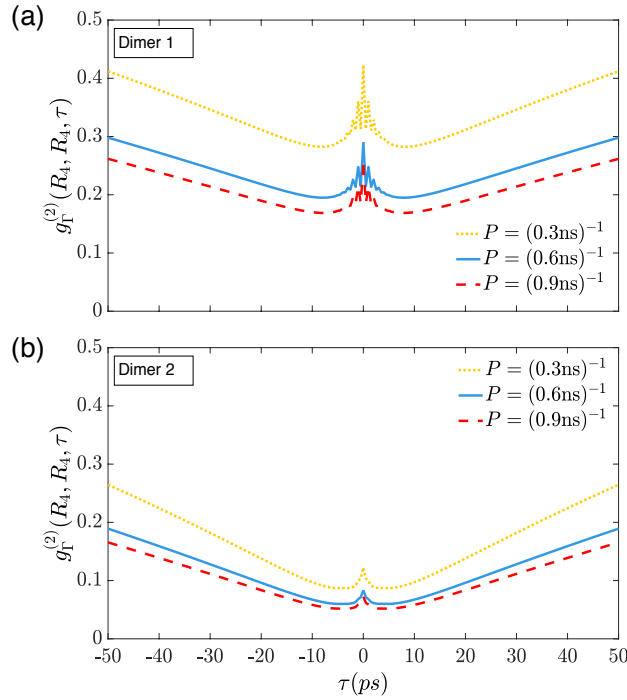


Figure 3.10: Frequency- and time-resolved auto-correlation functions  $g_{\Gamma}^{(2)}(R_4, R_4, \tau)$  for (a) dimer 1 (quasi-localised model) and (b) dimer 2 (more delocalised model), for different pumping rates  $P$ , with the other parameters in Fig.3.1(b) and 3.1(c).

In both Figs. 3.10 and 3.11 it can be observed that a larger pumping rate gives a higher intensity of the correlation function. Additionally, the auto-correlations in Fig.3.10(a) show the same oscillatory features observed in Fig.3.7.

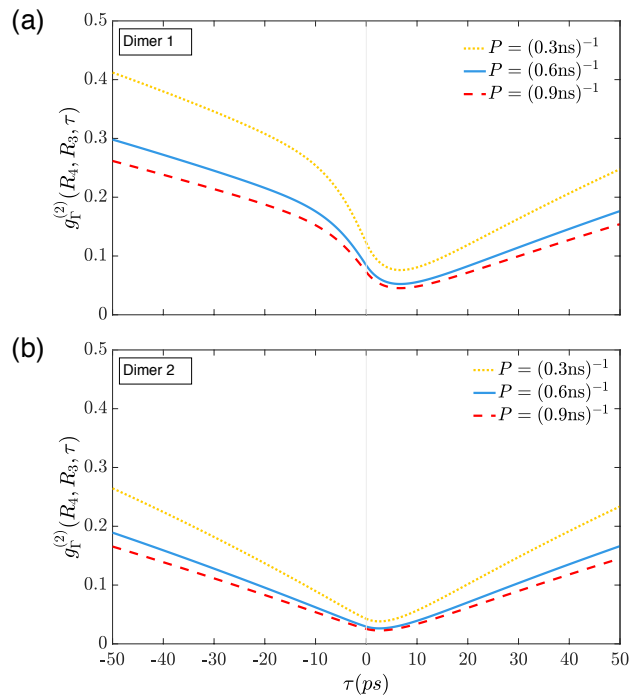


Figure 3.11: Frequency- and time-resolved cross-correlation functions  $g_{\Gamma}^{(2)}(R_4, R_3, \tau)$  for (a) dimer 1 (quasi-localised model) and (b) dimer 2 (more delocalised model), for different pumping rates  $P$ , with the other parameters in Fig.3.1(b) and 3.1(c).

The same analysis discussed before to evaluate the asymmetry of  $g_{\Gamma}^{(2)}(R_4, R_3, \tau)$  reveals that in Fig.3.11(a)  $f_- = 0.85, 0.60, 0.53$ , for the yellow, blue and red curve, respectively. In Fig.3.11(b), instead,  $f_- = 0.16, 0.11, 0.10$ , for the yellow, blue and red curve, respectively. This means that within both models, the cross-correlations exhibit more asymmetry when the pumping rate is bigger, namely when the system is pumped more often, being then driven towards classical conditions. Dimer 1 displays more asymmetry due to the quasi-localised nature of the excitons, which implies a light emission behaviour further from the purely quantum.

The analysis of the auto-correlations for different damping rates of the mode reveals that, within the model of dimer 1 (Fig.3.12(a)), the intermediate value of  $\Gamma_{th}$  (blue curve) guarantees the achievement of the equilibrium earlier, while the intensity of the correlation around  $\tau = 0$  ns increases when the coherences decay faster. In the case of more delocalisation (dimer 2), instead, a closer look at larger times shows that the smaller the damping rate is, the slower the system reaches the equilibrium (see Fig.3.12(b)).

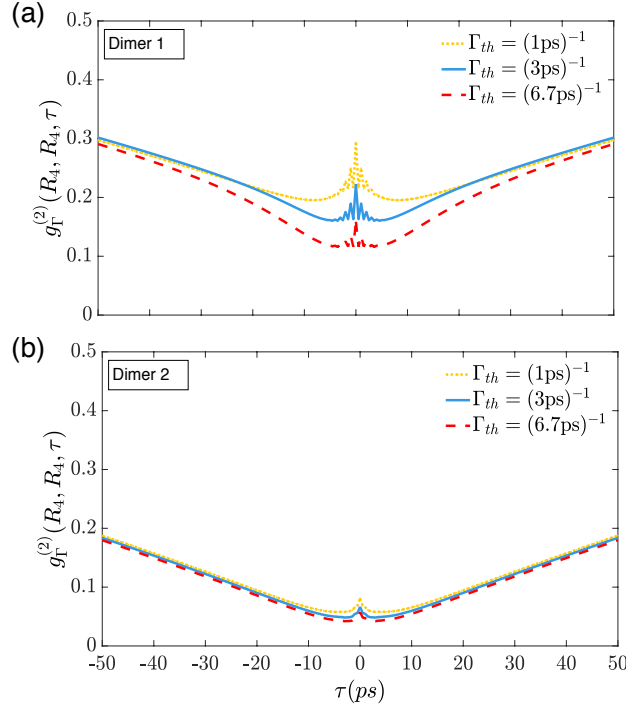


Figure 3.12: Frequency- and time-resolved auto-correlation functions  $g_{\Gamma}^{(2)}(R_4, R_4, \tau)$  for (a) dimer 1 (quasi-localised model) and (b) dimer 2 (more delocalised model), for different damping rates  $\Gamma_{th}$  for the mode, with the other parameters in Fig.3.1(b) and 3.1(c).

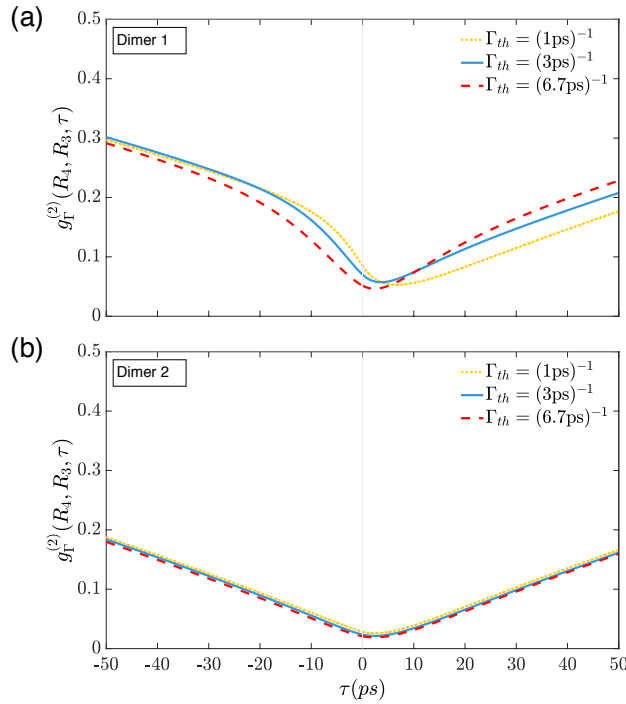


Figure 3.13: Frequency- and time-resolved cross-correlation functions  $g_{\Gamma}^{(2)}(R_4, R_3, \tau)$  for (a) dimer 1 (quasi-localised model) and (b) dimer 2 (more delocalised model), for different damping rates  $\Gamma_{th}$  for the mode, with the other parameters in Fig.3.1(b) and 3.1(c).

Regarding the cross-correlation analysis, in Fig.3.13(a) some similar features can be observed within the two regimes. In fact the values for the function  $f_-$  in Fig.3.13(a) are  $f_- = 0.6, 0.46, 0.3$ , for the yellow, blue and red curve, respectively. This means that within the model of dimer 1 the asymmetry is more evident for bigger values of  $\Gamma_{th}$  (see yellow curve). The direct implication of this result is that the more the asymmetry is emphasised in the cross correlation functions, the further the behaviour of the emitting system is from the perfect quantum emitter. Also the configuration for dimer 2 in Fig.3.13(b) displays that the asymmetry affects the correlation function slightly more when the thermal damping rate increases, with  $f_- = 0.0491, 0.0482, 0.0440$ , for the yellow, blue and red curve, respectively.

The comparison of these values for dimer 1 and dimer 2 highlights a very important aspect: a more evident asymmetry is a feature describing the quasi-localised nature of the excitons, while a cross-correlation function exhibiting more symmetry characterises the collective nature of the emission due to the bigger delocalisation of the excitons over the sites.

It is also worth noting that, in particular for dimer 1, we can observe two different rates of approaching the uncorrelated emission for positive and negative times. As already pointed out, positive and negative times correspond to detection of frequencies with inverted order. In other words, the first frequency probed at positive times is the second frequency detected at negative times. Different transitions correspond to different coherences: in this sense the peculiar behaviour shown by the correlation function witnesses that different coherences approach the equilibrium state at different rates.

### 3.6 Conclusion

In Chap.2 it has been highlighted that the theoretical approach developed to compute the frequency-filtered and time-resolved photon correlations allows to recover the correct behaviour of  $g_{\Gamma}^{(2)}(\omega_1, \omega_2, \tau)$  for long times. In this chapter, this method has been used to study some statistical properties of two prototypes of light harvesting complexes.

It has been proved that this photon counting analysis does capture features that colour blind detectors do not, reflecting the effects of the exciton-vibration interaction. The technique is also very promising, given the possibility to apply the theoretical approach to experimental setups. This would allow to focus on individ-

ual complexes in order to overcome the challenge dealt with the average behaviour of biomolecules ensembles in spectroscopic experiments.

To examine the effects of different electronic delocalisation, two different regimes have been investigated. The simulations show two fundamental aspects.

One is that the asymmetry observed in the cross correlation functions is more evident in the configuration of quasi-localised excitons, while a bigger delocalisation of the excitons over the sites, and then a more collective behaviour in the light emission, manifest themselves in a more symmetric shape of the correlation function.

Equally relevant is that in both configurations more asymmetry can be observed when vibronic coherences decay faster. This seems to suggest that a more symmetric correlation function characterises a system where a longer quantum interaction between these degrees of freedom takes place. However, this hypothesis needs further investigation.

In conclusion, even in such simple systems and in the steady state condition, this kind of study provides evidence of the exciton-vibration interaction. Frequency- and time-resolved photon correlation measurements can, indeed, probe coherent contributions to the emission statistics of light-harvesting complexes. Such correlations are affected by the vibronic coupling characterising biomolecules, witnessing coherences within the excited state manifold of the systems of interest. This implies that correlation functions carry clear signatures of quantum coherent dynamics and, therefore, they can be a very useful tool to investigate new features in simple systems as well as in more complicated biological antennae.

The results presented in this Chapter are in preparation for submission to a peer-review journal.

## Chapter 4

# Coloured photon counting statistics of bio-inspired dimers coupled to a cavity

In this chapter we consider the same bio-inspired vibronic dimers considered in Chap.3 but now in interaction with the confined mode of an optical cavity. We analyse the frequency-filtered and time-resolved statistics of the combined system-cavity, using the perturbative formalism developed in Chap.2. We consider the weak system-cavity coupling such that the presence of the cavity in this configuration has the effect of increasing the rate of light emission by our systems of interest. At the same time, the regime of weak coupling guarantees that the cavity does not affect significantly the internal quantum mechanical structure of the system of interest.

### 4.1 Introduction

In Chap.3 we have analysed how the frequency-filtered and time-resolved correlation functions can reveal important information about the dynamics of the system under study in free space. However, this configuration suffers from very low photon emission, which makes the measurements of such photon-statistics challenging. To improve this aspect the system can be coupled to a cavity mode, in order to enhance the photons detected [162–164].

Big steps forward have been made in the field of quantum optical phenomena, especially at single photon level [165], thanks to the use of optical cavities with high quality factors to analyse light-matter interaction for single atoms [166] or quantum dots [167]. Quantum optical phenomena have been explored also in the strong

system-cavity coupling [168], as well as in the ultra-strong [168–171] and in the deep strong [172] coupling regimes. The feature common to these three situations is that the coupling strength  $g_c$  between the system and the cavity dominates any decay rate  $\gamma_i$  involved in the dynamics [173], that is  $g_c > \gamma_i$ . However, the relationship between the coupling strength and the frequency of the cavity mode is different in each of these cases. In the ultra-strong regime the coupling strength is of some order of magnitude comparable to or larger than fractions of the cavity frequency, namely  $g_c \gtrsim 0.1\omega_c$  [168–171]. In the deep strong regime, instead, the coupling is comparable to or larger than the cavity frequency, that is  $g_c \gtrsim \omega_c$  [172]. In all these regimes system and cavity become interwoven and the system does not couple to its environment in an independent form. This means that they cannot be treated as separate systems and the master equation governing the dynamics has to be written in the dressed basis to have consistency in thermodynamics [174].

The presence of incoherent internal vibrations within biological molecules has made difficult to use them in quantum optical applications. Indeed, these molecules are characterised by specific transitions, with wavelength spanning from the microwave to the ultraviolet, depending on what they are related to (rotational, vibrational and electronic degrees of freedom). In the past few decades, the study of single molecules in solid state has been achievable thanks to high spatial and spectral resolutions, but these systems are still characterised by some decoherence due to the phononic coupling [175]. Nonetheless, it has recently been demonstrated that an organic molecule located inside a microcavity exhibits the same behaviour of a two-level quantum system [176]. Moreover, within the quantum biology field, the strong coupling between excitons of a photosynthetic light-harvesting antennae and a confined optical cavity mode has been investigated [177]. This strong coupling regime implies the formation of polariton states, whose energy differs from both the exciton and photon. As a consequence, the pathway of the energy transfer in photosynthetic antenna can be modified, yet without altering the molecular structure of the complex.

However, in this work we are not interested in cavity-system settings that modify the transfer pathways, but in settings where the weak coupling between the bio-inspired models and the optical cavity allows to investigate the dynamics of individual light-harvesting systems.

## 4.2 Motivation

The aim of this chapter is to analyse how the presence of a weakly coupled cavity affects the correlation functions of the system under scrutiny. We will apply the sensor formalism developed in Chap.2, coupling the sensors to the cavity mode, in order to examine the one- and two-coloured photon spectrum and extrapolate information about the dynamics of the vibronic system of interest. The system we envision is represented in Fig.4.1.

From a theoretical view point, cavity quantum electrodynamics setups have already been employed to investigate the excitation energy transfer dynamics in photosynthetic complexes in weak coupling regime [178]. This study considers the FMO (Fenna-Matthews-Olson) pigment-protein complex subject to coherent pumping and interacting with an optical microcavity, in order to analyse the statistical properties of the emitted photons. The goal was to gain information about the coherent quantum dynamics of the light harvesting system looking at the counting statistics associated with it. The authors claim that the zero time delay second order correlation  $g^{(2)}(0)$  depends on the amount of the dephasing involved in the dynamics, which could help understand the strength of interaction between the biomolecule and its environment.

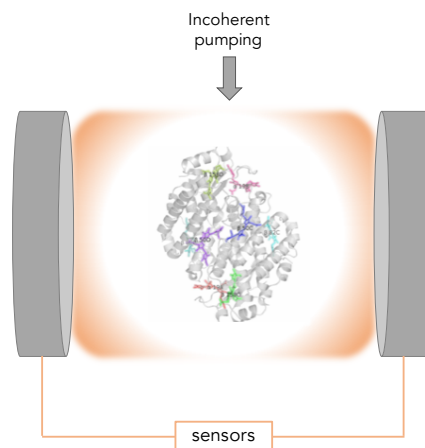


Figure 4.1: *Representation of the system we analyse in this chapter: a bio-inspired system, undergoing incoherent pumping, is located inside a cavity weakly coupled to sensors, which detect outgoing photons at specific frequencies.*

The reason behind our choice of weakly coupling the biological system to a cavity is to increase the emission of the photons coming out of the system. In a recent work [179], indeed, the authors have been able to create quantum dots single-photon sources, interacting with confined optical modes, that register a Purcell factor three

times bigger than the analogous situation in free space. We consider the two model systems described in the previous chapter (see Sec.3.2), so as to show the effect of a different delocalisation of the excitons over the sites.

### 4.3 Model: vibronic system coupled to a cavity

We focus the attention on the prototype biological dimers introduced in Sec.3.2, investigating two different regimes of exciton delocalisation. We consider the vibronic system with Hamiltonian given in Eq.(1.82) and fully explained in Sec.1.4. Here, we report its expression for clarity:

$$H_{\text{el-vib}} = \alpha M + \frac{\Delta\alpha}{2} \sigma_z + V\sigma_x + \omega_{\text{vib}}(d_1^\dagger d_1 + d_2^\dagger d_2) + \sum_{k=1}^2 g |k\rangle\langle k| (d_k^\dagger + d_k). \quad (4.1)$$

We remind the reader that in this case  $\sigma_z$  has been defined as  $\sigma_z = |1\rangle\langle 1| - |2\rangle\langle 2|$ , that is the population difference between local excited states. Similarly

$$\sigma_x = |1\rangle\langle 2| + |2\rangle\langle 1|.$$

The choice of operating in the site basis is due to the presence of the cavity introduced in the new setup, which does not allow to decouple the coordinates related to the mode centre of mass from those related to its relative displacement.

The cavity mode is described as a quantum harmonic oscillator of frequency  $\omega_c$  and creation and annihilation operators  $b_k$  and  $b_k^\dagger$ , respectively. The cavity excitation has been assumed on resonance with the highest exciton transition ( $\omega_c = E_1 = 18529 \text{ cm}^{-1}$ ). We also suppose local electronic states of the vibronic dimer coupled to the cavity with strength  $g_c$ , so that the cavity-system interaction is described by the Hamiltonian:

$$H_{\text{el-c}} = \omega_c b^\dagger b + \frac{1}{2} \sum_{k,k'=1}^2 g_c [(\sigma_k + \sigma_{k'})b^\dagger + (\sigma_k^\dagger + \sigma_{k'}^\dagger)b]. \quad (4.2)$$

Here, it has been assumed that the electronic degrees of freedom are weakly coupled to the cavity mode, therefore the rotating wave approximation has been applied in the equation above (the coupling is very weak in comparison to the electronic transitions).

As the system under scrutiny is a multilevel system, coupling it to a cavity mode in resonance with the exciton transitions allows to selectively increase such specific emission. Therefore, the analysis of the statistical properties of the light emitted by

the cavity in resonance with some characteristic frequency of the system of interest allows to gain information about it. Hence we assume the hypothetical sensors are weakly coupled to the cavity with a Hamiltonian taking the form given in Eqs. (1.97) and (1.98) and here reported:

$$H_{c-m} = \sum_m [\omega_m \varsigma_m^\dagger \varsigma_m + \epsilon_m (b \varsigma_m^\dagger + b^\dagger \varsigma_m)]. \quad (4.3)$$

Dissipations and dephasing channels for the system-cavity are introduced via a phenomenological master equation in the Lindblad form (see Sec.1.3.3.2). More specifically, the Lindblad master equation (see Eqs.(2.64) and (2.66)) is used to express the dephasing and relaxation processes happening during the evolution. Here, we report both Eqs. (2.64) and (2.66) together (adapted to the site basis we are working on), including also the relaxation term for the cavity:

$$\begin{aligned} \mathcal{L}(\hat{\rho}) = & -i [H_{\text{el-vib}} + H_{\text{el-c}} + H_{c-m}, \hat{\rho}] \\ & + \sum_{k=1,2} \frac{\gamma_{pd}}{2} \mathcal{L}_{A_k}(\hat{\rho}) + \frac{\gamma}{2} \sum_{v=1}^{2z} \sum_{r=1}^z \mathcal{L}_{\sigma_{vl}}(\hat{\rho}) + \frac{P_{X_1}}{2} \mathcal{L}_{\sigma_{X_1}^\dagger}(\hat{\rho}) \\ & + \sum_{k=1}^2 \frac{\Gamma_{th}(\eta(\omega_{\text{vib}}) + 1)}{2} \mathcal{L}_{b_k}(\hat{\rho}) + \frac{\Gamma_{th} \eta(\omega_{\text{vib}})}{2} \mathcal{L}_{b_k^\dagger}(\hat{\rho}) \\ & + \frac{\Gamma_c}{2} \mathcal{L}_c(\hat{\rho}) + \sum_m \frac{\Gamma}{2} \mathcal{L}_{\varsigma_m}(\hat{\rho}), \end{aligned} \quad (4.4)$$

where all the parameters are specified in Tables 3.1(b) and 3.1(c), in Sec.3.3. Since we are working in the site basis, we denote the vibrational eigenstates of the phonon modes with  $|l\rangle$  for mode 1 and  $|l'\rangle$  for mode 2, where  $l = 0, 1, \dots, L$  and  $l' = 0, 1, \dots, L'$ , with  $L$  and  $L'$  the maximum numbers set in the numerical simulation (we assumed  $L = L'$ ). We also indicate the eigenstate of the cavity mode with  $|l''\rangle$  where  $l'' = 0, 1, \dots, L''$ , with  $L''$  the maximum number set in the numerical simulation. In the Eq. above  $z = L * L' * L'' = L^2 * L''$ .  $\Gamma_c$  is the cavity decay rate and the choice of its value has been based on parameters used for cavity quantum electrodynamics experiments [180], considering an intermediate situation between a “good” or “bad” cavity, and with low dispersions and relatively high quality factor  $Q$ . The latter is defined as  $Q = \omega_c / \Gamma_c$  and for a realistic good cavity its value can be of the order of  $10^6$  [180]. The value of the cavity frequency has been chosen equal to the energy of the highest exciton  $\omega_c = E_1 = 18529 \text{cm}^{-1}$ , therefore for a quality factor of  $Q = 6 \cdot 10^6$ , the corresponding decay rate is  $\Gamma_c = (10 \text{ns})^{-1} = 10^8 \text{Hz}$ .

The size of the mixing angle  $\theta$  determines the degree of localisation of the excitons over the sites, through the expression displayed in Eq.(3.2). Here, our purpose is to investigate again two cases close to the two limits of quasi-localised and more delocalised excitons over the sites (more details are given in Sec.3.3). This delocalisation is expressed through the parameter  $\zeta = \tan(2\theta) = 2|V|/\Delta\alpha$ . The parameters related to these two situations are reported in table 3.1(b), that shows the common values in the two regimes, and in table 3.1(c), where the differences between them have been highlighted. For clarity, we specify that in our numerical calculations all wavenumbers given in the tables are multiplied by  $2\pi c$ , where  $c$  is the speed of light. Dimer 1 is inspired to the central dimer in the cryptophyte antennae PE545 [22,132], where  $\zeta_1 = 0.1$ . The second model instead, dimer 2, exhibits the same energy difference between the excitons ( $\Delta E_1 = \Delta E_2 = \Delta E$ ), as well as the same resonance condition between them and vibrational energy ( $\Delta E \sim \omega_{\text{vib}}$ ). However, the degree of delocalisation has been chosen to be slightly bigger,  $\zeta_2 = 0.5$ . Starting from these conditions, the coupling between the sites in dimer 2 is given by  $V_2 = \zeta_2 \Delta E / \left(2\sqrt{1 + \zeta_2^2}\right)$  and the energy splitting between them by  $\Delta\alpha_2 = \Delta E / \sqrt{1 + \zeta_2^2}$ .

## 4.4 Counting statistics in the cavity

### 4.4.1 Numerical simulations

Before presenting the results obtained, it is important to specify some aspects that make the numerical performance quite challenging. The main difficulty is due to the fact that, in principle, bosonic modes requires infinite excitations, then causing an exponential growth of the Hilbert space. However, in practice, it is necessary to restrict the Hilbert spaces of both the phonon modes and the cavity mode.

Regarding the vibrational modes, based on the analysis presented in Sec.3.3, we know that a maximum number of excitations  $L = 2$  suffices to analyse the photon statistics associated to the vibronic systems of interest, as shown in Appendix A.

The situation for the Hilbert space associated to the cavity mode requires a more careful thought. To show the reason behind this assertion, in Appendix B, we analyse the power spectra and the time-resolved correlation functions for both dimers, considering two different values of the coupling strength ( $g_c = (1.33\text{ps})^{-1} = 25 \text{ cm}^{-1}$  in Fig.B.1 and  $g_c = (0.67\text{ps})^{-1} = 50 \text{ cm}^{-1}$  in Fig.B.2). The figures compare the results obtained with two different values for the maximum number of excitations in the cavity mode,  $L'' = 3, 4$ .

As it can be noticed in Figs.B.1(a) and (b) and Figs.B.2(a) and (b), the power spec-

tra for both dimers and both values of couplings show convergence for  $L'' = 3$ . It has been verified that the same conclusion holds for the computation of the second order correlation at zero time delay. Concerning the cross correlation function at finite time delay, Fig.B.1(d) and Fig.B.2(d) show that for dimer 2 a maximum number of  $L'' = 3$  guarantees results qualitatively close to the those that converge. However, for dimer 1 such value of  $L''$  does not suffice to assure convergence at short time delays for either of the two  $g_c$  values considered. We therefore consider  $L'' = 4$ .

#### 4.4.2 First order correlations $S_{\Gamma}^{(1)}(\omega_1)$

We now investigate the statistical properties of the two bio-inspired systems of interest. First of all, we analyse the power spectra for different values of the coupling between the electronic degrees of freedom and the cavity. The aim is to highlight similarities with the power spectra found in free space (see Fig.3.4), in order to guarantee a condition for the cavity coupling that does not alter significantly the emission frequencies of the system under study.

The one-photon correlations reported in Fig.4.2 describe the situations for the two different models: dimer 1, with quasi-localised excitons (see Fig.4.2(a)), and dimer 2, with more delocalised excitons (see Fig.4.2(b)). It shows the frequencies emitted by the system of interest for both configurations: the main peaks are about the same and the feature common to both is that the larger the coupling, the more structured the spectrum becomes. In presence of the cavity the main frequencies emitted by the systems are:  $R_2 = 16330 \text{ cm}^{-1}$  and  $R_3 = 17450 \text{ cm}^{-1}$ ,  $R_4 = 18480 \text{ cm}^{-1}$ . When the system experiences more delocalisation, it can be observed a more emphasised splitting of the peak at  $R_3$  and a slightly different structure for the peak at  $R_4$  (see Fig.4.2(b)). The power spectrum exhibiting a more similar structure to that observed in free space (cf.Fig.3.4) is obtained for  $g_c = (1.33\text{ps})^{-1}$ , and therefore we choose this value to perform further simulations for the time-resolved analysis. In fact, although the condition of weak coupling for the decay rates  $g_c < \gamma_i$  is not met by the value  $g_c = (1.33\text{ps})^{-1}$ , it is still good enough to be considered for the purpose of this work, since  $g_c \ll \omega_c$ .

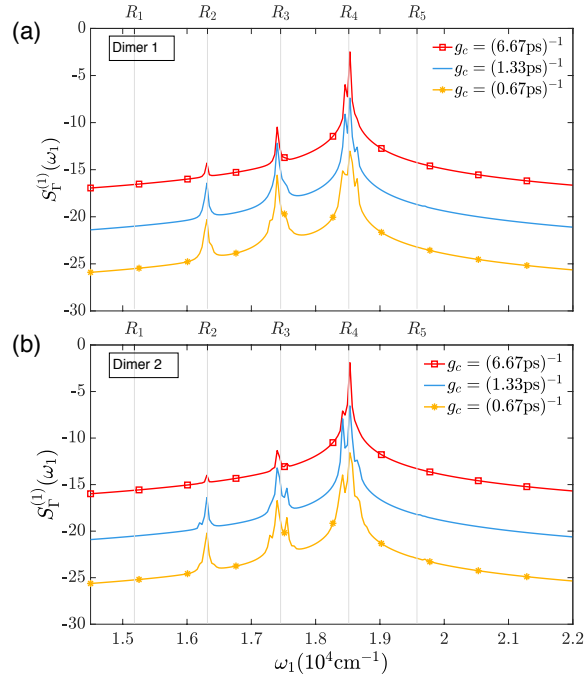


Figure 4.2: Power spectra for: (a) the quasi-localised model in dimer 1 and (b) the more delocalised in dimer 2, with parameters given in Tables 3.1(b) and 3.1(c). The yellow line corresponds to the spectrum with the largest value of coupling. The plots are in arbitrary units and the spectra have been translated with respect each other to better distinguish their features. The figure is in log scale.

#### 4.4.3 Zero time delay second order correlations $g_{\Gamma}^{(2)}(\omega_1, R_3)$

The computation of the second order frequency-filtered correlations at zero time delay in Fig.4.3 is carried out by fixing the frequency at the peak  $\omega_2 = R_3$  (one of the main peaks in both power spectra in fig.(4.2)), and letting the frequency of the other photon  $\omega_1$  vary over the whole spectral range. In this case, the comparison among the three different coupling parameters  $g_c$  is reported again for completeness. Fig.4.3 seems to suggest that antibunching is observed within both models for intermediate and smaller coupling, as well as for the largest system-cavity coupling in the more delocalised system. The only exception can be observed for the quasi-localised model, when the coupling parameter is the largest ( $g_c = (0.67ps)^{-1}$ ). In this case, the correlation between frequency  $R_3$  and frequencies slightly smaller than  $R_4$  shows bunching. Moreover, within this regime, the overall values of  $g_{\Gamma}^{(2)}(\omega_1, R_3)$  are closer to zero, indicating that such cross-correlated emission is more antibunched. Fig.4.3 also highlights that the correlation computed with  $g_c = (1.33ps)^{-1}$  is overall closer to zero for the more delocalised model, again meaning that the system in this configuration exhibits more antibunching.

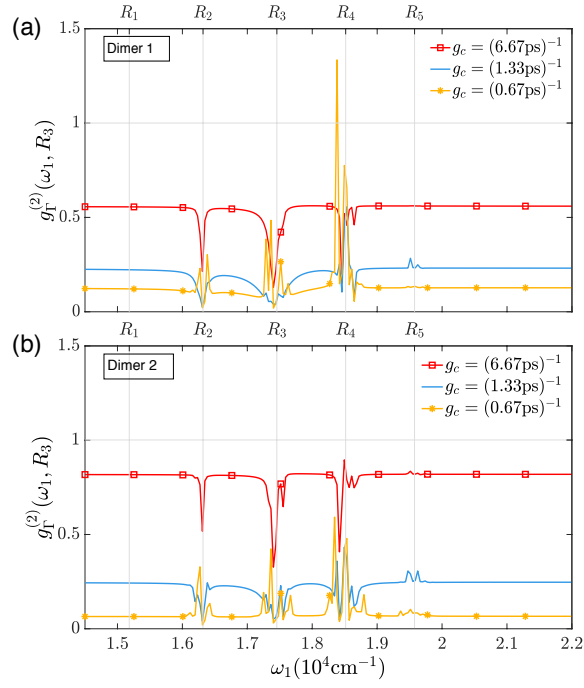


Figure 4.3: *Second order correlations at zero time delay for: (a) dimer 1 and (b) dimer 2, with parameters in Fig.3.1(b) and 3.1(c). The figure is in semilog scale. The yellow line corresponds to the spectrum with the largest value of coupling.*

#### 4.4.4 Finite time delay second order correlations $g_{\Gamma}^{(2)}(R_4, R_3, \tau)$

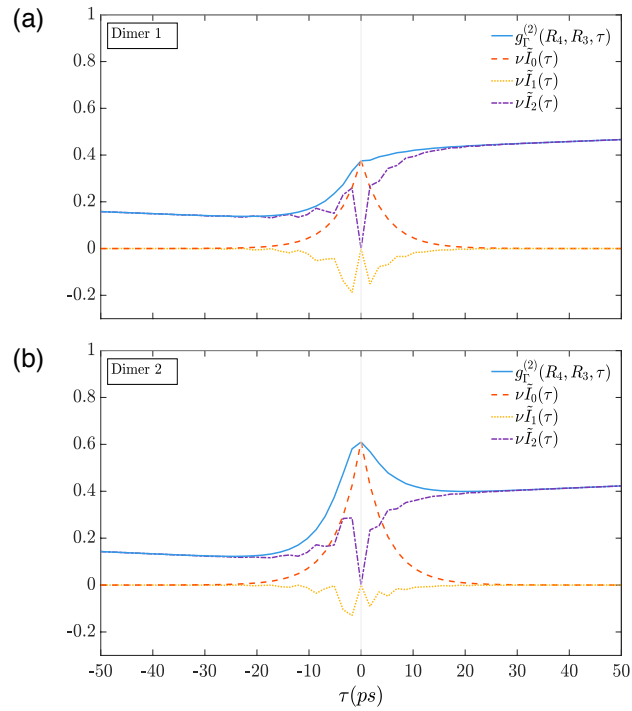


Figure 4.4: *Frequency- and time-resolved cross-correlation function  $g_{\Gamma}^{(2)}(R_4, R_3, \tau)$  for: (a) the quasi-localised configuration in dimer 1 and (b) the more delocalised model in dimer 2, with parameters in Fig.3.1(b) and 3.1(c).*

To better understand the nature of light emitted, the time-resolved second order cross-correlations  $R_4 - R_3$  have been computed at finite time delay, again for both configurations. Fig.4.4 seems to suggest that both dimers are emitting anti-bunched light, although the statistics observed is not trivial. In both regimes the presence of the cavity does alter the statistics of the light emitted by the system very significantly. In particular, the photon correlation observed for dimer 2 exhibits a completely different behaviour with respect to that shown in free space (cf. Fig.3.8), being now very far from the characteristic perfect quantum emitter correlation. It is also worth noticing that in both Figs.4.4(a) and (b) the derivatives at long times are positive, meaning that the correlation functions will eventually tend to 1, as expected (see Sec.2.4.2).

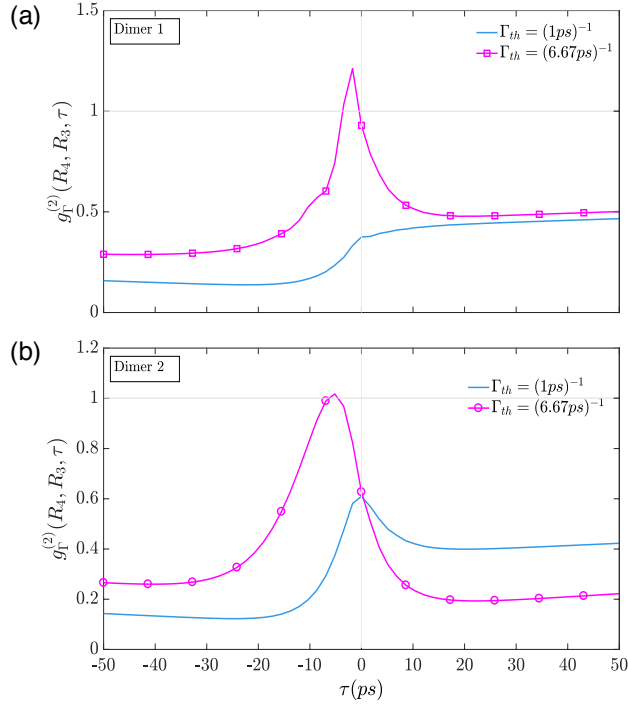


Figure 4.5: Frequency- and time-resolved cross-correlation functions  $g_{\Gamma}^{(2)}(R_4, R_3, \tau)$  for: (a) the quasi-localised configuration in dimer 1 and (b) the more delocalised model in dimer 2, for different damping rates  $\Gamma_{th}$  for the modes, with the other parameters in Fig.3.1(b) and 3.1(c).

As a further investigation, we examine the cross-correlation comparing different values of the thermal damping rates, to gain an insight of the effect of the vibrational relaxation on the statistical properties of the light emitted by the systems. Fig.4.5 represents the time-resolved correlation function within both regimes and for two values of the thermal damping:  $\Gamma_{th} = (1ps)^{-1}$  and  $\Gamma_{th} = (6.67ps)^{-1}$ . For slower vibrational relaxation, the photon statistics of dimer 1 changes from sub-Poissonian

to super-Poissonian as can be seen in Fig.4.5 (square markers).

To understand better the implications of this change from sub- to super-Poissonian statistics, we now analyse the Cauchy-Schwarz inequality (CSI) for these correlations [181]. The CSI states that correlations of the product of two variables  $X$  and  $Y$  are bounded by the product of the auto-correlations, namely  $|\langle XY \rangle|^2 \leq \langle X^2 \rangle \langle Y^2 \rangle$ . However, when the two variables are quantum observables, a violation of this inequality can occur [182–188]. This means that correlations between the observables can be strong enough to overcome the product of auto-correlations. In this context, the CSI inequality can be expressed through the correlators between the sensors. More specifically, we define  $g_{\Gamma,ij}^{(2)}(\tau)$  as in Eq.(2.31), considering the same linewidth for both sensors, that is:

$$g_{\Gamma,ij}^{(2)}(\tau) = g_{\Gamma}^{(2)}(\omega_i, \omega_j, \tau) = \frac{S_{\Gamma}^{(2)}(\omega_i, \omega_j, \tau)}{S_{\Gamma}^{(1)}(\omega_i) S_{\Gamma}^{(1)}(\omega_j)} = \frac{\langle \varsigma_i^{\dagger} \varsigma_j^{\dagger}(\tau) \varsigma_j(\tau) \varsigma_i \rangle}{\langle \varsigma_i^{\dagger} \varsigma_i \rangle \langle \varsigma_j^{\dagger} \varsigma_j \rangle}. \quad (4.5)$$

The CSI in time is then expressed through the ratio [189]:

$$R_{\Gamma,ij} = \frac{[g_{\Gamma,ij}^{(2)}(\tau)]^2}{g_{\Gamma,ii}^{(2)} g_{\Gamma,jj}^{(2)}} = \frac{\langle \varsigma_i^{\dagger} \varsigma_j^{\dagger}(\tau) \varsigma_j(\tau) \varsigma_i \rangle^2}{\langle (\varsigma_i^{\dagger} \varsigma_i)^2 \rangle \langle (\varsigma_j^{\dagger} \varsigma_j)^2 \rangle} < 1. \quad (4.6)$$

The calculation of this ratio for the quasi-localised configuration in dimer 1, with the smallest value of the thermal damping  $\Gamma_{th} = (6.67\text{ps})^{-1}$ , shows violation of the CSI for  $\tau < 0$ , implying the presence of nonclassical effects when frequency  $R_3$  is detected before  $R_4$ . This means that, although the statistics exhibits partial super-Poissonian distribution, the nature of the light emitted is quantum and presents antibunching. This effect has also been found in Ref. [139], where a two-level system was strongly coupled to a single mode of an optical cavity undergoing coherent pumping. The signature of the quantum nature of the emitter in our model is more evident when the thermal damping is smaller, namely when the vibronic coherences survive longer. The quantum behaviour of the light emitted reflects the quantum character of the interaction between the electronic degrees of freedom and the vibrational modes.

Finally, it is worth underlining an important point. In all the results presented above, we have coupled the sensors to the cavity mode. However, one could ask what happens if the sensors had been coupled to the electronic degrees of freedom. We have verified that the second order photon correlations remain qualitatively the same, but having coupled the sensors to the cavity has the advantage of increasing the intensity of the signal emitted. This has motivated our choice, as already mentioned at the beginning of this Chapter.

## 4.5 Conclusion

In this Chapter we aimed to complement the study of the second order photon correlation in free space, carried out in Chap.3. We have predicted frequency-filtered and time-resolved correlation functions of bio-inspired systems weakly coupled to a cavity mode, which probe coherent contributions to the emission statistics.

Having coupled the system to a cavity mode is often a good strategy to enhance the signal carrying out the quantum features of the emitter [83]. The use of the cavity has revealed to be very effective in our case. In fact, the light emitted by the system in free space can be difficult to capture, due to the low emission. The presence of the cavity allows to overcome this difficulty: increasing the coupling of the system to the cavity, the intensity of the emitted light is significantly enhanced. In principle this effect would continue when increasing the coupling even further. However, this would also alter the inner dynamics of the prototype photosynthetic complex, hybridising the states of the cavity and the system. For this reason the coupling strength has not been increased above a certain value, which guarantees a condition of weak coupling.

Moreover, the fact that we couple the system to the cavity has shown another interesting effect. The computation of the second order correlation function has, indeed, displayed super-Poissonian behaviour of the light emitted when the thermal damping of the phonon modes is reduced, meaning that the vibronic coherences of the system are more protected (see Fig.4.5). Even though a super-Poissonian distribution of the light emitted seems to be an indicator of classical light, one still needs to verify whether or not the correlation functions violate the CSI. In our case, we have indeed verified that the CSI is violated, which implies the quantum character of the light emitted. Therefore we have generated a beam of light that violates the CSI despite its super-Poissonian properties. This implies that the analysis of the statistics of the light emitted by the biomolecule of interest can provide information about the coherent contributions to the emission.

Our approach is very promising for the research in this field, since it could open the way to new experimental investigations that might be able to clarify and finally answer the main question debating in the community, that is whether or not photosynthetic complexes are characterised by non-trivial quantum coherence processes.

# Conclusions and outlook

In the field of quantum biology, photosynthesis has become the most paradigmatic process studied to understand the extremely high efficiency in the light harvesting process and energy transfer.

Experimentally, such effects have been investigated thanks to the development of two-dimensional electronic spectroscopy. In particular, it has revealed that the dynamics of biological systems presents oscillatory behaviour lasting up to picoseconds. These beatings survive for a surprising long time, given that electronic dephasing was expected to happen in a few hundreds of femtoseconds. One of the explanations proposed for these observations is intermolecular vibronic coupling, where excitons and some vibrational motions interact in a coherent form, promoting long-lasting coherent oscillations of quantum superpositions of excited states.

However, confirmations of this hypothesis with alternative techniques that can provide unambiguous signatures of these effects are needed.

Since one of the most powerful tools to identify quantum properties of light and emitters is the analysis of correlation functions, the aim of this thesis was to employ quantum optics techniques to explore quantum coherence interplay within prototype photosynthetic complexes.

Our first step (Chapter 2) has been to develop an alternative formulation of the sensor method to compute frequency-filtered and time-resolved correlation functions, both at zero and finite time delay. This method treats perturbatively the coupling between the system of interest and the sensors, and defines the photon correlations through a series of auxiliary matrices determined in the Hilbert space of the emitter only. These matrices also offer an insight into the physical processes involved in the measure of correlations. The expression for the time-resolved second order correlation function contains the sum of three contributions. Each of them gives an insight on the physical processes governing the correlations at different timescales.

The advantages of using this approach are several. First of all, the dimension of the Hilbert space results reduced, since the detectors are not included in the expression

of the photon correlations. Secondly, the results obtained do not rely on any assumption, meaning that they are valid also for non-Markovian systems. Moreover, within this approach correlation functions do not depend on the coupling parameter to the sensors, thus not requiring check for convergence of the results.

A further development of this research could be to prove the equivalence between the sensor method and the integral standard method used to compute photon correlations, without relying on quantum regression theorem and, therefore, on Markovian approximation. In such a case, we would be able to use the results obtained in our research even for non-Markovian quantum systems.

The following step (Chapter 3) has been to apply the method developed in Chapter 2 to compute frequency-filtered and time-resolved photon correlations to two different prototype photosynthetic complexes, in free space. This kind of analysis does capture features that the standard correlation function does not, therefore already proving the potential power of this tool. The two studied configurations differ for the degree of delocalisation of the excitons over the sites. The analysis shows important aspects.

Firstly, although the time-resolved correlation function exhibits sub-Poissonian statistics, it is not trivial to associate it to antibunching effects. Indeed, the cross-correlation shows asymmetry in the regime where the vibronic mechanism involves quasi-localised excitons, whereas the dimer characterised by more delocalisation presents a more symmetric correlation function. This is connected to the fact that the latter configuration is defined by a more collective behaviour in the light emission, therefore exhibiting features closer to the perfect quantum emitter. Nonetheless, the observed time-asymmetric fluctuations do indicate that the vibronic mechanism still affects the emission in this more delocalised system.

Secondly, but even more importantly, this frequency- and time-resolved photon correlation analysis is affected by the interplay between electronic and vibrational degrees of freedom. Indeed, it witnesses coherences, together with populations, within the excited state manifold of the system under study.

We have shown that frequency-filtered and time-resolved correlations capture quantum coherent contributions to excited states dynamics. This includes both populations and coherences. A further interesting investigation could be to understand the weight of each of these components. In addition, the computation of higher order correlations may shed light on the nature of the signal emitted by these biological complexes.

Finally (in Chapter 4), measurements of the frequency-filtered and time-resolved

correlation functions have been performed on the same two bio-inspired toy models, now weakly coupled to a cavity mode. Indeed, one of the main challenges in experiments when analysing single biomolecules using photoluminescence, is the weakness of the signal emitted. The presence of the cavity, however, enables to selectively increase the light emitted. In particular, as it is in resonance with one of the characteristic frequencies of the system, it allows to witness the electronic dynamics happening inside the biomolecule.

In principle, the larger the coupling, the more enhanced the light emitted. However, this coupling strength cannot be too large, due to the alteration it would cause to the internal dynamics of the system of interest. For this reason, a regime of weak coupling has been chosen for the purpose of this work. Nevertheless, exploring the regime of strong coupling could be interesting for a future investigation, since the emitted signal would probably increase even more. We point out that in this case one should consider a different master equation, as the two systems (cavity and vibronic part) would not be independently coupled to the different baths.

The coupling of the system to the cavity has shown interesting behaviours of the time-resolved cross-correlations. First of all, the signal emitted has increased due to the presence of the cavity. It exhibits super-Poissonian statistics, more evident in the configuration characterised by quasi-localised excitons and under a small thermal damping of the vibrational modes, meaning when the vibronic coherences of the system survive longer. Despite a super-Poissonian distribution of the light emitted seems to suggest a classical behaviour, a deeper analysis on the correlation function has been performed and we verified that the CSI is violated, implying the quantum nature of the light emitted.

Future works could analyse these correlations for more complex biological systems embedded in optical cavities. This approach appears, indeed, very promising thanks to the concrete possibility to experimentally measure filtered correlation functions of the light emitted by single molecules. The combination of such predictions with the experiments have the potential to unravel novel signatures of quantum coherent processes within biomolecules.

In conclusion, the research carried out in this thesis could pave the way to finally provide unambiguous proofs of quantum coherent processes occurring in the dynamics of single photosynthetic complexes.



# Appendix A

## Convergence for $L$ in free space

The analysis of both the power spectra (Fig.A.1(a)) and the zero (Fig.A.1(b)) and time resolved photon correlations (Fig.A.1(c)) for the system in free space shows that converged results can be obtained considering a maximum number of vibrational excitations of  $L = 4$ . However, even using only two excitations  $L = 2$  in the collective vibrational mode it is possible to obtain correct qualitative and quantitative results.

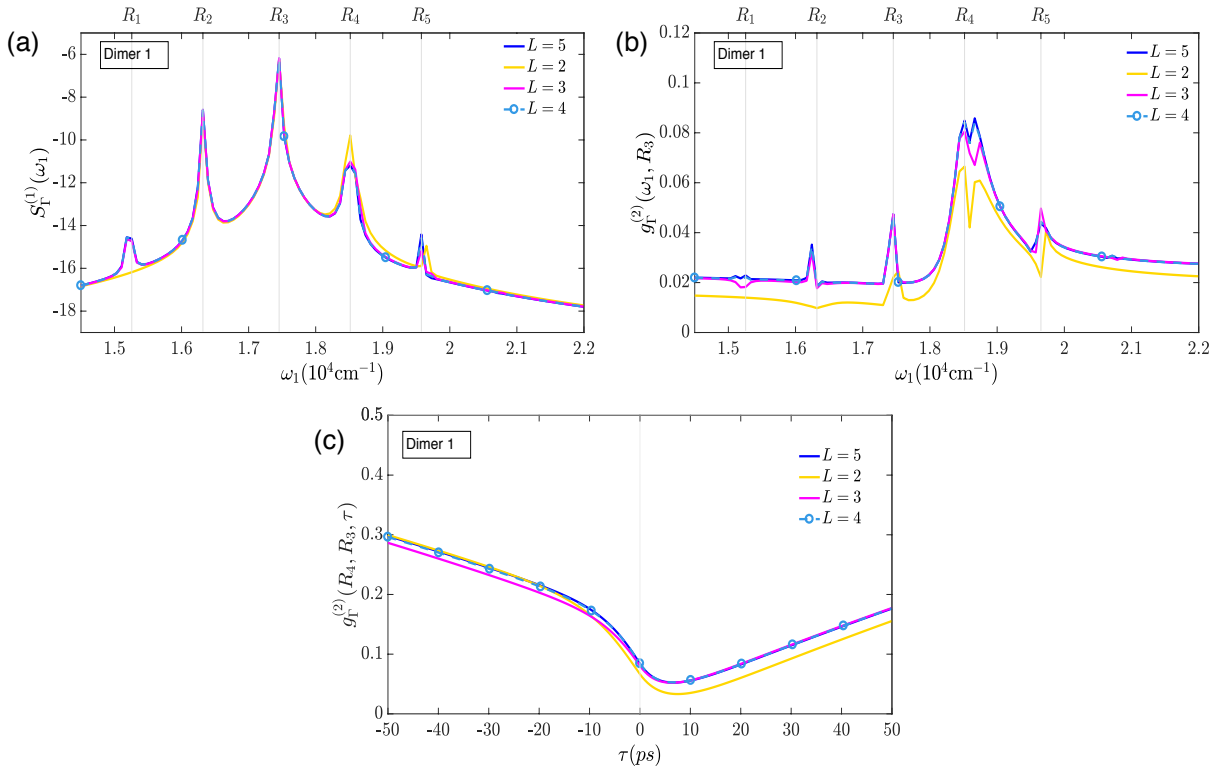


Figure A.1: The figure represents (a) the power spectra, (b) the zero time delay and (c) the time-resolved photon correlations for dimer 1, considering different values of the maximum number of excitations  $L$  in the collective vibrational mode.



## Appendix B

# Numerical checks in the cavity configuration

Fig.B.1 and Fig.B.2 analyse the power spectra and the time-resolved correlation functions for both dimers, considering two different values of the coupling strength ( $g_c = (1.33\text{ps})^{-1} = 25\text{ cm}^{-1}$  and  $g_c = (0.67\text{ps})^{-1} = 50\text{ cm}^{-1}$ , respectively). The figures compare the results obtained with two different values for the maximum number of excitations in the cavity mode,  $L'' = 3, 4$ .

It can be observed that the power spectra for both dimers and both values of couplings show convergence for  $L'' = 3$ . The same consideration holds for the cross correlation function of dimer 2 at finite time delay, as shown in Fig.B.1(d) and Fig.B.2(d). In this case, indeed, a maximum number of  $L'' = 3$  guarantees results qualitatively close to the those that converge. However, a different analysis needs to be done for dimer 1, since the value of  $L'' = 3$  does not suffice to assure convergence at short time delays for either of the two  $g_c$  values considered. We therefore consider  $L'' = 4$ .

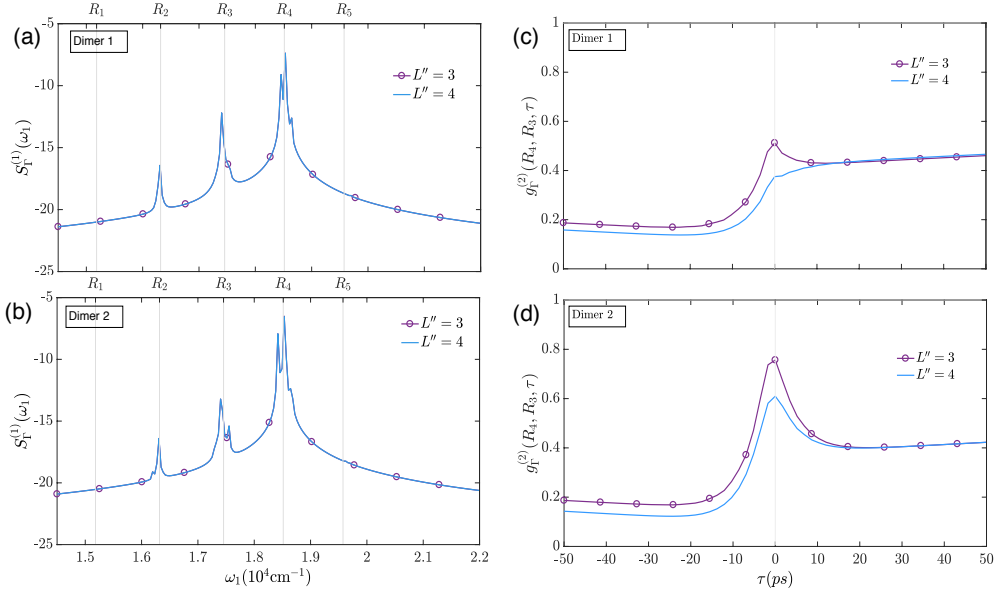


Figure B.1: Power spectra (a) and (b) and time-resolved correlation functions (c) and (d) for both dimers, with coupling to the cavity  $g_c = (1.33\text{ps})^{-1} = 25 \text{ cm}^{-1}$  and other parameters given in Tables 3.1(b) and 3.1(c), comparing different values of the maximum number of excitations  $L''$  in the cavity mode. (The figure for the power spectra is in log scale.)

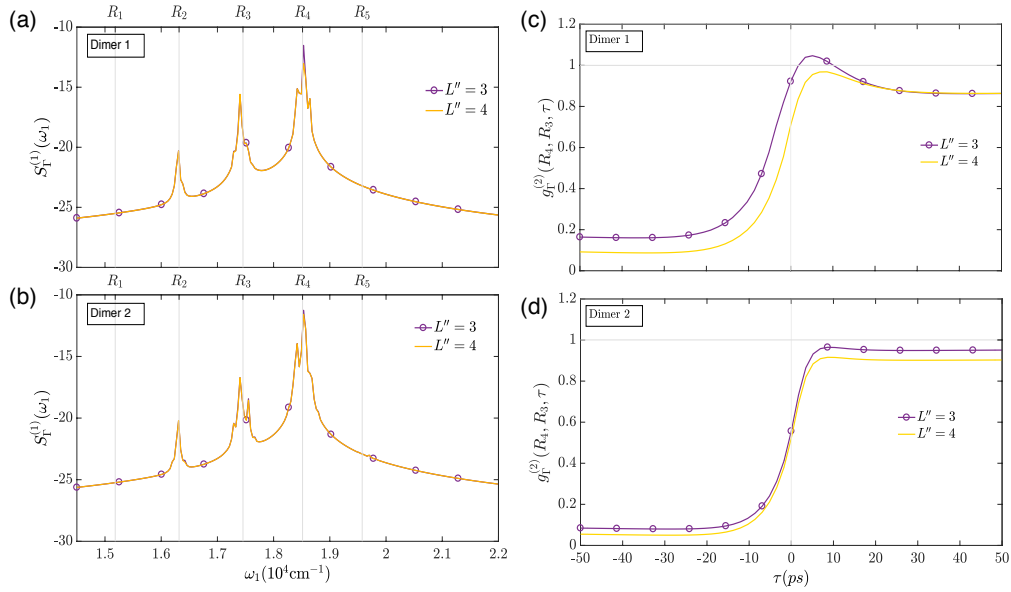


Figure B.2: Power spectra (a) and (b) and time-resolved correlation functions (c) and (d) for both dimers, with coupling to the cavity  $g_c = (0.67\text{ps})^{-1} = 50 \text{ cm}^{-1}$  and other parameters given in Fig.3.1(b) and 3.1(c), comparing different values of the maximum number of excitations  $L''$  in the cavity mode. (The figure for the power spectra is in log scale.)

# Bibliography

- [1] S. Huelga and M. Plenio, “Vibrations, quanta and biology,” *Contemp. Phys.*, vol. 54, pp. 181–207, 2013.
- [2] M. B. Plenio and S. F. Huelga, “Entangled light from white noise,” *Phys. Rev. Lett.*, vol. 88, p. 197901, 2002.
- [3] G. D. Scholes, G. R. Fleming, A. Olaya-Castro, and R. van Grondelle, “Lessons from nature about solar light harvesting,” *Nat. Chem.*, vol. 3, pp. 763–774, 2011.
- [4] H. van Amerongen, L. Valkunas, and R. van Grondelle, *Photosynthetic Excitons*. World Scientific Singapore, 2000.
- [5] R. J. Cogdell, A. Gall, and J. Köhler, “The architecture and function of the light-harvesting apparatus of purple bacteria: from single molecules to in vivo membranes,” *Quart. Rev. Biophys.*, vol. 39, pp. 227–324, 2006.
- [6] T. Ritz, A. Damjanović, and K. Schulten, “The quantum physics of photosynthesis,” *ChemPhysChem*, vol. 3, pp. 243–248, 2002.
- [7] R. Blankenship, *Molecular Mechanisms of Photosynthesis*. Blackwell Science, 2002.
- [8] V. I. Prokhorenko, A. R. Holzwarth, F. R. Nowak, and T. J. Aartsma, “Growing-in of optical coherence in the FMO antenna complexes,” *J. Phys. Chem. B*, vol. 106, pp. 9923–9933, 2002.
- [9] G. S. Engel, T. R. Calhoun, E. L. Read, T.-K. Ahn, T. Mančal, Y.-C. Cheng, R. E. Blankenship, and G. R. Fleming, “Evidence for wavelike energy transfer through quantum coherence in photosynthetic systems,” *Nature*, vol. 446, p. 782, 2007.

- [10] H. Lee, Y.-C. Cheng, and G. R. Fleming, “Coherence dynamics in photosynthesis: Protein protection of excitonic coherence,” *Science*, vol. 316, p. 1462, 2007.
- [11] G. Panitchayangkoon, D. Hayes, K. A. Fransted, J. R. Caram, E. Harel, J. Wen, R. E. Blankenship, and G. S. Engel, “Long-lived quantum coherence in photosynthetic complexes at physiological temperature,” *Proc. Natl. Acad. Sci. U.S.A.*, vol. 107, pp. 12766–12770, 2010.
- [12] E. Collini, C. Y. Wong, K. E. Wilk, P. M. G. Curmi, P. Brumer, and G. D. Scholes, “Coherently wired light-harvesting in photosynthetic marine algae at ambient temperature,” *Nature*, vol. 463, p. 644, 02 2010.
- [13] M. Mohseni, P. Rebentrost, S. Lloyd, and A. Aspuru-Guzik, “Environment-assisted quantum walks in photosynthetic energy transfer,” *J. Chem. Phys.*, vol. 129, p. 174106, 2008.
- [14] M. B. Plenio and S. F. Huelga, “Dephasing-assisted transport: quantum networks and biomolecules,” *New J. Phys.*, vol. 10, p. 113019, 2008.
- [15] A. Olaya-Castro, C. F. Lee, F. F. Olsen, and N. F. Johnson, “Efficiency of energy transfer in a light-harvesting system under quantum coherence,” *Phys. Rev. B*, vol. 78, p. 085115, 2008.
- [16] P. Rebentrost, M. Mohseni, I. Kassal, S. Lloyd, and A. Aspuru-Guzik, “Environment-assisted quantum transport,” *New J. Phys.*, vol. 11, p. 033003, 2009.
- [17] F. Caruso, A. W. Chin, A. Datta, S. F. Huelga, and M. B. Plenio, “Highly efficient energy excitation transfer in light-harvesting complexes: The fundamental role of noise-assisted transport,” *J. Chem. Phys.*, vol. 131, p. 105106, 2009.
- [18] A. W. Chin, A. Datta, F. Caruso, S. F. Huelga, and M. B. Plenio, “Noise-assisted energy transfer in quantum networks and light-harvesting complexes,” *New J. Phys.*, vol. 12, p. 065002, 2010.
- [19] F. Caruso, S. F. Huelga, and M. B. Plenio, “Noise-enhanced classical and quantum capacities in communication networks,” *Phys. Rev. Lett.*, vol. 105, p. 190501, 2010.

- [20] S. Shim, P. Rebentrost, S. Valleau, and A. Aspuru-Guzik, “Atomistic study of the long-lived quantum coherences in the Fenna-Matthews-Olson complex,” *Biophys. J.*, vol. 102, pp. 649–660, 2012.
- [21] J. Yuen-Zhou, J. J. Krich, M. Mohseni, and A. Aspuru-Guzik, “Quantum state and process tomography of energy transfer systems via ultrafast spectroscopy,” *Proc. Natl. Acad. Sci. U.S.A.*, vol. 108, p. 17615, 2011.
- [22] E. J. O’Reilly and A. Olaya-Castro, “Non-classicality of the molecular vibrations assisting exciton energy transfer at room temperature,” *Nat. Commun.*, vol. 5, p. 3012, 2014.
- [23] T. Brixner, T. Mančal, I. V. Stiopkin, and G. R. Fleming, “Phase-stabilized two-dimensional electronic spectroscopy,” *J. Chem. Phys.*, vol. 121, pp. 4221–4236, 2004.
- [24] D. M. Jonas, “Two-dimensional femtosecond spectroscopy,” *Annu. Rev. Phys. Chem.*, vol. 54, pp. 425–463, 2003.
- [25] E. Harel and G. S. Engel, “Quantum coherence spectroscopy reveals complex dynamics in bacterial light-harvesting complex 2 (lh2),” *Proc. Natl. Acad. Sci. U.S.A.*, vol. 109, pp. 706–711, 2012.
- [26] M. Maiuri, E. E. Ostroumov, R. G. Saer, R. E. Blankenship, and G. D. Scholes, “Coherent wavepackets in the Fenna–Matthews–Olson complex are robust to excitonic-structure perturbations caused by mutagenesis,” *Nat. Chem.*, vol. 10, p. 177, 2018.
- [27] E. Thyryhaug, R. Tempelaar, M. J. P. Alcocer, K. Židek, D. Bína, J. Knoester, T. L. C. Jansen, and D. Zigmantas, “Identification and characterization of diverse coherences in the Fenna–Matthews–Olson complex,” *Nat. Chem.*, vol. 10, pp. 780–786, 2018.
- [28] F. Ma, E. Romero, M. R. Jones, V. I. Novoderezhkin, and R. van Grondelle, “Both electronic and vibrational coherences are involved in primary electron transfer in bacterial reaction center,” *Nat. Commun.*, vol. 10, p. 933, 2019.
- [29] E. Romero, R. Augulis, V. I. Novoderezhkin, M. Ferretti, J. Thieme, D. Zigmantas, and R. van Grondelle, “Quantum coherence in photosynthesis for efficient solar-energy conversion,” *Nat. Phys.*, vol. 10, p. 676, 2014.

- [30] F. D. Fuller, J. Pan, A. Gelzinis, V. Butkus, S. S. Senlik, D. E. Wilcox, C. F. Yocum, L. Valkunas, D. Abramavicius, and J. P. Ogilvie, “Vibronic coherence in oxygenic photosynthesis,” *Nat. Chem.*, vol. 6, pp. 706 EP –, 2014.
- [31] A. Kolli, E. J. O’Reilly, G. D. Scholes, and A. Olaya-Castro, “The fundamental role of quantized vibrations in coherent light harvesting by cryptophyte algae,” *J. Chem. Phys.*, vol. 137, p. 174109, 2012.
- [32] G. H. Richards, K. E. Wilk, P. M. G. Curmi, H. M. Quiney, and J. A. Davis, “Coherent vibronic coupling in light-harvesting complexes from photosynthetic marine algae,” *J. Phys. Chem. Lett.*, vol. 3, pp. 272–277, 2012.
- [33] F. Novelli, A. Nazir, G. H. Richards, A. Roozbeh, K. E. Wilk, P. M. G. Curmi, and J. A. Davis, “Vibronic resonances facilitate excited-state coherence in light-harvesting proteins at room temperature,” *J. Phys. Chem. Lett.*, vol. 6, pp. 4573–4580, 2015.
- [34] J. C. Dean, T. Mirkovic, Z. S. D. Toa, D. G. Oblinsky, and G. D. Scholes, “Vibronic enhancement of algae light harvesting,” *Chem*, vol. 1, pp. 858–872, 2016.
- [35] A. W. Chin, J. Prior, R. Rosenbach, F. Caycedo-Soler, S. F. Huelga, and M. B. Plenio, “The role of non-equilibrium vibrational structures in electronic coherence and recoherence in pigment–protein complexes,” *Nat. Phys.*, vol. 9, p. 113, 2013.
- [36] H.-G. Duan, V. I. Prokhorenko, R. J. Cogdell, K. Ashraf, A. L. Stevens, M. Thorwart, and R. J. D. Miller, “Nature does not rely on long-lived electronic quantum coherence for photosynthetic energy transfer,” *Proceedings of the National Academy of Sciences*, vol. 114, p. 201702261, 2017.
- [37] W. H. Miller, “Perspective: Quantum or classical coherence?,” *J. Chem. Phys.*, vol. 136, p. 210901, 2012.
- [38] R. J. Glauber, “The quantum theory of optical coherence,” *Phys. Rev.*, vol. 130, pp. 2529–2539, 1963.
- [39] R. J. Glauber, “Nobel lecture: One hundred years of light quanta,” *Rev. Mod. Phys.*, vol. 78, pp. 1267–1278, 2006.

- [40] P. Grangier, G. Roger, and A. Aspect, “Experimental evidence for a photon anticorrelation effect on a beam splitter: A new light on single-photon interferences,” *Europhys. Lett.*, vol. 1, pp. 173–179, 1986.
- [41] B. Lounis and W. E. Moerner, “Single photons on demand from a single molecule at room temperature,” *Nature*, vol. 407, pp. 491–493, 2000.
- [42] A. Olaya-Castro, F. J. Rodríguez, L. Quiroga, and C. Tejedor, “Restrictions on the coherence of the ultrafast optical emission from an electron-hole-pair condensate,” *Phys. Rev. Lett.*, vol. 87, p. 246403, 2001.
- [43] P. Michler, A. Imamoglu, M. D. Mason, P. J. Carson, G. F. Strouse, and S. K. Buratto, “Quantum correlation among photons from a single quantum dot at room temperature,” *Nature*, vol. 406, pp. 968–970, 2000.
- [44] E. Moreau, I. Robert, J. M. Gérard, I. Abram, L. Manin, and V. Thierry-Mieg, “Single-mode solid-state single photon source based on isolated quantum dots in pillar microcavities,” *Appl. Phys. Lett.*, vol. 79, pp. 2865–2867, 2001.
- [45] E. Wientjes, J. Renger, A. G. Curto, R. Cogdell, and N. F. van Hulst, “Strong antenna-enhanced fluorescence of a single light-harvesting complex shows photon antibunching,” *Nat. Commun.*, vol. 5, p. 4236, 2014.
- [46] E. del Valle, A. Gonzalez-Tudela, F. P. Laussy, C. Tejedor, and M. J. Hartmann, “Theory of frequency-filtered and time-resolved  $n$ -photon correlations,” *Phys. Rev. Lett.*, vol. 109, p. 183601, 2012.
- [47] E. del Valle, A. Gonzalez-Tudela, F. P. Laussy, C. Tejedor, and M. J. Hartmann, “Erratum: Theory of frequency-filtered and time-resolved  $n$ -photon correlations [phys. rev. lett. 109, 183601 (2012)],” *Phys. Rev. Lett.*, vol. 116, p. 249902, 2016.
- [48] M. Peiris, K. Konthasinghe, and A. Muller, “Franson interference generated by a two-level system,” *Phys. Rev. Lett.*, vol. 118, p. 030501, 2017.
- [49] K. E. Dorfman and S. Mukamel, “Multidimensional photon correlation spectroscopy of cavity polaritons,” *Proc. Natl. Acad. Sci. USA*, vol. 115, p. 1451, 2018.
- [50] D. I. H. Holdaway, V. Notararigo, and A. Olaya-Castro, “Perturbation approach for computing frequency- and time-resolved photon correlation functions,” *Phys. Rev. A*, vol. 98, p. 063828, 2018.

- [51] P. Jordan, *Die Physik und das Geheimnis des Lebens*. 1943.
- [52] E. Schrödinger, *What is Life?* Cambridge University Press, 1944.
- [53] A.S.Davydov, *Biology and Quantum Mechanics*. Pergamon Press, 1982.
- [54] L. Hartmann, W. Dür, and H.-J. Briegel, “Steady-state entanglement in open and noisy quantum systems,” *Phys. Rev. A*, vol. 74, p. 052304, 2006.
- [55] M. d. Rey, A. W. Chin, S. F. Huelga, and M. B. Plenio, “Exploiting structured environments for efficient energy transfer: The phonon antenna mechanism,” *J. Phys. Chem. Lett.*, vol. 4, p. 903, 2013.
- [56] M. Mohseni, Y. Omar, G. Engel, and M. Plenio, *Quantum Effects in Biology*. Cambridge University Press, 2014.
- [57] F.-A. Miannay, Á. Bányász, T. Gustavsson, and D. Markovitsi, “Ultrafast excited-state deactivation and energy transfer in guanine cytosine dna double helices,” *J. Am. Chem. Soc.*, vol. 129, pp. 14574–14575, 2007.
- [58] N. Kollias, R. M. Sayre, L. Zeise, and M. R. Chedekel, “New trends in photobiology: Photoprotection by melanin,” *J. Photochem. Photobiol., B*, vol. 9, pp. 135–160, 1991.
- [59] M. Zarubin, S. Belkin, M. Ionescu, and A. Genin, “Bacterial bioluminescence as a lure for marine zooplankton and fish,” *Proc. Natl. Acad. Sci.*, vol. 109, p. 853, 2012.
- [60] J. C. Brookes, F. Hartoutsiou, A. P. Horsfield, and A. M. Stoneham, “Could humans recognize odor by phonon assisted tunneling?,” *Phys. Rev. Lett.*, vol. 98, p. 038101, 2007.
- [61] A. Ishizaki and G. R. Fleming, “On the interpretation of quantum coherent beats observed in two-dimensional electronic spectra of photosynthetic light harvesting complexes,” *J. Phys. Chem. B*, vol. 115, pp. 6227–6233, 2011.
- [62] R. A. Marcus and N. Sutin, “Electron transfers in chemistry and biology,” *Biochim. Biophys. Acta, Rev. Bioenerg.*, vol. 811, 1985.
- [63] H. B. Gray and J. R. Winkler, “Electron tunneling through proteins,” *Q. Rev. Biophys.*, vol. 36, pp. 341–372, 2003.

- [64] C. C. Page, C. C. Moser, X. Chen, and P. L. Dutton, “Natural engineering principles of electron tunnelling in biological oxidation–reduction,” *Nature*, vol. 402, pp. 47–52, 1999.
- [65] R. K. Allemann and N. S. Scrutton, *Quantum Tunnelling in Enzyme-Catalysed Reactions*. RSC Biomolecular Sciences, The Royal Society of Chemistry, 2009.
- [66] L. Turin, “A spectroscopic mechanism for primary olfactory reception,” *Chem. Senses*, vol. 21, pp. 773–791, 1996.
- [67] M. I. Franco, L. Turin, A. Mershin, and E. M. C. Skoulakis, “Molecular vibration-sensing component in drosophila melanogaster olfaction,” *Proc. Natl. Acad. Sci. U.S.A.*, vol. 108, pp. 3797–3802, 2011.
- [68] E. Wajnberg, D. Acosta-Avalos, O. C. Alves, J. F. de Oliveira, R. B. Srygley, and D. M. S. Esquivel, “Magnetoreception in eusocial insects: an update,” *J. R. Soc. Interface*, vol. 7, pp. S207–S225, 2010.
- [69] N. Lambert, Y.-N. Chen, Y.-C. Cheng, C.-M. Li, G.-Y. Chen, and F. Nori, “Quantum biology,” *Nat. Phys.*, vol. 9, p. 10, 2013.
- [70] S. Mekhilef, R. Saidur, and M. Kamalisarvestani, “Effect of dust, humidity and air velocity on efficiency of photovoltaic cells,” *Renewable Sustainable Energy Rev.*, vol. 16, pp. 2920 – 2925, 2012.
- [71] L. Urry, M. Cain, S. Wasserman, and J. Reece, *Campbell Biology*. Pearson Higher Education, 2016.
- [72] F. Fassioli, R. Dinshaw, P. C. Arpin, and G. D. Scholes, “Photosynthetic light harvesting: excitons and coherence,” *J. R. Soc. Interface*, vol. 11, p. 20130901, 2014.
- [73] F. Levi, S. Mostarda, F. Rao, and F. Mintert, “Quantum mechanics of excitation transport in photosynthetic complexes: a key issues review,” *Rep. Prog. Phys.*, vol. 78, p. 082001, 2015.
- [74] M. B. Oviedo and C. G. Sánchez, “Transition dipole moments of the qy band in photosynthetic pigments,” *J. Phys. Chem. A*, vol. 115, pp. 12280–12285, 2011.
- [75] F. Passarini, E. Wientjes, H. van Amerongen, and R. Croce, “Photosystem I light-harvesting complex Lhca4 adopts multiple conformations: Red forms

- and excited-state quenching are mutually exclusive,” *Biochim. Biophys. Acta (BBA) - Bioenergetics*, vol. 1797, pp. 501–508, 2010.
- [76] M. Sener and K. Schulten, *Energy Harvesting Materials*. ed David L Andrews, Singapore: World Scientific, 2005.
- [77] T. Brixner, J. Stenger, H. M. Vaswani, M. Cho, R. E. Blankenship, and G. R. Fleming, “Two-dimensional spectroscopy of electronic couplings in photosynthesis,” *Nature*, vol. 434, pp. 625–628, 2005.
- [78] R. Jimenez, S. N. Dikshit, S. E. Bradforth, and G. R. Fleming, “Electronic excitation transfer in the LH2 complex of Rhodobacter sphaeroides,” *J. Phys. Chem.*, vol. 100, pp. 6825–6834, 1996.
- [79] T. Pullerits, M. Chachivili, and V. Sundström, “Exciton delocalization length in the B850 antenna of Rhodobacter sphaeroides,” *J. Phys. Chem.*, vol. 100, pp. 10787–10792, 1996.
- [80] V. May and O. Kuhn, *Charge and Energy Transfer Dynamics in Molecular Systems*. Wiley, 2011.
- [81] H. Breuer and F. Petruccione, *The theory of open quantum systems*. Oxford University Press, 2002.
- [82] H. Carmichael, *An Open Systems Approach to Quantum Optics*. Springer-Verlag Berlin Heidelberg GmbH, 1993.
- [83] S. Haroche and J. Raimond, *Exploring the quantum atoms, cavities, and photons*. Oxford University Press, 2006.
- [84] I. S. Morag Am-Shalem, Amikam Levy and R. Kosloff, “Three approaches for representing Lindblad dynamics by a matrix-vector notation,” *arXiv:1510.08634v2*, 1996.
- [85] T. Renger, “Theory of optical spectra involving charge transfer states: Dynamic localization predicts a temperature dependent optical band shift,” *Phys. Rev. Lett.*, vol. 93, p. 188101, 2004.
- [86] L. Valkunas, D. Abramavicius, and T. Mancal, *Molecular Excitation Dynamics and Relaxation*. Wiley, 2013.
- [87] A. G. Redfield, “On the theory of relaxation processes,” *IBM J. Res. Dev.*, vol. 1, no. 1, pp. 19–31, 1957.

- [88] T. Förster, “Transfer mechanisms of electronic excitation energy,” *Radiation Research Supplement*, vol. 2, pp. 7–17, 1960.
- [89] Y.-C. Cheng and G. R. Fleming, “Coherence quantum beats in two-dimensional electronic spectroscopy,” *J. Phys. Chem. A*, vol. 112, pp. 4254–4260, 2008.
- [90] A. A. P. Chauvet, *Advances in Microfluidics. New Applications in Biology, Energy, and Materials Sciences*. IntechOpen, 2016.
- [91] S. Savikhin, D. R. Buck, and W. S. Struve, “Oscillating anisotropies in a bacteriochlorophyll protein: Evidence for quantum beating between exciton levels,” *Chem. Phys.*, vol. 223, pp. 303–312, 1997.
- [92] S. Mukamel, *Principles of nonlinear optical spectroscopy*. Oxford University Press, 1995.
- [93] P. Hamm, “Principles of nonlinear optical spectroscopy: A practical approach.” <http://www.mitr.p.lodz.pl/evu/lectures/Hamm.pdf>, 2005.
- [94] [https://web.stanford.edu/group/fayer/research\\_echo.html](https://web.stanford.edu/group/fayer/research_echo.html).
- [95] M. B. Plenio, J. Almeida, and S. F. Huelga, “Origin of long-lived oscillations in 2d-spectra of a quantum vibronic model: Electronic versus vibrational coherence,” *J. Chem. Phys.*, vol. 139, p. 235102, 2013.
- [96] A. F. Fidler, E. Harel, P. D. Long, and G. S. Engel, “Two-dimensional spectroscopy can distinguish between decoherence and dephasing of zero-quantum coherences,” *J. Phys. Chem. A*, vol. 116, no. 1, pp. 282–289, 2012.
- [97] J. Lim, D. Paleček, F. Caycedo-Soler, C. N. Lincoln, J. Prior, H. von Berlepsch, S. F. Huelga, M. B. Plenio, D. Zigmantas, and J. Hauer, “Vibronic origin of long-lived coherence in an artificial molecular light harvester,” *Nat. Commun.*, vol. 6, p. 7755, 2015.
- [98] J. R. Caram, A. F. Fidler, and G. S. Engel, “Excited and ground state vibrational dynamics revealed by two-dimensional electronic spectroscopy,” *J. Chem. Phys.*, vol. 137, p. 024507, 2012.
- [99] G. Panitchayangkoon, D. V. Voronine, D. Abramavicius, J. R. Caram, N. H. C. Lewis, S. Mukamel, and G. S. Engel, “Direct evidence of quantum transport in photosynthetic light-harvesting complexes,” *Proc. Natl. Acad. Sci. U.S.A.*, vol. 108, pp. 20908–20912, 2011.

- [100] M. M.O.Scully, *Quantum Optics*. Cambridge University Press, 1997.
- [101] W. Vogel and D. Welsch, *Quantum Optics*. Wiley-VCH Verlag GmbH and Co. KGaA, Weinheim, 2006.
- [102] M.Fox, *Quantum Optics*. Oxford University Press, 2006.
- [103] H.Carmichael, *An Open Systems Approach to Quantum Optics*. Springer-Verlag Berlin Heidelberg, 1993.
- [104] J. H. Eberly and K. Wódkiewicz, “The time-dependent physical spectrum of light\*,” *J. Opt. Soc. Am.*, vol. 67, pp. 1252–1261, 1977.
- [105] L. Knoll and G. Weber, “Theory of n-fold time-resolved correlation spectroscopy and its application to resonance fluorescence radiation,” *J. Phys. B*, vol. 19, p. 2817, 1986.
- [106] P. A. Apanasevich, S. Y. Kilin, and A. F. Fedorov, “Photon correlation in resonance scattering-a new approach to the investigation of the excited states of atoms and molecules,” *J. Phys. B: At. Mol. Phys.*, vol. 18, pp. L55–L58, 1985.
- [107] J. D. Cresser, “Intensity correlations of frequency-filtered light fields,” *J. Phys. B*, vol. 20, p. 4915, 1987.
- [108] G. Bel and F. L. H. Brown, “Theory for wavelength-resolved photon emission statistics in single-molecule fluorescence spectroscopy,” *Phys. Rev. Lett.*, vol. 102, p. 018303, 2009.
- [109] K. Kamide, S. Iwamoto, and Y. Arakawa, “Eigenvalue decomposition method for photon statistics of frequency-filtered fields and its application to quantum dot emitters,” *Phys. Rev. A*, vol. 92, p. 033833, 2015.
- [110] J. Wiersig, C. Gies, F. Jahnke, M. Aßmann, T. Berstermann, M. Bayer, C. Kistner, S. Reitzenstein, C. Schneider, S. Höfling, A. Forchel, C. Kruse, J. Kalden, and D. Hommel, “Direct observation of correlations between individual photon emission events of a microcavity laser,” *Nature*, vol. 460, pp. 245 EP –, 2009.
- [111] V. N. Shatokhin and S. Y. Kilin, “Correlation functions in resonance fluorescence with spectral resolution: Signal-processing approach,” *Phys. Rev. A*, vol. 94, p. 033835, 2016.

- [112] K.-H. Brenner and K. Wódkiewicz, “The time-dependent physical spectrum of light and the wigner distribution function,” *Opt. Commun.*, vol. 43, pp. 103 – 106, 1982.
- [113] A. Gonzalez-Tudela, F. P. Laussy, C. Tejedor, M. J. Hartmann, and E. del Valle, “Two-photon spectra of quantum emitters,” *New J. Phys.*, vol. 15, p. 033036, 2013.
- [114] A. González-Tudela, E. del Valle, and F. P. Laussy, “Optimization of photon correlations by frequency filtering,” *Phys. Rev. A*, vol. 91, p. 043807, 2015.
- [115] M. Peiris, B. Petrak, K. Konthasinghe, Y. Yu, Z. C. Niu, and A. Muller, “Two-color photon correlations of the light scattered by a quantum dot,” *Phys. Rev. B*, vol. 91, p. 195125, 2015.
- [116] H. Flayac and V. Savona, “Heralded preparation and readout of entangled phonons in a photonic crystal cavity,” *Phys. Rev. Lett.*, vol. 113, p. 143603, 2014.
- [117] G. Sallen, A. Tribu, T. Aichele, R. André, L. Besombes, C. Bougerol, M. Richard, S. Tatarenko, K. Kheng, and J. P. Poizat *Nat. Photonics*.
- [118] P. Grünwald, D. Vasylyev, J. Häggblad, and W. Vogel, “Quantum measurement of broadband nonclassical light fields,” *Phys. Rev. A*, vol. 91, p. 013816, 2015.
- [119] B. Silva, C. Sánchez Muñoz, D. Ballarini, A. González-Tudela, M. de Giorgi, G. Gigli, K. West, L. Pfeiffer, E. del Valle, D. Sanvitto, and F. P. Laussy, “The coloured Hanbury Brown–Twiss effect,” *Sci. Rep.*, vol. 6, p. 37980, 2016.
- [120] C. Dory, K. A. Fischer, K. Müller, K. G. Lagoudakis, T. Sarmiento, A. Rundquist, J. L. Zhang, Y. Kelaita, N. V. Saprà, and J. Vučković, “Tuning the photon statistics of a strongly coupled nanophotonic system,” *Phys. Rev. A*, vol. 95, p. 023804, 2017.
- [121] K. E. Dorfman and S. Mukamel, “Time-and-frequency-gated photon coincidence counting; a novel multidimensional spectroscopy tool,” *Phys. Scr.*, vol. 91, p. 083004, 2016.
- [122] Z. Zhang, P. Saurabh, K. E. Dorfman, A. Debnath, and S. Mukamel, “Monitoring polariton dynamics in the lhci photosynthetic antenna in a microcavity by two-photon coincidence counting,” *J. Chem. Phys.*, vol. 148, p. 074302, 2018.

- [123] T. Brixner, J. Stenger, H. M. Vaswani, M. Cho, R. E. Blankenship, and G. R. Fleming, “Two-dimensional spectroscopy of electronic couplings in photosynthesis,” *Nature*, vol. 434, pp. 625–628, 2005.
- [124] G. D. Scholes, G. R. Fleming, L. X. Chen, A. Aspuru-Guzik, A. Buchleitner, D. F. Coker, G. S. Engel, R. van Grondelle, A. Ishizaki, D. M. Jonas, J. S. Lundeen, J. K. McCusker, S. Mukamel, J. P. Ogilvie, A. Olaya-Castro, M. A. Ratner, F. C. Spano, K. B. Whaley, and X. Zhu, “Using coherence to enhance function in chemical and biophysical systems,” *Nature*, vol. 543, p. 647, 2017.
- [125] A. Ridolfo, E. del Valle, and M. J. Hartmann, “Photon correlations from ultrastrong optical nonlinearities,” *Phys. Rev. A*, vol. 88, p. 063812, 2013.
- [126] S. Tubasum, R. J. Cogdell, I. G. Scheblykin, and T. Pullerits, “Excitation-emission polarization spectroscopy of single light harvesting complexes,” *J. Phys. Chem. B*, vol. 115, pp. 4963–4970, 2011.
- [127] A. D. Cimmarusti, Z. Yan, B. D. Patterson, L. P. Corcos, L. A. Orozco, and S. Deffner, “Environment-assisted speed-up of the field evolution in cavity quantum electrodynamics,” *Phys. Rev. Lett.*, vol. 114, p. 233602, 2015.
- [128] N. Killoran, S. F. Huelga, and M. B. Plenio, “Enhancing light-harvesting power with coherent vibrational interactions: A quantum heat engine picture,” *J. Chem. Phys.*, vol. 143, p. 155102, 2015.
- [129] J. Hofkens, M. Cotlet, T. Vosch, P. Tinnefeld, K. D. Weston, C. Ego, A. Grimsdale, K. Mllen, D. Beljonne, J. L. Brdas, S. Jordens, G. Schweitzer, M. Sauer, and F. D. Schryver, “Revealing competitive Förster-type resonance energy-transfer pathways in single bichromophoric molecules,” *Proc. Natl. Acad. Sci. USA*, vol. 100, pp. 13146–13151, 2003.
- [130] C. G. Hübner, G. Zumofen, A. Renn, A. Herrmann, K. Müllen, and T. Basché, “Photon antibunching and collective effects in the fluorescence of single bichromophoric molecules,” *Phys. Rev. Lett.*, vol. 91, p. 093903, 2003.
- [131] F. Fassioli and A. Olaya-Castro, “Distribution of entanglement in light-harvesting complexes and their quantum efficiency,” vol. 12, p. 085006, 2010.
- [132] C. Curutchet, V. I. Novoderezhkin, J. Kongsted, A. Muñoz-Losa, R. van Grondelle, G. D. Scholes, and B. Mennucci, “Energy flow in the cryptophyte PE545 antenna is directed by bilin pigment conformation,” *J. Phys. Chem. B*, vol. 117, pp. 4263–4273, 2013.

- [133] J. C. López Carreño, E. del Valle, and F. P. Laussy, “Frequency-resolved Monte Carlo,” *Sci. Rep.*, vol. 8, p. 6975, 2018.
- [134] J. C. L. Carreño, E. Z. Casalengua, F. P. Laussy, and E. del Valle, “Joint subnatural-linewidth and single-photon emission from resonance fluorescence,” *Quantum Sci. Technol.*, vol. 3, p. 045001, 2018.
- [135] H. Carmichael, *An Open Systems Approach to Quantum Optics*. Springer-Verlag Berlin Heidelberg, 1993.
- [136] H. Paul, “Photon antibunching,” *Rev. Mod. Phys.*, vol. 54, pp. 1061–1102, 1982.
- [137] X. T. Zou and L. Mandel, “Photon-antibunching and sub-poissonian photon statistics,” *Phys. Rev. A*, vol. 41, pp. 475–476, 1990.
- [138] R. J. Brecha and H. J. Carmichael, “Nonclassical photon correlations in cavity QED,” in *Coherence and Quantum Optics VI*, Springer US, 1989.
- [139] S. L. Mielke, G. T. Foster, and L. A. Orozco, “Nonclassical intensity correlations in cavity QED,” *Phys. Rev. Lett.*, vol. 80, pp. 3948–3951, 1998.
- [140] W. Choi, J.-H. Lee, K. An, C. Fang-Yen, R. R. Dasari, and M. S. Feld, “Observation of sub-poisson photon statistics in the cavity-QED microlaser,” *Phys. Rev. Lett.*, vol. 96, p. 093603, 2006.
- [141] C. Lang, D. Bozyigit, C. Eichler, L. Steffen, J. M. Fink, A. A. Abdumalikov, M. Baur, S. Filipp, M. P. da Silva, A. Blais, and A. Wallraff, “Observation of resonant photon blockade at microwave frequencies using correlation function measurements,” *Phys. Rev. Lett.*, vol. 106, p. 243601, 2011.
- [142] D. Bozyigit, C. Lang, L. Steffen, J. M. Fink, C. Eichler, M. Baur, R. Bianchetti, P. J. Leek, S. Filipp, M. P. da Silva, A. Blais, and A. Wallraff, “Antibunching of microwave-frequency photons observed in correlation measurements using linear detectors,” *Nat. Phys.*, vol. 7, p. 154, 2010.
- [143] P. Rabl, “Photon blockade effect in optomechanical systems,” *Phys. Rev. Lett.*, vol. 107, p. 063601, 2011.
- [144] F. Caruso, S. K. Saikin, E. Solano, S. F. Huelga, A. Aspuru-Guzik, and M. B. Plenio, “Probing biological light-harvesting phenomena by optical cavities,” *Phys. Rev. B*, vol. 85, p. 125424, 2012.

- [145] Q. Xie, H. Zhong, M. T. Batchelor, and C. Lee, “The quantum Rabi model: solution and dynamics,” *J. Phys. A*, vol. 50, p. 113001, 2017.
- [146] J. M. Womick and A. M. Moran, “Vibronic enhancement of exciton sizes and energy transport in photosynthetic complexes,” *J. Phys. Chem. B*, vol. 115, pp. 1347–1356, 2011.
- [147] V. I. Novoderezhkin, A. B. Doust, C. Curutchet, G. D. Scholes, and R. van Grondelle, “Excitation dynamics in phycoerythrin 545: modeling of steady-state spectra and transient absorption with modified redfield theory,” *Biophys. J.*, vol. 99, pp. 344–352, 2010.
- [148] A. Miranowicz, J. Bajer, W. Leoński, and R. Tanaś, “Various approaches to photon antibunching in second-harmonic generation,” *Proceedings*, 1997.
- [149] D. Roy, C. M. Wilson, and O. Firstenberg, “Colloquium: Strongly interacting photons in one-dimensional continuum,” *Rev. Mod. Phys.*, vol. 89, p. 021001, 2017.
- [150] X. Gu, A. F. Kockum, A. Miranowicz, Y.-X. Liu, and F. Nori, “Microwave photonics with superconducting quantum circuits,” *Phys. Rep.*, vol. 718-719, pp. 1–102, 2017.
- [151] Y.-L. L. Fang and H. U. Baranger, “Waveguide QED: Power spectra and correlations of two photons scattered off multiple distant qubits and a mirror,” *Phys. Rev. A*, vol. 91, p. 053845, 2015.
- [152] X. H. H. Zhang and H. U. Baranger, “Quantum interference and complex photon statistics in waveguide QED,” *Phys. Rev. A*, vol. 97, p. 023813, 2018.
- [153] L. Onsager, “Reciprocal relations in irreversible processes. i.,” *Phys. Rev.*, vol. 37, pp. 405–426, 1931.
- [154] A. Denisov, H. M. Castro-Beltran, and H. J. Carmichael, “Time-asymmetric fluctuations of light and the breakdown of detailed balance,” *Phys. Rev. Lett.*, vol. 88, p. 243601, 2002.
- [155] K. Tomita and H. Tomita, “Irreversible circulation of fluctuation,” *Progr. Theor. Phys.*, vol. 51, pp. 1731–1749, 1974.
- [156] R. Graham, *Springer Tracts in Modern Physics*, vol. 51. Springer-Verlag, Berlin, 1973.

- [157] R. Graham and H. Haken, “Generalized thermodynamic potential for Markoff systems in detailed balance and far from thermal equilibrium,” *Phys.*, vol. 243, p. 289, 1971.
- [158] C. A. Schrama, G. Nienhuis, H. A. Dijkerman, C. Steijsiger, and H. G. M. Heideman, “Destructive interference between opposite time orders of photon emission,” *Phys. Rev. Lett.*, vol. 67, pp. 2443–2445, 1991.
- [159] H. Z. Zhao, Z. H. Lu, and J. E. Thomas, “Phase-dependent resonance fluorescence and time ordering in photodetection,” *Phys. Rev. Lett.*, vol. 79, pp. 613–616, 1997.
- [160] E. Moreau, I. Robert, L. Manin, V. Thierry-Mieg, J. M. Gérard, and I. Abram, “Quantum cascade of photons in semiconductor quantum dots,” *Phys. Rev. Lett.*, vol. 87, p. 183601, 2001.
- [161] A. W. Chin, E. Manguaud, O. Atabek, and M. Desouter-Lecomte, “Coherent quantum dynamics launched by incoherent relaxation in a quantum circuit simulator of a light-harvesting complex,” *Phys. Rev. A*, vol. 97, p. 063823, 2018.
- [162] E. M. Purcell, “Spontaneous emission probabilities at radio frequencies,” *Phys. Rev.*, vol. 69, p. 681, 1946.
- [163] G. M. Akselrod, C. Argyropoulos, T. B. Hoang, C. Ciraci, C. Fang, J. Huang, D. R. Smith, and M. H. Mikkelsen, “Probing the mechanisms of large purcell enhancement in plasmonic nanoantennas,” *Nat. Photonics*, vol. 8, p. 835, 2014.
- [164] M. Boroditsky, R. Vrijen, R. Coccioli, R. Bhat, and E. Yablonovitch, “Spontaneous emission extraction and Purcell enhancement from thin-film 2-d photonic crystals,” *J. Lightwave Technol.*, vol. 17, p. 2096, 1999.
- [165] G. Khitrova, H. M. Gibbs, M. Kira, S. W. Koch, and A. Scherer, “Vacuum Rabi splitting in semiconductors,” *Nat. Phys.*, vol. 2, pp. 81–90, 2006.
- [166] H. Mabuchi and A. C. Doherty, “Cavity quantum electrodynamics: Coherence in context,” *Science*, vol. 298, p. 1372, 2002.
- [167] F. P. Laussy, E. del Valle, M. Schrapp, A. Laucht, and J. J. Finley, “Climbing the Jaynes-Cummings ladder by photon counting,” *J. Nanophotonics*, vol. 6, pp. 1–10, 2012.

- [168] L. Garziano, A. Ridolfo, R. Stassi, O. Di Stefano, and S. Savasta, “Switching on and off of ultrastrong light-matter interaction: Photon statistics of quantum vacuum radiation,” *Phys. Rev. A*, vol. 88, p. 063829, 2013.
- [169] F. Beaudoin, J. M. Gambetta, and A. Blais, “Dissipation and ultrastrong coupling in circuit QED,” *Phys. Rev. A*, vol. 84, p. 043832, 2011.
- [170] A. Ridolfo, M. Leib, S. Savasta, and M. J. Hartmann, “Photon blockade in the ultrastrong coupling regime,” *Phys. Rev. Lett.*, vol. 109, p. 193602, 2012.
- [171] A. Ridolfo, S. Savasta, and M. J. Hartmann, “Nonclassical radiation from thermal cavities in the ultrastrong coupling regime,” *Phys. Rev. Lett.*, vol. 110, p. 163601, 2013.
- [172] J. Casanova, G. Romero, I. Lizuain, J. J. García-Ripoll, and E. Solano, “Deep strong coupling regime of the jaynes-cummings model,” *Phys. Rev. Lett.*, vol. 105, p. 263603, 2010.
- [173] H. Shi and M. Bhattacharya, “Quantum mechanical study of a generic quadratically coupled optomechanical system,” *Phys. Rev. A*, vol. 87, p. 043829, 2013.
- [174] H. Zoubi, M. Orenstien, and A. Ron, “Coupled microcavities with dissipation,” *Phys. Rev. A*, vol. 62, p. 033801, 2000.
- [175] W. Moerner, M. Orrit, U. Wild, and T. Basch, *Single-Molecule Optical Detection, Imaging and Spectroscopy*. Wiley, New York, 1996.
- [176] D. Wang, H. Kelkar, D. Martin-Cano, D. Rattenbacher, A. Shkarin, T. Utikal, S. Göttinger, and V. Sandoghdar, “Turning a molecule into a coherent two-level quantum system,” *Nat. Phys.*, vol. 15, pp. 483–489, 2019.
- [177] D. M. Coles, Y. Yang, Y. Wang, R. T. Grant, R. A. Taylor, S. K. Saikin, A. Aspuru-Guzik, D. G. Lidzey, J. K.-H. Tang, and J. M. Smith, “Strong coupling between chlorosomes of photosynthetic bacteria and a confined optical cavity mode,” *Nat. Commun.*, vol. 5, p. 5561, 2014.
- [178] F. Caruso, S. K. Saikin, E. Solano, S. F. Huelga, A. Aspuru-Guzik, and M. B. Plenio, “Probing biological light-harvesting phenomena by optical cavities,” *Phys. Rev. B*, vol. 85, p. 125424, 2012.

- [179] L. Sapienza, M. Davanço, A. Badolato, and K. Srinivasan, “Nanoscale optical positioning of single quantum dots for bright and pure single-photon emission,” *Nature Communications*, vol. 6, p. 7833, 2015.
- [180] M. Aspelmeyer, T. J. Kippenberg, and F. Marquardt, “Cavity optomechanics,” *Rev. Mod. Phys.*, vol. 86, pp. 1391–1452, 2014.
- [181] G. Hardy, J. Littlewood, and G. Pólya, *Inequalities*. Cambridge Mathematical Library, 1952.
- [182] J. F. Clauser, “Experimental distinction between the quantum and classical field-theoretic predictions for the photoelectric effect,” *Phys. Rev. D*, vol. 9, pp. 853–860, 1974.
- [183] M. A. Rowe, D. Kielpinski, V. Meyer, C. A. Sackett, W. M. Itano, C. Monroe, and D. J. Wineland, “Experimental violation of a bell’s inequality with efficient detection,” *Nature*, vol. 409, pp. 791–794, 2001.
- [184] A. Kuzmich, W. P. Bowen, A. D. Boozer, A. Boca, C. W. Chou, L. M. Duan, and H. J. Kimble, “Generation of nonclassical photon pairs for scalable quantum communication with atomic ensembles,” *Nature*, vol. 423, pp. 731–734, 2003.
- [185] V. Balić, D. A. Braje, P. Kolchin, G. Y. Yin, and S. E. Harris, “Generation of paired photons with controllable waveforms,” *Phys. Rev. Lett.*, vol. 94, p. 183601, 2005.
- [186] J. K. Thompson, J. Simon, H. Loh, and V. Vuletić, “A high-brightness source of narrowband, identical-photon pairs,” *Science*, vol. 313, pp. 74–77, 2006.
- [187] A. M. Marino, V. Boyer, and P. D. Lett, “Violation of the Cauchy-Schwarz inequality in the macroscopic regime,” *Phys. Rev. Lett.*, vol. 100, p. 233601, 2008.
- [188] K. V. Kheruntsyan, J.-C. Jaskula, P. Deuar, M. Bonneau, G. B. Partridge, J. Ruaudel, R. Lopes, D. Boiron, and C. I. Westbrook, “Violation of the cauchy-schwarz inequality with matter waves,” *Phys. Rev. Lett.*, vol. 108, p. 260401, 2012.
- [189] C. Sánchez Muñoz, E. del Valle, C. Tejedor, and F. P. Laussy, “Violation of classical inequalities by photon frequency filtering,” *Phys. Rev. A*, vol. 90, p. 052111, 2014.